

https://dspace.org/

Investigation into the impact of wind generation on the inter-area and local oscillation modes of power systems

Chidzikwe, Cliff

2018

https://hdl.handle.net/10539/26738

Chidzikwe, Cliff (2018) Investigation into the impact of wind generation on the inter-area and local oscillation modes of power systems, University of the Witwatersrand, Johannesburg, https://hdl.handle.net/10539/26738

Downloaded from a DSpace repository. https://dspace.org/

Investigation into the impact of wind generation on the inter-area and local oscillation modes of power systems



Cliff Chidzikwe

A dissertation submitted to the Faculty of Engineering and the Built Environment

of the University of the Witwatersrand

in fulfilment of the academic requirements for the

MASTER OF SCIENCE DEGREE IN ELECTRICAL ENGINEERING

School of Electrical and Information Engineering

University of the Witwatersrand

Johannesburg

DECLARATION

I declare that this dissertation entitled "**Investigation into the impact of wind generation on inter-area and local oscillation modes of power systems**" is my own unaided work. Where secondary material has been used, it has been acknowledged and referenced according to the faculty requirements. It is submitted for a Master of Science degree in Electrical Engineering at the University of the Witwatersrand. It has not been submitted before for any degree or examination to any other university.

Signed on the _____day of _____2018

_____

Cliff Chidzikwe

ACKNOWLEDGEMENTS

I am proud to acknowledge all those who contributed to the success of the work contained in this dissertation with their inestimable contribution.

Firstly, I would like to thank God for availing me His unmerited favour. Secondly, I would like to acknowledge my academic supervisor Dr. J. M. Van Coller of the School of Electrical and Information Engineering, University of the Witwatersrand and my industrial supervisor Mr. T. Modisane of Eskom Holdings SOC, System Operations for their constant guidance and support throughout the duration of this work.

I would like to express my gratitude to:

- Eskom Power Plant Engineering Institute (EPPEI) for their financial support;
- My friends and loved ones for their support and encouragements;
- Lastly but not least, my family for their unfailing support and encouragement throughout the duration of my studies. I love you all!

UNIVERSITY OF THE WITWATERSRAND
JOHANNESBURG

We speak of electrical energy as current: it exists only while it runs away; we use it only by delaying its escape

-Wendell Berry, "The Use of Energy," The Unsettling of America, 1977

ABSTRACT

The operation and dynamic characteristics of power system grids with mixed generation technologies in particular synchronous generators and wind turbine generators are receiving great attention towards the better understanding of the modern power system stability. Wind power generation introduces new types of non-conventional generators that are being operated in parallel with conventional generation. However, as the penetration of wind energy increases, the power system dynamics and behaviour are modified. It is thus important to understand and quantify the impact of wind energy technologies on the performance of the interconnected power systems. The investigation in this dissertation focuses on the impact of wind power generation on the power system small-signal stability. The focus is on the variable-speed Type 4 Wind Turbine Generators (WTGs) and the Wind Power Plants (WPPs) impact on the inter-area and local oscillation modes of the power systems. An aggregated WPP model based on the generic IEC 61400-27-1 (2015) Type 4 WTG of varying capacities was used in this investigation together with a multi-machine small-scale power system comprising conventional synchronous generators and their associated controls. The Power System Stabilizer (PSS), an additional generator control, is widely used to resolve the power system small-signal stability problems by providing additional damping to the inter-area and local oscillation modes. This investigation considered the impact of wind power on the inter-area and local oscillation modes without and with PSSs installed on the synchronous generators. The procedure involved employing small-signal stability analysis through eigenvalue analysis and tracking the oscillation modes after the integration of wind power generation sources. The investigation has shown that the introduction of wind power in parallel with synchronous generators alter the generator operating conditions and the power flows causing the inter-area and local oscillation mode characteristics to change. As the wind power penetration increases, the inter-area and local mode frequencies decrease. The decrease in frequencies has been attributed to the change in the operating conditions of synchronous generators when operated in parallel with wind turbine generators. It was further found that wind power can have negative or positive impact on the damping of inter-area and local modes. However, for the particular case studies examined, this investigation suggests that PSSs already installed in the absences of wind power generation sources do not require retuning. The work recommends that power system small-signal stability requirements in the presence of wind power should be investigated as this is a unique characteristic for a given network.

UNIVERSITY OF THE WITWATERSRAND JOHANNESBURG

DEDICATION

I dedicate this dissertation to my parents (Mr. Ernest and Mrs. Marjory Chidzikwe) and my brothers (Tendai, Baldwin and Fortune) and my sisters (Constance and Sharon). I further dedicate this work to my sisters-in-law (Faith and Caroline) and my late grandfather Oliver Mwashita.

UNIVERSITY OF THE WITWATERSRAND
JOHANNESBURG

TABLE OF CONTENTS

Declaration i

Acknowledgements ii

Abstract iii

Dedication iv

List of Figures ix

List of Tables xii

Chapter 1 : Introduction 1

1.1. Background and Motivation 1

1.2. Power System Rotor Angle Stability 2

1.3. Research Questions 5

1.4. Methodology 6

1.5. Dissertation Outline 7

Chapter 2 : Theoretical Background 8

2.1. Small - Signal Stability Analysis 8

2.1.1. State-Space Representation 8

2.1.2 Linearization 9

2.1.3 Modal Analysis 11

2.1.4 Modal Matrices 15

2.1.5 Decoupling the State Equations 15

2.1.6 Transfer Function 17

2.1.7 Eigenvalue Sensitivity 19

2.1.8 Participation Factor 20

UNIVERSITY OF THE WITWATERSRAND JOHANNESBURG

2.2. Theory of the Power System Stabilizer (PSS) 20

2.3. Conventional Power System Stabilizer (PSS) design method 25

2.3.1 Phase-compensation design 27

2.3.2 Washout filter block selection 27

2.3.3 PSS gain 28

2.3.4 PSS output limiters 28

2.4. Power System Component Modelling 28

2.4.1 Synchronous Generator 28

2.4.2 Electrical Load 40

2.4.3 Transmission Lines 41

2.4.4 Power Transformers 42

2.4.5 Capacitors 44

2.5. Study System Configuration - Two-Area-Multi-Machine (TAMM) System 44

2.6. Summary 46

Chapter 3 : Type 4 Wind Turbine Generator (WTG) 47

3.1. An Introduction to Wind Turbine Generators (WTGs) 47

3.1.1 Fixed-Speed Wind Turbine Generators (WTG) 48

3.1.2 Variable-Speed Wind Turbine Generators (WTGs) 49

3.2. Wind Turbine Generator (WTG) Generic Models 51

3.3. IEC 61400-27-1 Type 4 Wind Turbine Generator (WTG) model 51

3.3.1 Aerodynamic Model 53

3.3.2 Mechanical Model 55

UNIVERSITY OF THE WITWATERSRAND JOHANNESBURG

3.3.3 Generator System 56
3.3.4 Grid Protection Model 57
3.3.5 Control Block Model 58
3.4. Aggregation of Wind Power Plants (WPPs) 67
3.5. Development of the Aggregated Wind Power Plant (WPP) Model 68
3.6. Summary 71
Chapter 4 : Power System Stabilizer (PSS) Design 73
4.1. Small-Signal Analysis of the Two-Area-Multi-Machine (TAMM) System 73
4.1.1 Synchronous generator operating with manual control 74
4.1.2 Synchronous generators operating with automatic excitation control 75
4.1.3 Time Domain Simulation 76
4.2. Selection of Power System Stabilizers (PSSs) Location 78
4.3. Determination of the generator phase-lag 79
4.4. IEEE Power System Stabilizer (PSS2B) Design 80
4.4.1 Washout Filter Time Constants 82
4.4.2 Torsional (or Ramp-Tracking) Filter 83
4.4.3 Phase Compensation and Gain Design 84
4.5. Power System Stabilizer (PSS) Performance Evaluation 88
4.1.1. Test Cases 89
4.1.2. Modal Analysis 90
4.1.3. Time Domain Performance Evaluation 95

UNIVERSITY OF THE WITWATERSRAND JOHANNESBURG

4.6. Summary 104

Chapter 5 : Wind Power Generation Impact on the Small-Signal Stability 105

5.1. Impact of Wind Generation on Inter-Area and Local Oscillation Modes without Power System Stabilizers (PSSs) 105

5.1.1. Wind Power Replacing Conventional Generation 107

5.1.2. Wind Power Supplying Increasing System Load 118

5.2. Impact of Wind Generation on Power System Stabilizers (PSSs) Tuned for Damping Inter-Area and Local Oscillation Modes 129

5.2.1. Wind power supplying increasing load with generators equipped with PSSs 130

5.3. Summary 138

Chapter 6 : Conclusion and Recommendation 142

References 143

Appendix A 147

Generator 01 – 04 Governor parameters 147

UNIVERSITY OF THE WITWATERSRAND JOHANNESBURG

LIST OF FIGURES

Figure 1.1: Worldwide trend in installed wind generation capacity from 2000 to 2010 1

Figure 1.2: Classification of power system stability [6] 3

Figure 1.3: Block diagram for a synchronous generator excitation system [7] 4

Figure 1.4: Basic PSS structure block diagram [3] 5

Figure 2.1: Single Machine Infinite Bus (SMIB) system 22

Figure 2.2: Linearized SMIB system 22

Figure 2.3: Eigenvalue movement/locus due to the presence of the PSS 26

Figure 2.4 : Cross sectional view of a three-phase salient-pole synchronous generator [3] 29

Figure 2.5: Synchronous generator stator and rotor circuits [3] 30

Figure 2.6: Synchronous generator open-circuit characteristic 38

Figure 2.7: π-model for medium length lines 42

Figure 2.8: Single phase equivalent circuit of a three-phase two winding transformer 43

Figure 2.9: Two-Area-Multi-Machine (TAMM) test system 45

Figure 2.10: Block diagram of the IEEE AC4 excitation system 46

Figure 3.1: Typical wind farm or Wind Power Plant [31] 47

Figure 3.2: Type 1 fixed-speed WTG configuration 49

Figure 3.3: Type 2 variable-speed WTG configuration 49

Figure 3.4: Type 3 variable-speed WTG configuration 50

Figure 3.5: Type 4 variable-speed WTG configuration 50

Figure 3.6: Interface between the WT model, grid model and WPP model 52

Figure 3.7: Modular structure of the IEC 61400-27-1, Type 4B (herein referred to as Type 4 WT) 53

Figure 3.8: Block diagram of a constant aerodynamic torque model 55

Figure 3.9: Block diagram for two-mass model [36] 55

Figure 3.10: WT fault-ride through characteristics 57

UNIVERSITY OF THE WITWATERSRAND JOHANNESBURG

Figure 3.11: Type 4 WT control block structure [36] 58
Figure 3.12: Block diagram implementation of the P control model 59
Figure 3.13: Block diagram implementation of the Q Control model 63
Figure 3.14: Block diagram implementation of the current limitation model 65
Figure 3.15: Block diagram implementation for QP and QU limitation model 66
Figure 3.16: Single-machine equivalent WPP model layout 67
Figure 3.17: Simulated WPP model in DIgSilent PowerFactory 69
Figure 3.18: WPP point of connection terminal voltage, active power and reactive power responses 70
Figure 3.19: WPP model eigenvalue plot 71
Figure 4.1: Two-Area-Multi-Machine (TAMM) test system 73
Figure 4.2: Inter-area power flow over transmission line 1 76
Figure 4.3: Inter-area power flow Fast Fourier Transform (FFT) 77
Figure 4.4: Rotor angle speed of the generators without the PSSs 78
Figure 4.5: Phase-lag between generator (Gen 03) electrical torque and excitation system reference voltage phase-lag 80
Figure 4.6: IEEE Type PSS2B-dual-input PSS structure 80
Figure 4.7: Frequency response of a single washout filter and double or cascaded single washout filters 82
Figure 4.8: Frequency response of typical torsional (or ramp tracking) filters 83
Figure 4.9: Phase compensation of the example designed phase-lead 85
Figure 4.10: System root loci with increasing PSS gain 86
Figure 4.11: System modes' frequency change with increasing PSS gains 87
Figure 4.12: Graphical presentation of the inter-area mode damping comparison 92
Figure 4.13: Graphical presentation of the area 1 local mode damping comparison 93
Figure 4.14: Graphical presentation of area 2 local oscillation mode damping comparison 94
Figure 4.15: Case 1 generator rotor angles response with reference to reference machine (Gen 03) without and with designed PSSs 97
Figure 4.16: Case 1 generator speeds response to the 3-phase fault with and without designed PSSs 98
Figure 4.17: Case 1 generators active powers response to the 3-phase fault without and with designed PSSs 99
Figure 4.18: Case 3 generator rotor angles response with reference to reference machine (Gen 03) without and with designed PSSs 101

UNIVERSITY OF THE WITWATERSRAND JOHANNESBURG

Figure 4.19: Case 3 generator speeds response to the 3-phase fault with and without designed PSSs 102

Figure 4.20: Case 3 generator speeds response to the 3-phase fault with and without designed PSSs 103

Figure 5.1: Eigenvalue plot of the TAMM system without WPP 106

Figure 5.2: Two-Area Multi-Machine (TAMM) system with generator 03 replaced with a Wind Power Plant (WPP) 108

Figure 5.3: Eigenvalue plot of the TAMM system with WPP 109

Figure 5.4: Comparison of the eigenvalues of the TAMM system without and with WPP (100 MW) 109

Figure 5.5: Two-Area Multi-Machine (TAMM) system with generator 02 replaced with a Wind Power Plant (WPP) (no PSSs) 112

Figure 5.6: Two-Area Multi-Machine (TAMM) system with generator 04 replaced with a Wind Power Plant (WPP) (no PSSs) 113

Figure 5.7: Local oscillation modes damping ratios with gradual increase in wind power without PSSs 116

Figure 5.8: Two-Area Multi-Machine (TAMM) system with Wind Power Plant (WPP) in area 1 supplying increasing load (Load 1) (no PSSs) 119

Figure 5.9: Two-Area Multi-Machine (TAMM) system with Wind Power Plant (WPP) in area 2 supplying increasing load in area 2 (no PSSs) 119

Figure 5.10: Inter-area and local oscillation modes' frequency variation with wind power supplying increasing area 1 load (no PSSs) 120

Figure 5.11: Inter-area and local modes damping ratios variation with wind power supplying increasing area 1 load (no PSSs) 121

Figure 5.12: Inter-area and local oscillation mode frequency variation with wind power supplying increasing area 2 load (no PSSs) 125

Figure 5.13: Local oscillation mode damping ratio variation with increasing wind power penetration (no PSSs) 125

Figure 5.14: Inter-area oscillation mode damping ratio variation with increasing wind power (with PSSs) 131

Figure 5.16: Inter-area oscillation mode frequency variation with wind power (with PSSs) 132

Figure 5.17: Wind power connected between the two interconnected areas 134

Figure 5.18: Local oscillation mode frequency change with increasing wind power (with PSSs) 136

Figure 5.19: Local oscillation mode damping ratio with increasing wind power (with PSSs) 137

Figure 5.20: Generator 01 rotor angle response with 100 – 300 MW wind power with reference to the reference machine response with increasing wind power with PSSs 140

Figure 5.21: Generator 01 rotor angle response with 400 – 700 MW wind power with reference to the reference machine response with increasing wind power with PSSs 140

Figure 5.22: Generator 02 rotor angle response with 100 – 300 MW wind power with reference to the reference machine response with increasing wind power with PSSs 141

Figure 5.23: Generator 02 rotor angle response with 400 – 700 MW wind power with reference to the reference machine response with increasing wind power with PSS 141

LIST OF TABLES

Table 2.1: Generator data 45

Table 2.2: IEEE AC4 excitation system parameters 46

Table 3.1: Parameters for the two-mass mechanical model 56

Table 3.2: Type 4 WT generator settings 57

Table 3.3: P control settings 59

Table 3.4: Q control mode and associated settings (M_{qG}) [37] 60

Table 3.5: Description of $FLVRT$ flag signal values 61

Table 3.6: Low-voltage ride through modes and associated settings (M_{qLVRT}) [36] 61

Table 3.7: WT Q-control model settings 62

Table 3.8: Current limiter settings 64

Table 3.9: WT voltage and maximum active and reactive current settings 64

Table 3.10: Q-limitation (or QP and QP limitation) model 66

Table 3.11: WT power dependency of reactive power 66

Table 3.12: WT voltage dependency of reactive power 67

Table 3.13: Sample of equivalent collector system parameters [12] 68

Table 4.1: Small-signal stability analysis with manual excitation control 74

Table 4.2: Mode shapes with manual excitation control 74

Table 4.3: Small-signal stability analysis with automatic excitation control on the generators 75

Table 4.4: Generator speed participation factors towards the inter-area mode 79

Table 4.5: System generator, excitation system and generators phase-lags 79

Table 4.6: Torsional (or ramp tracking) filter typical parameters 84

Table 4.7: Designed PSS2B settings 88

Table 4.8: Test cases operating conditions 89

Table 4.9: Test cases eigenvalue analysis results used for testing the designed PSSs settings 90

UNIVERSITY OF THE WITWATERSRAND JOHANNESBURG

Table 4.10: Inter-area oscillation mode damping comparison with the designed PSS settings 91

Table 4.11: Area 1 local mode damping comparison without and with designed PSSs 93

Table 4.12: Area 2 local mode damping comparison without and with designed PSSs 94

Table 5.1: Eigenvalue analysis results without wind power 106

Table 5.2: Inter-area oscillation mode with increasing wind power (no PSSs) 110

Table 5.3: Percentage change in inter-area mode frequency with reference to case without wind power 111

Table 5.4: Different load flows for the integration of WPPs of different capacity for the inter-area mode investigation 112

Table 5.5: Local oscillation mode with increasing wind power (no PSSs) (as generator Gen 02 in area 1 dispatch was gradually replaced with wind power) 114

Table 5.6: Inter-area active power flows for the integration of WPPs of different capacity for the area 1 local mode investigation 115

Table 5.7: Area 2 local oscillation mode with increasing wind power (no PSSs) (as generator Gen 04 in area 2 dispatch was gradually replaced with wind power) 115

Table 5.8: Local modes characteristic with increasing wind power compensating synchronous generator dispatch variation 117

Table 5.9: Different load flows for the integration of WPPs of different capacity for the area 2 local mode investigation 118

Table 5.10: Inter-area oscillation mode characteristic with wind power supplying increasing area 1 load (no PSSs) 122

Table 5.11: Local oscillation modes characteristic with wind power supplying increasing area 1 load 122

Table 5.12: Local modes change in frequency and damping ratio when wind power supplies increasing load in area 1 (no PSSs) 123

Table 5.13: Power flow changes when wind power supplies increasing system load in area 1 124

Table 5.14: Inter-area oscillation mode characteristic with wind power supplying increasing area 2 load (no PSSs) 126

Table 5.15: Local oscillation modes characteristic with wind power supplying increasing area 2 load (no PSSs) 128

Table 5.16: Local mode change in frequency and damping ratio when wind power supplies increasing load in area 2 (no PSS) 128

Table 5.17: Power flow changes when wind power supplies increasing system load in area 2 129

Table 5.18: TAMM system small-signal characteristic with PSS in service without wind generation 130

Table 5.19: Inter-area mode characteristics with increasing wind power supplying increasing system load (with PSSs) 131

Table 5.20: Percentage change in the tuned inter-area mode's damping ratio with increasing wind power (with PSSs) 133

Table 5.21: Power flows when wind power was integrated between the two interconnected areas 133

Table 5.22: Inter-area mode characteristic when load 2 is increased and compensated with wind power located in area 2 (with PSSs) 135

Table 5.23: Local mode characteristics with increasing wind power with PSSs (with PSSs) 136

Table 5.24: Local modes damping ratio changes with increasing wind power (with PSSs) 138

Table A.1: IEEE governor parameters 147

UNIVERSITY OF THE WITWATERSRAND JOHANNESBURG

CHAPTER 1 : INTRODUCTION

1.1. Background and Motivation

The current world's population is expected to double by 2040 with an increase of 25% in the energy demand – which will vary across different nations [1]. The 21st century has already witnessed this increasing demand for energy and the introduction of new generation technologies. Renewable energy resources such as wind energy have increased their penetration in the power system because of environmental concerns and the limited fossil-fuel reserves. The generation of electricity using wind energy is favoured because of its environmentally friendly and economic benefits compared to conventional generation technologies using fossil-fuels. Globally, the installed wind generation capacity increased exponentially from 17.4 GW in 2000 to 197 GW by the end of 2010 [2]. This trend is illustrated in Figure 1.1 below.

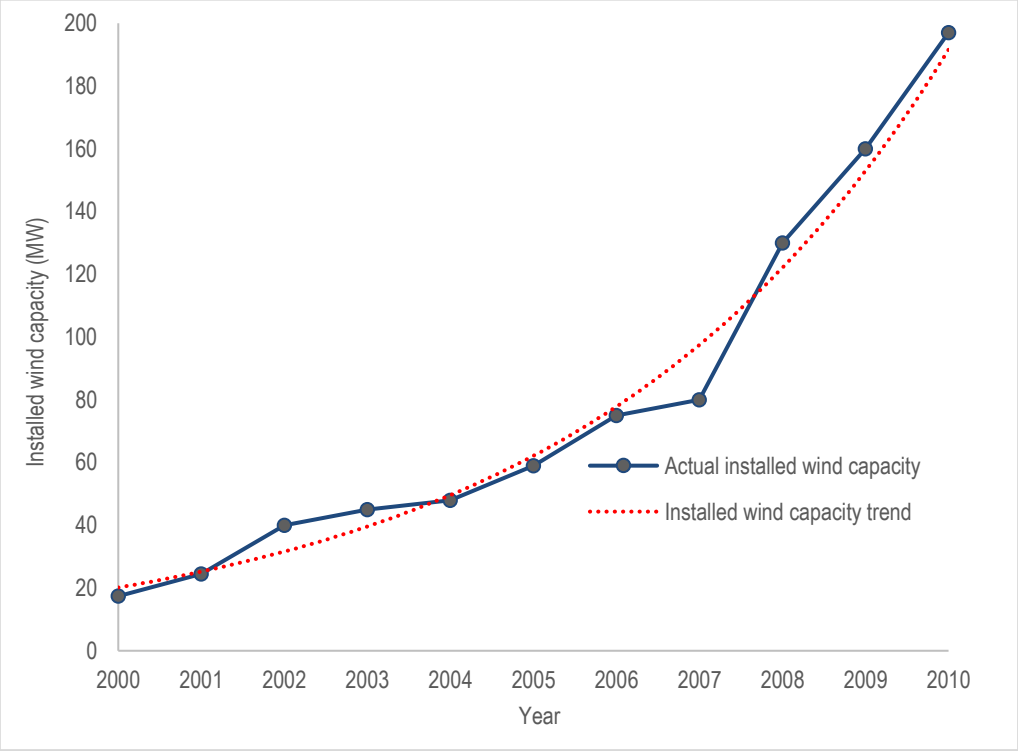

Figure 1.1: Worldwide trend in installed wind generation capacity from 2000 to 2010

Power systems are very complex structures characterised by transmission lines and conventional generation schemes (coal and hydro). The challenge associated with the power systems has been to ensure that they supply electricity in a stable and reliable way [3]. Renewable energy resources, such as wind energy, introduce new types of non-conventional generators in significant amounts into the power system

which are being operated in parallel with the conventional generation technologies or replacing the conventional synchronous generators. As the penetration of wind energy increases, the power system dynamics and behaviour are modified. This is strongly related to the wind energy penetration levels [4]. Initially, the Wind Turbine Generators (WTGs) used in old Wind Power Plants (WPPs) were of much lower ratings - typically 0.75 MW but now WTGs of larger ratings are being introduced that can significantly affect the network behaviour. Several countries around the world have the Grid Code requirements for Renewable Power Plants (RPPs) to be connected to the power system. For example, the South African Grid Code requirements [5] and others require RPPs to have the capabilities to positively contribute towards the stable operation of the power system. The focus of the current Grid Code requirements has been on power quality, voltage and frequency stability. As the penetration of wind energy increases, this modifies the overall system dynamics. The investigation in this dissertation focuses on the power system small-signal stability with high penetration of wind power.

Power system stability is defined as the "*the ability of an electric power system, for a given initial operating condition, to regain a state of operating equilibrium after being subjected to a physical disturbance, with most system variables bounded so that practically the entire system remains intact"* [6]. The power system stability is largely influenced by the dynamics of conventional synchronous generators which form the principal source of electric energy. As such, the evaluation of the power system stability is primarily concerned with the behaviour of the interconnected synchronous generators. A stable power system should be able to remain intact with all the synchronous generators returning to their original or new stable operating point while an unstable power system results in new operating conditions and subsequent variations in the power transfers, synchronous generator rotor speeds, voltages and frequencies. To this end, the understanding of power system stability is facilitated by the classification of stability into rotor-angle stability, voltage stability and frequency stability as illustrated in Figure 1.2. Although the focus of this research is on the power system rotor-angle stability which is further described in the following section, voltage stability and frequency stability are equally important. Voltage stability is the ability of the power system to maintain steady voltages at all buses in the system after being subjected to a disturbance from a given initial operating condition whereas frequency stability focuses on the ability of the power system to maintain steady frequency following a severe system upset resulting in a significant imbalance between generation and load. These two forms of power system stability are described in detail in reference [6].

1.2. Power System Rotor Angle Stability

Rotor angle stability is the ability of interconnected synchronous machines of a power system to remain in synchronism [3] [7]. Rotor angle instability may result from an imbalance between the generator input mechanical torque and output electromechanical torque which causes the rotors of generators to either accelerate or decelerate. The resulting change of the electromechanical torque of the generators following disturbances is composed of the synchronising torque in phase with the generator rotor angle deviation and the damping torque in phase with the generator speed deviation. The synchronous operation of interconnected generators and power system stability is dependent on the existence of both components of the torque for each of the synchronous machines [3]. Lack of sufficient synchronizing torque results in

non-oscillatory instability characterized with aperiodic drift in the generator rotor angles while the lack of sufficient damping torque results in oscillatory instability.

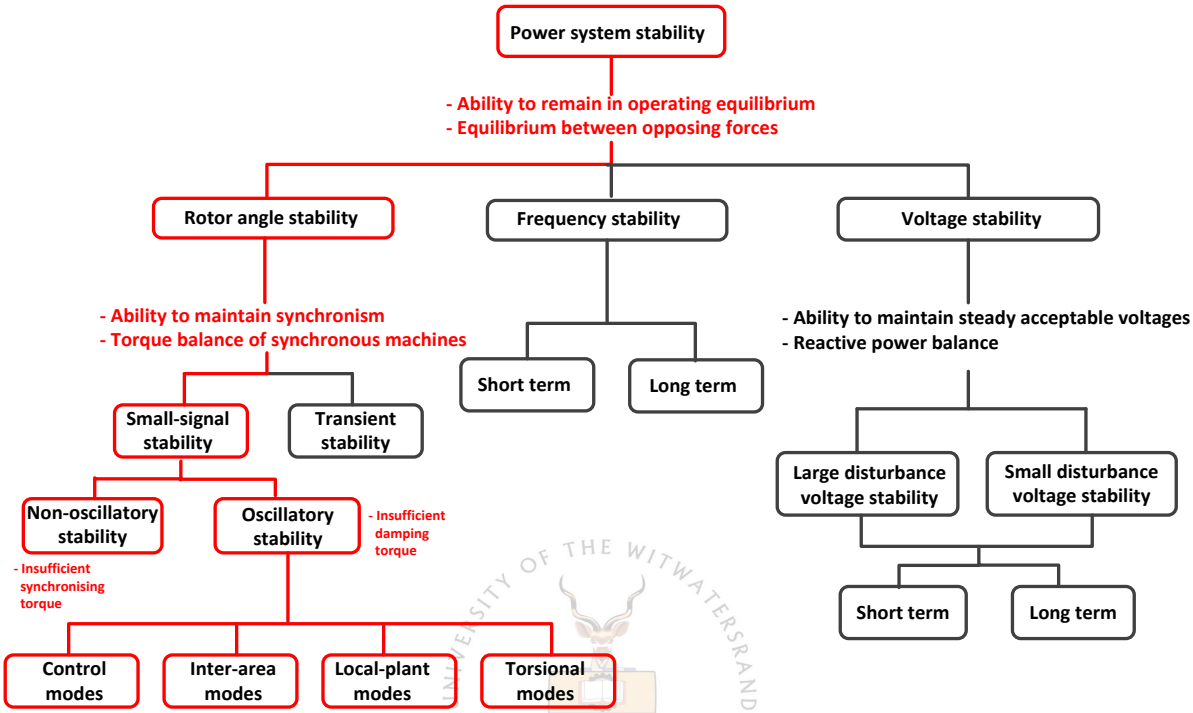

Figure 1.2: Classification of power system stability [6]

Rotor angle stability is classified into small-signal stability, which is the focus of this investigation, and transient stability. Small-signal stability is the ability of the power system to maintain synchronism under small disturbances [3]. The small disturbances continually take place and are in the form of small variations in load and generation. Small-signal instability can be in the form of a steady increase in the generator rotor angles due to insufficient synchronising torque or rotor oscillations of increasing amplitude due to insufficient damping torque. The power system response to small disturbances is dependent on several factors which include initial operating condition, transmission system strength and type of synchronous generator excitation control system [3]. In today's practical power systems, small-signal instability is largely a problem of insufficient damping of oscillations. The small-signal stability problem is concerned with the synchronous generator rotor angle electromechanical oscillations at frequencies ranging from 0.2 Hz to 3 Hz [8]. The oscillations are distinguished into local modes and inter-area modes. Local modes are associated with the swinging of units at a generating station at frequencies ranging from 0.8 Hz to 3 Hz while inter-area oscillation modes involve small groups of closely interconnected synchronous generators oscillating relative to each other. The frequencies of the inter-area modes are lower than those of the local modes and range from 0.25 Hz to 0.8 Hz [8]. The lack of damping torque results in the rotor oscillations increasing in amplitude which can lead to loss of synchronism.

Transient stability, which is the other type of rotor angle stability, is defined as the ability of the power system to maintain synchronism when subjected to a severe transient disturbance [3]. The use of automatic control devices, such as Automatic Voltage Regulators (AVRs) and high-response exciters, required to maintain transient stability, adversely affects the power system damping torque [3] [7]. This is worsened by decreasing the transmission system strength relative to the size of the generation stations. The small-signal instability problem related to inter-area modes is worsened by weak links transferring large power. For the purposes of studying the oscillations, models used for local modes consist of a single machine connected to the power system represented as an infinite bus using the Thevenin equivalent impedance at the machine terminals. For studying inter-area modes, the impedance linking the generators in different areas need to be modelled.

The Power System Stabilizer (PSS) is widely used to resolve the power system small-signal stability problem. The PSS is a supplementary control device installed as an element of the synchronous generator excitation control system to modulate the excitation voltage in order to provide additional damping torque [7]. To achieve this, PSSs use auxiliary stabilizing signals (usually the generator shaft speed, terminal frequency, and electrical power) to produce a component of the electrical torque in phase with the rotor speed deviations through the AVR. The combination of the AVR and PSS can meet the conflicting exciter performance needed for the system transient stability while at the same time providing additional damping to the generator rotor oscillations. Figure 1.3 shows a block diagram showing the various excitation control subsystems including the PSS.

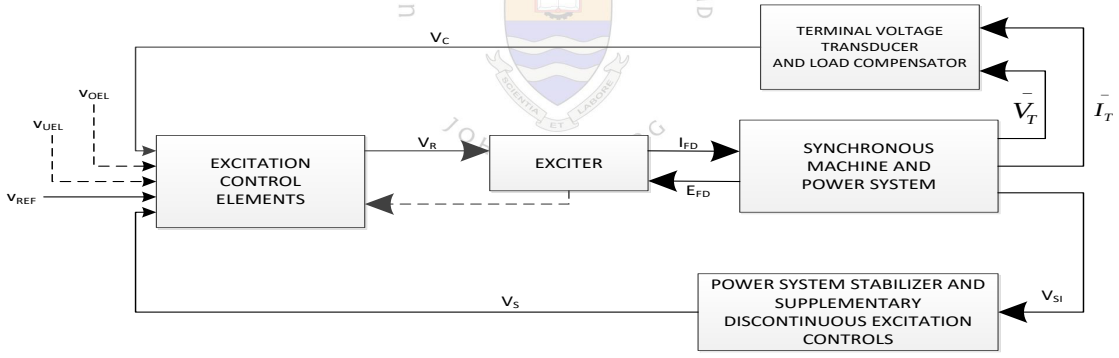

Figure 1.3: Block diagram for a synchronous generator excitation system [9]

Figure 1.4 shows a block diagram implementation of the single input PSS which consists of distinct stages (a signal washout filter block, a phase compensation block, a gain block, and a limiter block) with specific functions to collectively provide damping of the generator rotor oscillations. The function of each block and its design are described in Chapter 2. In practice, power systems are designed to operate above some defined minimum damping requirements for all possible operating conditions. The design and selection of the PSS settings to meet the power system small-signal stability requirements without compromising other categories of stability is a complex task.

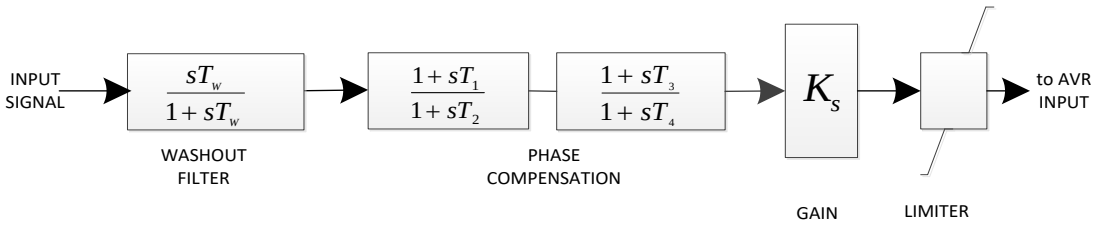

Figure 1.4: Basic PSS structure block diagram [3]

The impact of substantial amounts of wind power on the interconnected power system small-signal stability, among other aspects, is not considered in the currently used Grid Codes and standard planning practices. The aspect of small-signal stability is equally important because it involves inter-area and local oscillation modes of power systems and designed PSSs of the synchronous generators that would have been previously tuned in the absence of wind power plants. Several studies in the literature have been conducted on the investigation of the impact of wind generation on the inter-area and local modes but this was mainly on the fixed-speed WTGs and the Type 3 variable-speed WTGs [4] and concluded that wind power generation does not introduce new electromechanical oscillation modes because the wind power generators are decoupled from the power system grid by the power converters [10]. However, this did not cover the impact of wind power generation on the power system damping. The impact of WPPs comprising newer Type 4 variable-speed WTGs on the inter-area and local modes has received less attention and has not been investigated. In addition, the extent to which wind power generation impacts on the power system damping in the presence of PSSs has not been addressed in the literature. The contribution of this work is that it investigates Type 4 variable-speed WTGs on their impact on the power system small-signal inter-area modes and local modes and specified the power system damping. To put into context, a recent study done in South Africa [11] focused on the improvement of an inter-area mode damping between the South-Western Cape and North-Eastern Mpumalanga areas which was resolved by retuning the Koeberg PSSs. However, further north, approximately 200 km from Koeberg power station is the 100 MW Sere Wind Farm using Type 4 variable-speed WTGs. This proximity triggered an investigation into how the inclusion of significant amounts of wind power impact on the power system small-signal stability. Therefore, this dissertation presents a theoretical investigation into the impact of the wind power generation from Type 4 variable-speed WTGs on the power system small-signal stability.

1.3. Research Questions

The main research question to be answered from this dissertation is *What is the impact of wind power on the power system small-signal oscillation damping*?

The following two sub-questions were outlined to address the main question:

- To what extent can PSSs provide damping to both inter-area and local oscillation modes?
- What are the impacts of Type 4 variable-speed WTGs on PSSs tuned for damping inter-area and local oscillation modes?

The research objective aimed at investigating the impact of wind power on power system small-signal stability to determine its impact on the PSS settings.

1.4. Methodology

To achieve the above objective, detailed simulations were performed using a commercially-available power system software programme, DIgSilent PowerFactory. A well-known small-scale study power system, the Two-Area Multi-Machine (TAMM) system from [3] was adopted since the data was readily available. The approach used firstly illustrated the effects of synchronous generator controls on the power system small-signal stability with the goal of determining the requirements of PSSs. A modern dual-input PSS structure was adopted. The settings of PSSs were determined using conventional root-locus methods to achieve damping ratios above the defined minimum acceptable criteria [7]. After the PSS settings selection, the small-signal stability margins of the system were determined to verify the PSSs setting performance under different operating conditions. Non-linear time-domain techniques were also used to confirm the small-signal stability results.

The inherent difference between conventional synchronous generators and WPPs can be reflected in the approach and suite of studies for analysing the impact of WPPs on the power system dynamics. The impact of wind power on power systems require representation of WPPs by aggregating all WTGs into a single WTG connected to a lumped pad-mount transformer and the equivalent WPP cable system [12]. The transformers feeding into the power system grid and the WPP reactive power compensation are explicitly represented. The equivalent aggregated WPP capacity is equal to the number of generators times the individual generator MVA rating. The lumped transformer rating is determined by the product of the single transformer rating and the number of transformers used. Aggregated data of realistic WPPs (WPPs size and collector system) in [12] was adopted and used to develop a 100 MW WPP using the IEC 61400-27-1 (2015) Type 4 WTG model rated at 2 MVA with unity power factor. Different WPP capacities were then realized by increasing the number of the parallel machines, pad-mount transformers, and the equivalent collector WPP cable system and the station transformers. The IEC 61400-27-1 (2015) Type 4 WTG model, developed by various WTG manufacturers to reproduce the behaviour of their wind turbines suitable for power system stability studies, was used to develop the WPP using DIgSilent PowerFactory. In DIgSilent PowerFactory, IEC 61400-27-1 (2015) Type 4 variable-speed WTG model is implemented as a template with default generic settings covering a wide range of Type 4 variable-speed WTGs on the market [13]. Due to the unavailability of the Original Equipment Manufacturer (OEM) data during this investigation, these generic settings were adopted. A similar approach was used in [14] since the default parameters emulate a realistic WTG model. In practice, the WPP reactive power compensation is required at the WPP level but in this dissertation, this is not considered since focus is only on active power.

The WPPs were to be integrated at various locations of the test power system to identify the potential impacts of wind generation on inter-area and local modes of power systems. The first approach used in this investigation involved integrating WPP and reducing an equivalent amount of the conventional generation dispatch to balance the load demand. For this approach, it was deemed convenient to choose a conventional generator with reduced dispatch balanced by increased dispatch from a WPP and carefully observing the power system small-signal stability characteristics. The other approach involved gradual increment of the system load and integrating wind power to supply the load increase. This approach had practical reasoning that the conventional generation could not be curtailed. Load flow analysis is essential for the integration of new generation capacity into the power system [2]. The objective in load flow analysis is to determine the power system components' loading, transmission line power flows and the system voltages. Hence, load flow analysis was firstly conducted to establish the steady-state system requirements with each wind power integration scenario prior to power system small-signal stability analysis.

1.5. Dissertation Outline

Chapter 1 is the introduction consisting of the background and motivation, the research questions and objective, and the used methodology.

Chapter 2 presents the theoretical basis of small-small signal stability analysis of power systems, the concept of the PSS including the distinct types of PSS and the conventional control design approaches used in this dissertation. The chapter reviews the modelling of components relevant to this investigation before presenting the test system to be used for this study.

Chapter 3 focuses on the development of an aggregated WPP, based on the IEC 6400-27-1 Type 4 variable-speed WTG model in DIgSilent PowerFactory. The WPP model is used to derive WPPs of different capacities whilst investigating the impact of wind generation on the inter-area and local modes of power systems.

Chapter 4 presents the application of small-signal stability analysis to the test system considering two generator control strategies viz manual excitation control and closed loop, high gain excitation system control (i.e. automatic excitation control) with the intension to designing PSSs.

Chapter 5 presents the impact of wind power generation on the inter-area and local modes of power systems. The first part of the chapter focuses on the impact of wind power generation on the inter-area and local modes without PSSs installed on the synchronous generators while the final part considered the synchronous generators equipped with PSSs providing additional damping to the oscillation modes.

Chapter 6 provides the conclusion and recommendation based on the work contained in this dissertation.

CHAPTER 2 : THEORETICAL BACKGROUND

This chapter presents the theory related to research topic which include the theory of small-signal stability, the concept of the PSS including the distinct types of PSS with their practical advantages and disadvantages. The design of the PSS is a complex task which must ensure that the PSS provides damping over a wide range of operating conditions. Various modern design methods such as the adaptive control [15], H∞ optimal control [16] and variable structure control [17] have been researched in designing PSSs. These methods have been shown to produce better results; however, their application in practical systems is limited due to the lack of confidence in the methods. Instead, the conventional control design approaches (lead-lag and root locus) are preferred by utilities as these approaches have been successfully applied for many years. Thus, the conventional control method approach was adopted in this investigation and this chapter presents its application in the design of PSSs. The chapter also presents the modelling of electrical components relevant to this investigation.

2.1. Small - Signal Stability Analysis

Small-signal stability, as defined in the previous chapter, is the ability of the power system to maintain synchronism when subjected to small disturbances. The disturbances involved are considered small if the power system equations that describe the resulting response can be linearized about an operating point [3]. This section provides the power system small-signal stability analysis using the linear technique to obtain information about the dynamic characteristics of the power system.

UNIVERSITY OF THE WITWATERSRAND JOHANNESBURG

2.1.1. State-Space Representation

The state-space representation is used to represent the behaviour of a dynamic system, such as that of a power system, using a set of *n* first order non-linear ordinary differential equations of the form given in Eq. (2.1)

$$\dot{x}_i = f_i(x_1, x_2, \cdots, x_n; u_1, u_2, \cdots, u_r; t); i = 1,2, \dots, n \tag{2.1}$$

-where *n* is the order of the system and *r* is the number of the inputs that can be written in vector-matrix notation:

$$\dot{\mathbf{x}} = \mathbf{f}(\mathbf{x}, \mathbf{u}, \mathbf{t}) \tag{2.2}$$

-where

$$\mathbf{x} = \begin{bmatrix} x_1 \\ x_2 \\ \vdots \\ x_n \end{bmatrix} \qquad \mathbf{u} = \begin{bmatrix} u_1 \\ u_2 \\ \vdots \\ u_r \end{bmatrix} \qquad \mathbf{f} = \begin{bmatrix} f_1 \\ f_2 \\ \vdots \\ f_n \end{bmatrix}$$

The column vector $\mathbf{x}$ is the state vector and its elements x_i are state variables. The column vector $\mathbf{u}$ is the vector of inputs to the system that influence the performance of the system. The column vector $\mathbf{f}$ is a vector of non-linear function of the state and input variables. Time is represented by *t*, and the derivative of a state variable $\boldsymbol{x}$ with respect to time is denoted by $\dot{\boldsymbol{x}}$. The state variables are defined as the minimal set of variables that, along with the inputs to the system, provide a complete description of the system behaviour [3]. For power systems, the state variables may be the synchronous generator physical quantities such as rotor angles, speed deviation or voltage. If the derivatives of state variables are not explicit functions of time, the system is called an autonomous system, where in this case Eq. (2.2) simplifies to:

$$\dot{\mathbf{x}} = \mathbf{f}(\mathbf{x}, \mathbf{u}) \tag{2.3}$$

The output variables which can be observed on the system in terms of the state variables and the input variables can be written in the form:

$$\mathbf{y} = \mathbf{g}(\mathbf{x}, \mathbf{u}) \tag{2.4}$$

-where: $\mathbf{y} = \begin{bmatrix} y_1 \\ y_2 \\ \vdots \\ y_m \end{bmatrix}$ $\mathbf{g} = \begin{bmatrix} g_1 \\ g_2 \\ \vdots \\ g_m \end{bmatrix}$

$\mathbf{y}$ is the vector of output variables;

$\mathbf{g}$ is a vector of non-linear functions relating the state and input variables to output variables;

2.1.2 Linearization

The procedure for linearizing Eq. (2.3) involves selecting an operating point where $\mathbf{x_0}$ is the initial state vector and $\mathbf{u_0}$ is the initial input vector corresponding to the equilibrium point at which the small-signal performance is being investigated. At this selected operating point, we have,

$$\dot{\mathbf{x_0}} = \mathbf{f}(\mathbf{x_0}, \mathbf{u_0}) = 0 \tag{2.5}$$

When the system is perturbed by small disturbances from the above state, the system state and input variables change to:

$$\mathbf{x} = \mathbf{x_0} + \Delta\mathbf{x} \qquad\qquad \mathbf{u} = \mathbf{u_0} + \Delta\mathbf{u}$$

-where the prefix Δ denotes a small deviation or change from the initial selected point. The new state must satisfy Eq. (2.3) as follows:

$$\dot{\mathbf{x}} = \dot{\mathbf{x_0}} + \Delta\dot{\mathbf{x}} = \mathbf{f}\left[(\mathbf{x_0} + \Delta\mathbf{x}), (\mathbf{u_0} + \Delta\mathbf{u})\right] \tag{2.6}$$

Since the perturbations are considered to be small, the non-linear system equations $\mathbf{f}(\mathbf{x}, \mathbf{u})$ can be expressed in Taylor's series expansion where the expansion's first terms are considered only and the second and higher order powers of Δx and Δu are neglected [3]. We can write Eq. (2.3) and Eq. (2.4) as:

$$\begin{aligned} \dot{x}_i &= \dot{x}_{io} + \Delta\dot{x}_\iota = f_i\left[(\mathbf{x_0} + \Delta\mathbf{x}), (\mathbf{u_0} + \Delta\mathbf{u})\right] \\ &= f_i\left(\mathbf{x_0}, \mathbf{u_0}\right) + \frac{\partial f_i}{\partial x_1}\Delta x_1 + \cdots + \frac{\partial f_i}{\partial x_n}\Delta x_n + \frac{\partial f_i}{\partial u_1}\Delta u_1 + \cdots + \frac{\partial f_i}{\partial x_r}\Delta u_r \end{aligned} \tag{2.7}$$

Since $\dot{\boldsymbol{x}}_{\boldsymbol{io}} = f_i\left(\mathbf{x_0}, \mathbf{u_0}\right)$ Eq.(2.7) simplifies to Eq.(2.8) where $i = 1, 2, \cdots n$

$$\Delta\dot{x}_\iota = \frac{\partial f_i}{\partial x_1}\Delta x_1 + \cdots + \frac{\partial f_i}{\partial x_n}\Delta x_n + \frac{\partial f_i}{\partial u_1}\Delta u_1 + \cdots + \frac{\partial f_i}{\partial x_r}\Delta u_r \tag{2.8}$$

Then Eq. (2.4) simplifies to Eq. (2.9) where $j = 1, 2, \cdots m$

$$\Delta y_j = \frac{\partial g_j}{\partial x_1}\Delta x_1 + \cdots + \frac{\partial g_j}{\partial x_n}\Delta x_n + \frac{\partial g_j}{\partial u_1}\Delta u_1 + \cdots + \frac{\partial g_j}{\partial x_r}\Delta u_r \tag{2.9}$$

The resulting linearized forms of Eq. (2.3) and (2.4) around the operating point $\mathbf{x_0}$ and $\mathbf{u_0}$ are given by:

$$\Delta\dot{\mathbf{x}} = \mathbf{A}\,\Delta\mathbf{x} + \mathbf{B}\,\Delta\mathbf{u} \tag{2.10}$$

$$\Delta\mathbf{y} = \mathbf{C}\,\Delta\mathbf{x} + \mathbf{D}\,\Delta\mathbf{u} \tag{2.11}$$

-where $\mathbf{A} = \begin{bmatrix} \frac{\partial f_1}{\partial x_1} & \cdots & \frac{\partial f_1}{\partial x_n} \\ \vdots & \ddots & \vdots \\ \frac{\partial f_n}{\partial x_1} & \cdots & \frac{\partial f_n}{\partial x_n} \end{bmatrix}$ $\mathbf{B} = \begin{bmatrix} \frac{\partial f_1}{\partial u_1} & \cdots & \frac{\partial f_1}{\partial u_r} \\ \vdots & \ddots & \vdots \\ \frac{\partial f_n}{\partial u_1} & \cdots & \frac{\partial f_n}{\partial u_r} \end{bmatrix}$

$\mathbf{C} = \begin{bmatrix} \frac{\partial g_1}{\partial x_1} & \cdots & \frac{\partial g_1}{\partial x_n} \\ \vdots & \ddots & \vdots \\ \frac{\partial g_m}{\partial x_1} & \cdots & \frac{\partial g_m}{\partial x_n} \end{bmatrix}$ $\mathbf{D} = \begin{bmatrix} \frac{\partial g_1}{\partial u_1} & \cdots & \frac{\partial g_1}{\partial u_r} \\ \vdots & \ddots & \vdots \\ \frac{\partial g_m}{\partial u_1} & \cdots & \frac{\partial g_m}{\partial u_r} \end{bmatrix}$

UNIVERSITY OF THE WITWATERSRAND JOHANNESBURG

$\Delta\mathbf{x}$ is the linearized state vector of dimension *n*

$\Delta\mathbf{y}$ is the linearized output vector of dimension *m*

$\Delta\mathbf{u}$ is the linearized input vector of dimension *r*

$\mathbf{A}$ is the state matrix, size (*n x n*)

$\mathbf{B}$ is the input matrix, size (*n x r*)

$\mathbf{C}$ is the output matrix, size (*m x n*)

$\mathbf{D}$ is the feed forward matrix, size (*m x r*)

2.1.3 Modal Analysis

Once the state space model has been established, useful information pertaining to the power system stability can be extracted. The state space model allows the determination of the system eigenvalues, eigenvector properties and participation factors.

Eigenvalues

The eigenvalues are the scalar parameters λ for which there exist non-trivial solutions of matrix **A,** obtained by solving the following equation

$$\mathbf{A\Phi} = \lambda\mathbf{\Phi} \tag{2.12}$$

-where **A** is an *n x n* state matrix and $\mathbf{\Phi}$ is an *n x 1* vector. The eigenvalues are found by solving Eq.(2.13) (i.e. Eq.(2.12) rearranged), which is called the characteristics equation where $\mathbf{I}$ is an identity matrix

$$\det(\mathbf{A} - \lambda\mathbf{I}) = 0 \tag{2.13}$$

The ***n*** solutions of the characteristic equation $\lambda = \lambda_1, \lambda_2, \ldots, \lambda_n$ are the eigenvalues of the *n x n* state matrix $\mathbf{A}$. These eigenvalues can be real or complex. If the state matrix $\mathbf{A}$ is real, the complex eigenvalues occur in conjugate pairs of the form given by (2.14):

$$\lambda_i = \sigma \pm j\omega \tag{2.14}$$

-where σ and ω are the real and imaginary components of the eigenvalue respectively.

The eigenvalues contain useful information pertaining to the power system stability and each of the eigenvalues is associated with a mode of oscillation. The stability of the linearized power system at an operating point (x_0, u_0) can be visualized on the complex plane through the eigenvalues. A system is said to be stable at an operating point if all the eigenvalues of the system are in the left-half of the complex plane and unstable otherwise. A real positive eigenvalue corresponds to an increasing non-oscillatory mode whereas a negative real eigenvalue corresponds to a decaying non-oscillatory mode [3]. The larger the magnitude of the eigenvalue real component, the faster the rate of decay. For complex conjugate pairs, each oscillation mode corresponds to an oscillatory mode whereby the real component gives the damping of the oscillation and it determines if the mode is oscillatory stable or unstable while the imaginary component gives the frequency of oscillation. Thus, for a complex eigenvalue, the frequency of oscillation in Hertz is given by Eq.(2.15).

$$f = \frac{\omega}{2\pi} \tag{2.15}$$

Generally, the frequency determined using Eq. (2.15) falls into different frequency ranges for inter-area and local modes as described in Chapter 1. However, the mode shape, explained later, is used to definitively determine the nature of an oscillatory mode and to identify the generators oscillating against each other. The damping ratio of an oscillation mode quantifies how much an oscillation mode is damped. The damping ratio is given by Eq.(2.16).

$$\zeta = \frac{-\sigma}{\sqrt{\sigma^2 + \omega^2}} \tag{2.16}$$

-where σ is the real component of the eigenvalue and ω is the imaginary component of the eigenvalue.

The damping ratio of an oscillation mode is usually expressed as a percentage (i.e. ζ×100%). Power systems are designed to operate with minimum damping ratios of 5% under all possible operating conditions [7]. An oscillation mode damping ratio determines the rate of decay of the oscillation amplitude. From Eq.(2.16), a positive real component of the eigenvalue implies a negative damping ratio while a negative real component of the eigenvalue implies a positive damping ratio.

UNIVERSITY OF THE WITWATERSRAND JOHANNESBURG

Eigenvectors

More information other than the frequency and damping of the oscillations relating to the nature of the oscillations can be determined from the right and left eigenvectors. Using the right and left eigenvectors, the way in which each oscillation mode contributes to a state may be determined. For any eigenvalue λ_i, the *n x 1*-column vector $\boldsymbol{\Phi_i}$ which satisfies Eq. (2.17) is called the right eigenvector of the state matrix $\mathbf{A}$ associated with the eigenvalue λ_i, where $i = 1, 2, \cdots, n$

$$\mathbf{A}\boldsymbol{\Phi_i} = \lambda_i \boldsymbol{\Phi_i} \tag{2.17}$$

The right eigenvector $\boldsymbol{\Phi_i}$ is a column vector with length equal to the number of state variables and is of the form:

$$\Phi_i = \begin{bmatrix} \Phi_{1i} \\ \Phi_{2i} \\ \vdots \\ \Phi_{ni} \end{bmatrix}$$

The right eigenvector gives the relative activity of the state variables in a dynamic mode [3]. This is also referred to as the mode shape. In this dissertation, ***REV*** is used for reporting the right eigenvectors. Eigenvectors are not unique and remain valid eigenvalues when multplied by any scalar qauntity [7]. Similarly, the *1 x n*-row vector $\boldsymbol{\Psi_i}$ satisfing Eq.(2.18) is called the left eigenvector associated with eigenvalue λ_i

$$\boldsymbol{\Psi_i A} = \lambda_i \boldsymbol{\Psi}_i \tag{2.18}$$

-where $i = 1, 2, \cdots, n$.

The elements of the left eigenvector measure the contribution of the activity of a state variable in a mode. The left and right eigenvalues corresponding to different eigenvalues are orthogonal [3]. i.e., if λ_i is not equal to λ_j

UNIVERSITY OF THE WITWATERSRAND JOHANNESBURG

$$\boldsymbol{\Psi_j \Phi_i} = 0 \tag{2.19}$$

However, in the case of eigenvalues corresponding to the same eigenvalue,

$$\boldsymbol{\Psi_i \Phi_i} = \mathrm{C_i} \tag{2.20}$$

The ratio between left and right eigenvector elements is unique, and it is common practice to normalize by an arbitrary constant [3]. This is normally chosen such that the normalized vectors satisfy Eq.(2.21):

$$\boldsymbol{\Psi_i \Phi_i} = 1 \tag{2.21}$$

This orthogonality property allows the state vector to be expanded as a series combination of the system modes.

2.1.4 Modal Matrices

To express the eigenproperties of state matrix $\mathbf{A}$ the following modal matrices are introduced [3].

$$\mathbf{\Phi} = [\mathbf{\Phi_1}\ \mathbf{\Phi_2}\ \cdots\ \mathbf{\Phi_n}] \tag{2.22}$$

$$\mathbf{\Psi} = \left[\mathbf{\Psi_1}^T\ \mathbf{\Psi_2}^T \cdots\ \mathbf{\Psi_n}^T\right]^T \tag{2.23}$$

$$\mathbf{\Lambda} = \text{diagonal matrix, with the eigenvalues } \lambda_1,\ \lambda_2, \ldots,\ \lambda_n \tag{2.24}$$

In terms of these modal matrices Eq.(2.17) and Eq.(2.21) can be re-written as Eq.(2.25) and Eq.(2.26) respectively after matrix manipulation and simplifications where $\mathbf{\Lambda}$ is a diagonal matrix of eigenvalues.

UNIVERSITY OF THE WITWATERSRAND JOHANNESBURG

$$\mathbf{A\Phi} = \mathbf{\Phi\Lambda} \tag{2.25}$$

$$\mathbf{\Psi\Phi} = \mathbf{I} \tag{2.26}$$

Then Eq. (2.25) can be further re-written as given by Eq. (2.27),

$$\mathbf{\Phi}^{-1}\mathbf{A\Phi} = \mathbf{\Lambda} \tag{2.27}$$

2.1.5 Decoupling the State Equations

The response of the state variables in the state equations Eq. (2.11) when the system responds to a set of initial conditions with zero input derived from physical considerations is often not the best means of analytical studies of motion as it results in cross-coupling between state variables. The problem is that the rate of change of each state variable is a linear combination of all the state variables [3]. As a result of the coupling between state variables, it is difficult to isolate parameters that significantly influence the system behaviour. In order to eliminate the coupling between the state variables, a new state vector **z** is considered which is related to the original state vector by the transformation:

$$\Delta \mathbf{x} = \mathbf{\Phi z} \tag{2.28}$$

-where $\mathbf{\Phi}$ is the modal matrix defined by Eq.(2.22).

Due to the orthogonal property of the right and left eigenvectors the system state space representation in terms of the transformed variable vector **z**, is given as:

$$\begin{aligned} \mathbf{\Phi \dot{z}} &= \mathbf{A\ \Phi\ z + B\ \Delta u} \\ \Delta \mathbf{y} &= \mathbf{C\ \Phi\ z + D\ \Delta u} \end{aligned} \tag{2.29}$$

The resulting decoupled state space representation of the power system equations is then given as:

UNIVERSITY OF THE WITWATERSRAND JOHANNESBURG

$$\dot{\mathbf{z}} = \mathbf{\Lambda\ z + B'\Delta u} \tag{2.30}$$

$$\Delta \mathbf{y} = \mathbf{C'z + D\ \Delta u} \tag{2.31}$$

-where

$$\mathbf{B'} = \mathbf{\Phi^{-1}B} \tag{2.32}$$

$$\mathbf{C'} = \mathbf{C\Phi} \tag{2.33}$$

Referring to Eq. (2.30), if any row of the matrix $\mathbf{B'}$is zero the respective input has no effect on the corresponding mode and the mode is uncontrollable. The matrix $\mathbf{C'}$ in Eq. (2.31) determines if the variable z_i contributes to the formation of the outputs and hence if any column of the matrix is zero, then the corresponding mode is unobservable. Thus, *n x r* matrix $\mathbf{B'} = \mathbf{\Phi^{-1}B}$ is called the mode controllability matrix and the *m x n* matrix $\mathbf{C'} = \mathbf{C\Phi}$ is called the mode observability matrix. By inspection of matrices $\mathbf{B'}$and $\mathbf{C'}$ the oscillation modes can be classified into either controllable and observable; controllable and unobservable; uncontrollable and observable; and uncontrollable and unobservable. To contextualize this, in South Africa the trend is to tune PSSs to provide damping to local modes only, yet the network

also experiences inter-area modes [11]. Based on the above theory, it can be argued that the inter-area modes could be observable but uncontrollable which further makes tuning PSSs for the inter-area modes difficult.

2.1.6 Transfer Function

The state space representation can describe both the complete internal behaviour and the input-output properties of the system. The transfer function representation specifies only the input to output behaviour which allows arbitrary selection of the system state variables. On the other hand, state space representation is a complete description of the system which allows the transfer function to be uniquely defined [3]. For small-signal stability analysis of power systems, the eigenvalue analysis of the state matrix described in the previous section suffices; however, for controller design the open loop transfer function between specific variables is important. From the state space representation Eq.(2.10) and Eq.(2.11), and if the output, ***y*** is not a direct function of the input, ***u*** (i.e. $\mathbf{D}$ = 0*)* we may write:

$$\Delta\dot{\mathbf{x}} = \mathbf{A}\,\Delta\mathbf{x} + \mathbf{B}\,\Delta\boldsymbol{u} \tag{2.34}$$

$$\Delta\boldsymbol{y} = \mathbf{C}\,\Delta\mathbf{x} \tag{2.35}$$

-where $\mathbf{A}$ is the state matrix, $\Delta\mathbf{x}$ is the state variable vector, Δu is a single input variable, Δy is a single output variable, $\mathbf{C}$ is a row vector and $\mathbf{B}$ is a column vector. The transfer function between the variables ***y*** and ***u*** is obtained by applying the Laplace transform:

$$G(s) = \frac{\Delta y(s)}{\Delta u(s)} = \mathbf{C}\,(\mathrm{s}\mathbf{I} - \mathbf{A})^{-\mathbf{1}}\,\mathbf{B} \tag{2.36}$$

Eq. (2.36) has the following general form, assuming $D(\mathrm{s})$ and $N(\mathrm{s})$ can be factored:

$$G(s) = K\,\frac{N(\mathrm{s})}{D(\mathrm{s})} = K\,\frac{(s-z_1)(s-z_2)\cdots(s-z_l)}{(s-p_1)(s-p_2)\cdots(s-p_n)} \tag{2.37}$$

-where $z_1, z_2, \ldots, z_l$ are called the zeros for which $G(s)$ becomes zero and $p_1, p_2, \ldots, p_n$ are called the poles of $G(s)$

The values of poles and zero uniquely determine the system transfer function. The transfer function can be expanded in partial fractions as:

$$G(s) = \frac{R_1}{(s - p_1)} + \frac{R_2}{(s - p_2)} + \cdots + \frac{R_n}{(s - p_n)} \tag{2.38}$$

-where $R_i$is called the residue of $G(s)$ at pole p_i.

The transfer function in terms of the eigenvalues and eigenvectors can be obtained by expressing the state variables $\Delta\mathbf{x}$ in terms of the transformed variable ***z*** defined by Eq. (2.28) can thus be written as:

$$G(s) = \frac{\Delta y(s)}{\Delta u(s)} = \mathbf{C}\,\mathbf{\Phi}(s\mathbf{I} - \mathbf{\Lambda})^{-1}\,\mathbf{\Psi B} \tag{2.39}$$

Since $\mathbf{\Lambda}$ is a diagonal matrix, $G(s)$ may be written as:

$$G(s) = \sum_{i=1}^{n} \frac{R_i}{s - \lambda_i} \tag{2.40}$$

-where the residues in terms of the eigenvectors are:

$$R_i = \mathbf{C\Phi_i\Psi_i B} \tag{2.41}$$

Referring to Eq. (2.40), the poles of $G(s)$ are given by the eigenvalues of $\mathbf{A}$ and the solution of Eq. (2.42) gives the zeros of $G(s)$.

$$\sum_{i=1}^{n} \frac{R_i}{s - \lambda_i} = 0 \tag{2.42}$$

2.1.7 Eigenvalue Sensitivity

Eigenvalue sensitivity is a useful property in control studies used to assess the effect of the change of a system parameter. Eigenvalue sensitivity is the sensitivity to change in the elements of the state matrix [3]. The relationship between the state matrix, eigenvalues and right eigenvectors is defined in Eq. (2.17) which when differentiated with respect to a_{kj} (the element of $\mathbf{A}$ in the *k*th row and *j*th column) gives:

$$\frac{\partial \mathbf{A}}{\partial a_{kj}}\boldsymbol{\Phi_i} + \mathbf{A}\frac{\partial \boldsymbol{\Phi_i}}{\partial a_{kj}} = \frac{\partial \lambda_i}{\partial a_{kj}}\boldsymbol{\Phi_i} + \lambda_i \frac{\partial \boldsymbol{\Phi_i}}{\partial a_{kj}} \tag{2.43}$$

Eq.(2.43) can be simplified by pre-multiplying with the *i*th left eigenvector and rearranging to yield Eq.(2.44):

$$\boldsymbol{\Psi_i}\frac{\partial \mathbf{A}}{\partial a_{kj}}\boldsymbol{\Phi_i} + \boldsymbol{\Psi}_i(\mathbf{A} - \lambda_i \mathbf{I})\frac{\partial \boldsymbol{\Phi_i}}{\partial a_{kj}} = \boldsymbol{\Psi_i}\boldsymbol{\Phi_i}\frac{\partial \lambda_i}{\partial a_{kj}} \tag{2.44}$$

Eq. (2.44) can be simplified to Eq. (2.45) considering that $\boldsymbol{\Psi_i}\boldsymbol{\Phi_i} = 1$ and $\boldsymbol{\Psi_i}(\mathbf{A} - \lambda_i \mathbf{I}) = 0$

$$\boldsymbol{\Psi}_\mathbf{i}\frac{\partial \mathbf{A}}{\partial a_{kj}}\boldsymbol{\Phi_i} = \frac{\partial \lambda_i}{\partial a_{kj}} \tag{2.45}$$

It is important to note that all the elements of the derivative of the state matrix (left hand side of Eq.(2.45)) are equal to zero and 1 for those elements in the *k*th row and *j*th column which yields the eigenvalue sensitivity Eq.(2.46).

$$\frac{\partial \lambda_i}{\partial a_{kj}} = \Psi_{\mathrm{ik}}\Phi_{\mathrm{ji}} \tag{2.46}$$

The sensitivity of the eigenvalue, λ_i to the element a_{kj} of the state matrix is equal to the product of the left eigenvector element Ψ_{ik} and the right eigenvector element Φ_{ji}.

2.1.8 Participation Factor

The right and left eigenvectors individually can be used to identify the relationship between the state variables and the modes as described earlier. However, the problem in using the eigenvectors is that their elements depend on the units and scaling associated with state variables. The solution to this is the matrix called the participation factor matrix $\mathbf{P}$, which combines the right and left eigenvectors as a measure of the association between the state variables and the modes [3].

$$\mathbf{P} = [\mathbf{p_1} \quad \mathbf{p_2} \cdots \quad \mathbf{p_n}] \tag{2.47}$$

$$\text{with } \mathbf{p_i} = \begin{bmatrix} p_{1i} \\ p_{2i} \\ \vdots \\ p_{ni} \end{bmatrix} = \begin{bmatrix} \Phi_{1i}\Psi_{i1} \\ \Phi_{2i}\Psi_{i2} \\ \vdots \\ \Phi_{ni}\Psi_{in} \end{bmatrix}$$

where Φ_{ki}= is the element on the kth row and ith column of the modal matrix $\mathbf{\Phi}$

= kth entry of the right eigenvector Φ_i

Ψ_{ik} = the element on the ith row and kth column of the modal matrix $\mathbf{\Psi}$

= kth entry of the left eigenvector Ψ_i

The element $p_{ki} = \Psi_{ki}\Phi_{ik}$is called the participation factor which is a measure of the relative participation of the *k*th state variable in the *i*th mode and vice versa. The effect of multiplying the elements of the left and right eigenvectors is to make p_{ki} dimensionless.

In power systems, not all the synchronous generators may require the addition of PSSs to ensure adequate damping of the system oscillation modes. The participation factor is a good indication of the importance of a state variable to the mode and it is particularly useful as a screen for the PSS optimal placement [7]. In general, adding damping to the generators with positive participation factors will improve the oscillation mode damping while generators exhibiting negative participation factors will have an adverse effect when equipped with damping equipment. If the participation factor is zero, the corresponding generator will not contribute to the oscillation mode damping [7].

2.2. Theory of the Power System Stabilizer (PSS)

The two main elements of synchronous machines are the field winding and the armature winding which are found on the machine's rotor and stator respectively. The field winding is excited by direct current from the excitation system to produce a rotating magnetic field. The magnetic field induces alternating three phase voltages in the stator armature windings. Three phase stator currents will develop when a

load is connected. The resulting stator currents will produce another rotating magnetic field rotating at the same speed as the generator rotor field under steady-state conditions. The tendency of the stator and rotor fields to align themselves result in an electromagnetic torque which opposes rotation of the rotor. In order to sustain the rotation, a mechanical torque must be applied from the generator turbine. An increase in the mechanical torque input advances the rotor field to a new position relative to the rotating stator magnetic field while a reduction of the mechanical torque input retards the rotor field position. Under steady-state operating conditions, the rotor field and the stator field have the same speed with an angular separation between them depending on the generator electromagnetic torque [3].

The change in the electromagnetic torque ΔT_E can be resolved into the synchronising torque in phase with the rotor angle deviation and the damping torque in phase with the speed deviation following a disturbance. This can be expressed mathematically through Eq. (2.48).

$$\Delta T_E = T_S \Delta\delta + T_D \Delta\omega \tag{2.48}$$

-where: $T_S \Delta\delta$ is the component of torque change in phase with the rotor angle deviation $\Delta\delta$, and is referred to as the synchronising torque component; where T_S is the synchronizing torque coefficient;

$T_D \Delta\omega$ is the component of torque in phase with the rotor speed deviation $\Delta\omega$, and is referred to as the damping torque component; where T_D is the damping torque coefficient;

Referring to Eq. (2.48), the PSS should operate in such a way that a component of the electrical torque proportional to the rotor speed deviation should be produced and the logical signal input to the PSS is the speed deviation. The theoretical basis for PSS operation can be explained using a single machine connected to a large system through an external impedance as shown in Figure 2.1 where X_{eq} is the equivalent impedance of a transmission line and the generator transformer, E_T is the generator terminal voltage, P_g and Q_g are the generator active and reactive power respectively, V∞ is the infinite bus voltage. The arrangement is known as a Single Machine Infinite Bus (SMIB). The SMIB system was first presented in [18] to provide insights into the effects of excitation systems and to establish understanding of the stabilizing requirements through excitation control – i.e. the PSS.

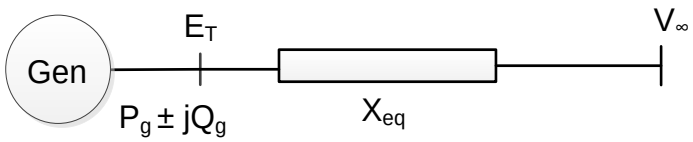

Figure 2.1: Single Machine Infinite Bus (SMIB) system

Figure 2.2 shows the linearized block diagram model of the SMIB comprising the simplified exciter, AVR and a voltage transducer adapated from [3]. The figure shows the relationship between the various exictation control system variables (the block diagram also include the PSS loop).

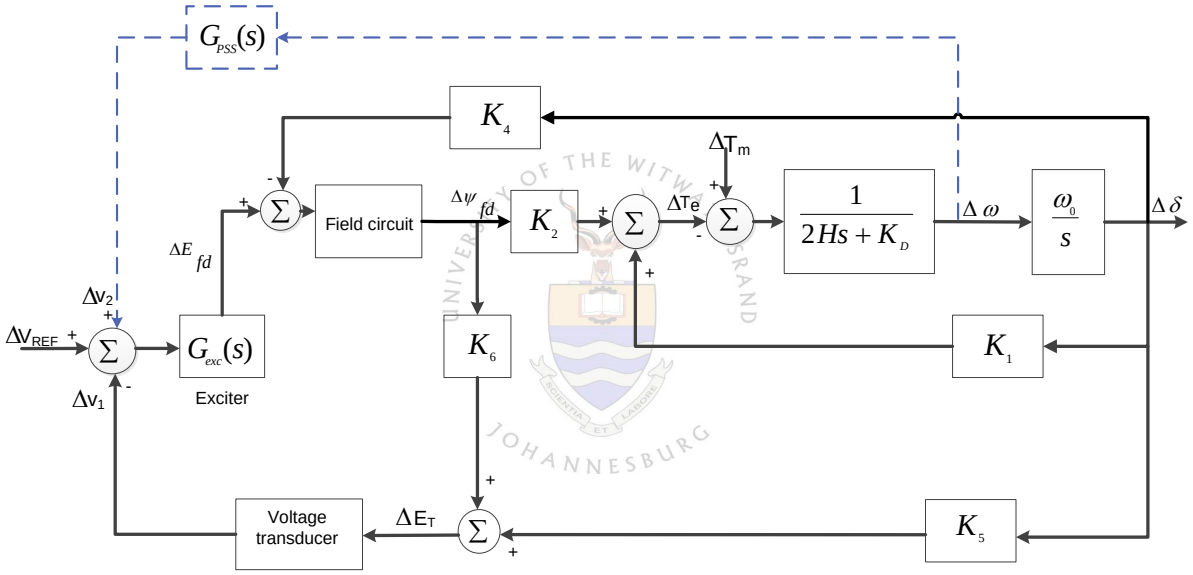

Figure 2.2: Linearized SMIB system

In Figure 2.2, Δ denotes the small excursions about an initial operating point, where: v_1 is the voltage transducer output signal; v_2 is the PSS output signal; V_{REF} is the reference voltage signal; E_{fd} is the field voltage; E_T is the generator terminal voltage; ω_0 is rated angular velocity of the rotor $2\pi/f$ where f is the supply frequency; H is the inertia constant and K_D is a component of damping torque. The parameters $K_1 - K_6$ are functions of the generator, system impedance and system operation condition which are dependent on the system loading and network strength [3]. The definition of the parameters are as follows:

$K_1 = \frac{\Delta T_e}{\Delta \delta} |_{E_q'}$ represents the change in electrical torque ΔT_e for a change in the rotor angle $\Delta\delta$ with constant flux linkages in the d axis,

$K_2 = \frac{\Delta T_e}{\Delta E_q'} |_{\delta}$ represents the change in electrical torque ΔT_e for a change in the d-axis flux linkages $\Delta E_q'$ with constant rotor angle δ.

$K_3 = \frac{X_d' + X_{eq}}{X_d + X_{eq}}$ represents the case where the external impedance is modelled as a pure reactance - impedance factor.

$K_4 = \frac{1}{K_3} \frac{\Delta E_q}{\Delta \delta}$ represents the demagnetizing effect for a change in the rotor angle $\Delta\delta$

$K_5 = \frac{\Delta E_T}{\Delta \delta} |_{E_q'}$ represents the change in terminal voltage ΔE_T with change in rotor angle $\Delta\delta$ for constant d-axis flux linkage E_q'

$K_6 = \frac{\Delta E_T}{\Delta E_q'} |_{\delta}$ represents the change in terminal voltage ΔE_T with change in E_q' for constant rotor angle, δ

Referring to Figure 2.2, $G_{exc}(s)$ is the transfer function of the AVR and exciter, and the transfer function of the generator is between ΔE_{fd} and ΔT_e. In analysing the small-signal oscillations, better insight of the excitation control system and theoretical concept of PSSs is found using frequency response [18]. The response between the exciter input and the generator electrical torque exhibits a frequency dependent gain and phase shift [3] for which the PSS transfer function $G_{PSS}(s)$ will compensate (gain and phase-lead). The phase-lag between the exciter input and the generator electrical torque changes with changes in the power system operating conditions [3]. Consequently, a suitable PSS phase-lead needs to be provided over the rotor oscillation range of frequencies, rather than a single frequency. The frequency range of interest is from 0.1 Hz to 2 Hz. In general, a compromise must be made when determining the phase-lead acceptable for different system operating conditions. However, if the exciter and generator transfer functions were pure gains a direct feedback of the rotor speed deviation would result in a damping torque component.

A PSS may be included in the excitation system, with either rotor speed, accelerating power or frequency as the input signal or a combination of these auxiliary input signals. As mentioned previously, the most advocated and logical auxiliary signal is the rotor speed, however, the other inputs can be used and have different advantages and disadvantages. Standardized and commercially used PSSs are documented in IEEE Std. 421.5-2005 [9]. The effectiveness of PSSs in damping the power system rotor oscillations depend on several factors which among them include the input signal used. Alternative forms of PSSs have been developed based on the various input signals namely speed-based PSSs, frequency-based PSSs and power-based PSSs.

- Speed-based PSSs

Rotor speed can be directly measured and used as an input signal to the PSS. The rotor-speed based PSSs were successfully used on hydraulic and thermal generating units with reliable measure of both local and inter-area oscillation modes [19]. However, several practical limitations were experienced [20]. For example, vertically mounted units require filters to remove low frequency noise from the rotor-speed signal due to shaft lateral movement. In such units, lateral shaft movement mitigation techniques are required. In addition, specially designed filters are required to remove low frequency noise components and use of several transducers around the generator shafts. The challenges associated with this technique are increased costs and high maintenance. Horizontally mounted turbo units result in torsional modes in the rotor-speed signals due to twisting of the generator shaft. Torsional filters also known as ramp tracking filters were used in such cases, but this affected the PSS performance by introducing phase-lags at lower frequencies. This has a destabilizing effect on the exciter modes which eventually limits the PSS gain hence impacts the desired damping. The torsional filters require custom design based on each of the generator torsional characteristics making this approach more expensive. The speed-based PSSs are best tuned when the generator is at full-output while connected to a strong system [21].

- Frequency-based PSSs

The generator rotor speed deviations can be estimated from the frequency. The frequency is calculated from the generator terminal voltages and terminal currents. This type of input is more sensitive to the inter-area modes than local modes [20] [21]. However, the power system frequency usually contains other frequency components such as the torsional modes. In the case of torsional modes and for thermal units, frequency-based PSS require torsional filters which result in the same difficulties as the speed-based PSSs. The sensitivity of the frequency to speed-deviations increases as the power system interconnection becomes weak [21]. Thus, this leads to the frequency-based PSSs being tuned for best performance under weak interconnection conditions which is when PSS's damping is required the most. The frequency-based PSSs often have smaller gains than speed-based PSSs.

- Power-based PSSs

Power-based PSS operation can be explained with reference to the equation of motion of the machine rotor called the swing equation Eq. (2.49) derived in reference [3]

$$2H\frac{d}{dt}\Delta\omega = \Delta P_m - \Delta P_e \tag{2.49}$$

-where: H is the generator per unit inertia constant;

ΔP_m is the change in per unit mechanical power;

ΔP_e is the change in per unit electrical power;

Due to difficulties involved in measuring mechanical power, early power-based PSSs assumed constant mechanical power. Referring to Eq. (2.49), this assumption leads to the rotor-speed changes being proportional to changes in electrical power which were easily measured and used as an input signal. However, it was noticed that when there is a change in the mechanical power, the PSS would undesirably respond. In addition, during rapid load changes power-based PSSs would respond and this resulted in large reactive power swings [22]. The setbacks have been corrected by use of limiters to prevent the PSS from responding but it restricted the overall gain and damping of power-based PSS and they are of limited practicality. The limitations of the pure power-based PSSs are mitigated by the use of the integral of accelerating power as the input (e.g. the IEEE Std. 421.5- PSS2B). The integral of accelerating power-based PSS is the modern and almost universally adopted PSS type. The requirement of this work was to adopt a modern dual-input (power and speed or frequency) PSS structure. For this reason, the IEEE PSS2B model was used. The IEEE PSS2B implementation and parameter selection is presented in detail in Chapter 4. However, the principle of operation of the integral of accelerating power-based PSS is illustrated by rewriting Eq. (2.49) as:

$$\Delta\omega = \frac{1}{2H}\int (\Delta P_m - \Delta P_e)\, dt \tag{2.50}$$

Referring to Eq. (2.50), the integral of accelerating-power can be derived from changes in the generator rotor speed deviations by measuring the mechanical power and the electrical power changes. The problem in this case, is to measure the integral of change in mechanical power free of torsional modes unless the torsional filters are used. Nevertheless, the major advantage is that the torsional filters are not in the main stabilizing path which involve the change in the electrical power signal. This consequently alleviates the exciter modes stability problem which allows higher gain and thus better damping by the PSS.

2.3. Conventional Power System Stabilizer (PSS) design method

The PSS objective is to move an unstable or poorly damped eigenvalue, λ_i into the left-half of the complex plane. The movement can be explained using Figure 2.3. As previously described, for an ideal case where the PSS phase characteristic is an exact inverse of the exciter and the generator phase characteristic, a poorly damped eigenvalue will move along the locus indicated by L_2 in Figure 2.3. In this case the PSS introduces a pure damping torque component.

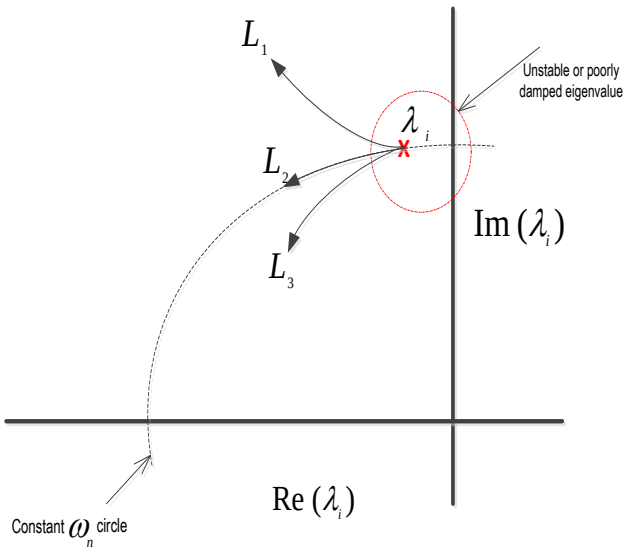

Figure 2.3: Eigenvalue movement/locus due to the presence of the PSS

The poorly damped eigenvalue could move along locus L_1 or L_3 indicated in Figure 2.3. The eigenvalue moves along the locus L_1 due to the PSS action as the PSS gain increases. This locus is when the PSS introduces damping torque with increasing synchronizing torque. In this case, the frequency of the oscillation mode increases. In the case whereby the eigenvalue moves along the locus path L_3 the PSS introduces damping torque with decreasing synchronizing torque which compromises the transient stability of the system. If an eigenvalue moves along path L_3 this implies that the frequency of the oscillation mode is decreasing, and the PSS is providing too much phase-lead. Hence when determining the required phase compensation of the PSS, intentional slight under-compensation to overcompensation is considered so that the PSS significantly increases the damping torque with slight increase in the synchronising torque [3] [23].

The system phase characteristic between the generator and the exciter from the AVR input reference to the generator electrical torque is used to design the PSS. The frequency response-based method is the commonly used approach. Frequency response analysis is simple, and it clearly indicates the way the system phase characteristics should be modified to achieve the desired performance and the approach can be used in field tests. From a simulation point of view, the frequency response method relies on linearizing the power system at an operating point and determining the frequency response between the AVR input reference to the generator electrical torque. When performing the frequency response analysis, the generator inertia is set to infinity to avoid feedback due to change in generator rotor angle [24].

2.3.1 Phase-compensation design

Once the system phase characteristic has been determined the PSS phase compensation settings are designed to provide the necessary phase-lead to compensate the system phase-lag. The phase-lead requirements at the frequency of the oscillation mode of interest and the number of phase-lead blocks required are determined from the system phase-lag. A single PSS phase-lead block should not exceed 55º [7]. Thus, if the phase-lag at the oscillation mode of interest exceeds 55º, more than one phase-lead block should be used, and this can be divided equally among the available phase-lead blocks. The phase-lead characteristic is provided by Eq. (2.51).

$$H_P(s) = \left(\frac{1 + a\mathrm{Ts}}{1 + \mathrm{Ts}}\right) \qquad (a > 1) \tag{2.51}$$

-where a is a scaling factor is and T is a time constant.

To minimize the high frequency gain which amplifies the signal noise level, the scaling factor a in Eq. (2.51) should be as small as possible [25]. The maximum phase lead angle, $\emptyset_m$ obtained with the phase advance unit is given by Eq.(2.52). The time constant T in Eq. (2.51) determines the frequency ω_{m} where f_{osc} is the oscillation mode frequency at which the maximum phase-lead angle occurs. This maximum phase-lead angle will occur at the frequency given by Eq.(2.53).

$$\emptyset_m = sin^{-1}\left(\frac{a-1}{a+1}\right) \tag{2.52}$$

$$\omega_{\mathrm{m}} = 2\pi f_{osc} = \frac{1}{T\sqrt{\alpha}} \tag{2.53}$$

2.3.2 Washout filter block selection

The signal washout block of the PSS shown in Figure 1.4 is a high pass filter which allow signals associated with the rotor oscillations to pass unaltered. The washout filter block allows the PSS to respond only to changes in speed. Without it, steady changes in speed would modify the terminal voltage. In general, the signal washout filter time constant should be high enough to allow signals associated with the rotor oscillations to pass but not so long that it leads to undesirable generator voltage excursions during system-islanding conditions [3]. Islanding is when a location is no longer supplied from the main grid. The washout filter time constant ranges from 1 to 20 seconds [3].

2.3.3 PSS gain

The PSS gain block determines the amount of damping introduced by the PSS. The root-locus technique is generally used to determine the PSS gain. The system stability as a function of the gain can be determined by varying the gain and the trajectories of the critical mode eigenvalues are established. The gain of the PSS should provide a maximum damping ratio to critical oscillation modes without adversely affecting other system oscillation modes such as the exciter mode. The critical oscillation mode damping ratio increases with gain up to a gain beyond which further increase results in decreased damping [23]. Due to practical issues, such as signal noise, the final PSS gain is determined during field commissioning and it is generally one-third of the gain which results in the exciter mode being unstable [23] [21]. This gain is obtained through small incremental adjustment during transient tests until oscillations are observed. The oscillations indicate instability due to an exciter mode or excessive amplification of input signal noise.

2.3.4 PSS output limiters

The PSS positive and negative output limiters have important effects on the performance of the PSS. In general, the positive output limiter is set at a relatively large value in the range of 0.1 to 0.2 p.u [3]. This allows a high level of contribution from the PSS during large swings. The PSS negative output limiter can be set in the range of -0.05 to -0.1 p.u which allows sufficient control range while at the same time providing satisfactory transient response [3]. The PSS limiter block must be set such that it does not interfere with the action of the AVR. For small-disturbance analysis, these limiters are not considered as interest is on a linearized model about an operating point.

2.4. Power System Component Modelling

To accurately capture the relevant dynamics of interest, power system components must be modelled with great accuracy. This section presents a review of the modelling of key components which are relevant to this investigation namely the synchronous generator, electrical loads, transformers, transmission lines and capacitors.

2.4.1 Synchronous Generator

There are two types of synchronous generators, namely salient pole and round rotor generators which are based on the rotor structure and speed. Salient pole synchronous generators rotate at lower speeds due to their relatively large number of poles and are used in hydro-power plants. These rotors often have damper windings or amortisseur windings in the form of copper or brass rods embedded in the pole face which are intended to damp out speed oscillations. However, the damper windings cause high fault currents which affect the generator protection [26]. Round rotor synchronous generators operate at high speed and they have two or four field poles formed by distributed windings placed in slots milled in the solid rotor and held in place by steel wedges [3]. Round rotor synchronous generators are used in

thermal power plants and they often do not have special damper windings. This study will consider the round rotor synchronous generator type. The correct prediction of power system small-signal stability behaviour is sensitive to the models of synchronous generators. Higher order models of the synchronous generators are recommended for the small-signal stability analysis because such models fully capture the generators' characteristics [8]. In this dissertation, the round rotor synchronous generator 6th order models were used. The mathematical equations representing the synchronous generator model consider both its electrical and mechanical behaviour. The major elements of physical synchronous machines, the stator and rotor, were introduced earlier in Section 2.2.

Figure 2.4 adapted from reference [3] is a cross sectional view of a three-phase salient-pole synchronous generator physical arrangement indicating the stator, rotor and their respective windings with a pair of field poles. The armature windings, on the stator uniformly distributed 120º apart in space, are responsible for generating the three phase voltages displaced 120º in time. Under balanced operating conditions, the armature winding produces a magnetic field in the air-gap which rotates at the same synchronous speed as the field produced by the direct current in the field winding.

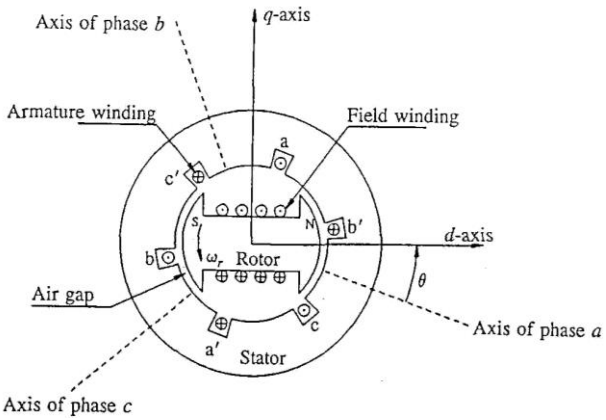

Figure 2.4 : Cross sectional view of a three-phase salient-pole synchronous generator [3]

The number of field poles is determined by the mechanical speed of the rotor and electric supply frequency of the stator. The synchronous speed is given by Eq.(2.54):

$$n = \frac{120f}{p_f} \tag{2.54}$$

-where n is the speed in revolution per minute (rpm); f is the supply frequency (Hz); and p_f is the number of field poles.

Mathematical model

For the purposes of modelling and identifying synchronous generator characteristics, two axes are defined, the direct ***d*** axis and quadrature ***q*** axis. The ***d***-axis is assumed to be aligned with the magnetic axis of the field winding and the ***q***-axis leads ***d***-axis by 90 electrical degrees [3]. The position of the rotor relative to the stator is measured by an angle θ between the ***d***-*axis* and magnetic axis of phase ***a*** winding. It is also assumed that the stator winding is sinusoidally distributed around the air gap, stator slots cause no appreciable variation of the rotor inductance with the rotor position and that the magnetic hysteresis is negligible [3].

The modelling of the generator electrical behaviour considers the generator's stator circuit which consists of three-phase armature windings carrying alternating current and the rotor circuit comprising the field winding connected to a direct current source and amortisseur windings as shown in Figure 2.5

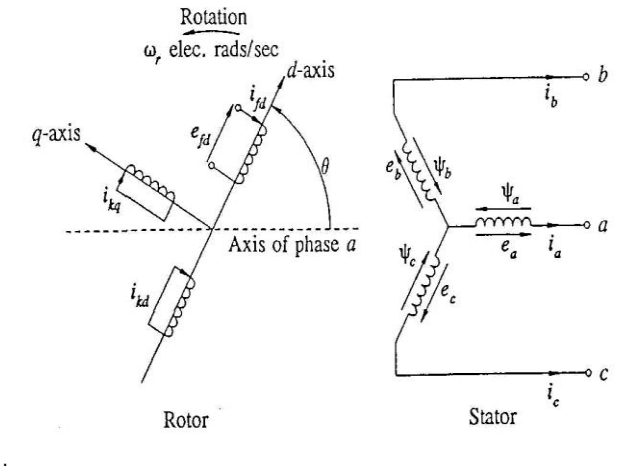

Figure 2.5: Synchronous generator stator and rotor circuits [3]

Figure 2.5 includes one set of closed amortisseur winding circuits in the ***d***- and ***q***-axes. For the purposes of analysis and simplification and when the interest is on the generator's characteristic as seen from the stator and the rotor terminals one set of the amortisseur winding circuit suffices [3].

The dynamic performance of the generator is described by the stator and rotor circuits together with the generator torque equation. The stator and rotor equations are derived from the relationship between the electric circuits and magnetic field of their coupled circuits. The equations are derived assuming that the positive direction of the stator winding current to be out of the machine whereas the field and the amortisseur currents are positive when pointed into the machine [3]. Thus, using Faraday's law, the stator voltages are:

$$e_a = p\psi_a - R_a i_a$$

$$e_b = p\psi_b - R_a i_b \quad (2.55)$$

$$e_c = p\psi_c - R_a i_c$$

-where: e_a, e_b, e_c represent the instantaneous stator phase to neutral voltages; $p = d/dt$ is a differential operator, R_a is the armature resistance; i_a, i_b, i_c represent instantaneous stator currents in phases ***a, b, c*** and ψ presents the flux linkage for the three phases which can be given in terms of self and mutual inductances:

$$\psi_a = -L_{aa}i_a - L_{ab}i_b - L_{ac}i_c + L_{afd}i_{fd} + L_{akd}i_{kd} + L_{akq}i_{kq}$$

$$\psi_b = -L_{bb}i_b - L_{ab}i_a - L_{ac}i_c + L_{afd}i_{fd} + L_{akd}i_{kd} + L_{akq}i_{kq}$$

$$\psi_c = -L_{cc}i_c - L_{ab}i_b - L_{ac}i_a + L_{afd}i_{fd} + L_{akd}i_{kd} + L_{akq}i_{kq}$$

UNIVERSITY OF THE WITWATERSRAND JOHANNESBURG

-where:L_{aa}, L_{bb}, L_{cc} are the self-inductances of the stator windings

L_{ab}, L_{bc}, L_{ca} are the mutual-inductances between the stator windings

$L_{afd}, L_{akd}, L_{akq}$ are the mutual inductance between stator and rotor windings;

i_{fd}, i_{kd}, i_{kq} are the field and amortisseur currents.

The difficulty involved in analysing the above stator voltage equations is that the inductances are functions of the rotor position and thus the inductances are time varying [3]. The Park's transformation is used to simplify the generator equations by reducing the complexity resulting from the time varying inductances. The purpose of the Park's transformation is to transform the stator phase stationary quantities (voltages, currents, reactances and flux linkages) to the rotating rotor reference frame. For balanced steady-state operation, the transformation allows alternating phase currents to appear as direct currents. From a practical point of view, the transformation allows the associated parameters of synchronous machines to be measured directly from the generator terminals and be able to provide a visual description of machine model detailing the transient and sub-transient behaviour. The stator circuit is transformed into ***dq0***-axes reference frame using trigonometric

functions of angle θ such that the resulting inductances are constant and independent of the rotor position. In addition, the per unit system is further used to conveniently normalise the generator characteristics in the Park's transform reference to simplify computations and to remove arbitrary constants. The per unit system expresses all the quantities as dimensionless ratios and allows the equations to be used for equivalent circuits.

The transformation from ***abc*** phase variables into ***dq0*** variables and the inverse in matrix form are given by (2.56) and (2.57) respectively [3].

$$\begin{bmatrix} i_d \\ i_q \\ i_0 \end{bmatrix} = \frac{2}{3}\begin{bmatrix} \cos\theta & \cos\theta & \cos(\theta+\alpha) \\ -\sin\theta & -\sin(\theta-\alpha) & -\sin(\theta+\alpha) \\ \frac{1}{2} & \frac{1}{2} & \frac{1}{2} \end{bmatrix}\begin{bmatrix} i_a \\ i_b \\ i_c \end{bmatrix} \tag{2.56}$$

$$\begin{bmatrix} i_a \\ i_b \\ i_c \end{bmatrix} = \begin{bmatrix} \cos\theta & -\sin\theta & 1 \\ \cos(\theta-\alpha) & -\sin(\theta-\alpha) & 1 \\ \cos(\theta+\alpha) & -\sin(\theta+\alpha) & 1 \end{bmatrix}\begin{bmatrix} i_d \\ i_q \\ i_0 \end{bmatrix} \tag{2.57}$$

-where $\alpha = 2\pi/3$ and i_0 is the zero-sequence component associated with symmetrical components defined such that the three phase currents are transformed into three variables and this component is zero under balanced conditions. According to [3] the widely-used practice for normalizing stator quantities is to use machine ratings (such as the volt-ampere rating of the machine in VA, peak phase to neutral rate voltage in V, the rated frequency in Hz and the peak line current in A) as base values from which other remaining quantities can be derived.

By applying ***dq0*** transformation (2.56) and using stator base quantities, the stator voltage equation Eq. (2.55) becomes:

$$e_d = p\psi_d - \psi_q p\theta - R_a i_d$$

$$e_q = p\psi_q + \psi_d p\theta - R_a i_q \tag{2.58}$$

$$e_0 = p\psi_0 - R_a i_0$$

Referring to the transformed stator equations, the term $p\theta = \omega_r$ represents the rotor angular velocity. The terms $\psi_q p\theta$ and $\psi_d p\theta$ are called the speed voltages due to the flux change in space resulting from the transformation of a stationary reference to a rotating reference whereas the terms $p\psi_d$ and $p\psi_q$are called transformer voltages due to flux changes in time. For steady-state conditions, the transformer voltage terms are omitted in the stator voltage equations without causing an error because they are negligible in comparison with the speed voltages [3]. The signs associated with the speed voltage terms are related to the sign conventions assumed for voltage and flux linkage relationship and to the assumed relative positions of the ***d-*** and ***q-***axes. Similarly, using Faraday's law the rotor circuit voltage equations are:

$$e_{fd} = p\psi_{fd} + R_{fd} i_{fd}$$

$$0 = p\psi_{kd} + R_{kd} i_{kd} \tag{2.59}$$

$$0 = p\psi_{kd} + R_{kq} i_{kq}$$

UNIVERSITY OF THE WITWATERSRAND JOHANNESBURG

The rotor circuit self-inductances and mutual inductances between each other do not vary with the rotor position because of the stator's cylindrical structure. However, rotor to stator mutual inductances vary periodically as given in the rotor circuit flux linkages below [3].

$$\psi_{fd} = L_{ffd} i_{fd} + L_{fkd} i_{kd} - L_{afd}[i_a \cos\theta + i_b cos(\theta - \alpha) + i_c cos(\theta + \alpha)]$$

$$\psi_{kd} = L_{fkd} i_{fd} + L_{kkd} i_{kd} - L_{akd}[i_a \cos\theta + i_b cos(\theta - \alpha) + i_c cos(\theta + \alpha)]$$

$$\psi_{kq} = L_{kkd} i_{kq} + L_{akq}[i_a \sin\theta + i_b \sin(\theta - \alpha) + i_c \sin(\theta + \alpha)]$$

The rotor flux linkages in the ***dq0*** components can be obtained by substituting i_d and i_q from (2.56) in the above equations to yield:

$$\psi_{fd} = L_{ffd} i_{fd} + L_{fkd} i_{kd} - k_d L_{afd} i_d$$

$$\psi_{kd} = L_{fkd} i_{fd} + L_{kkd} i_{kd} - k_d L_{akd} i_d$$

$$\psi_{kq} = L_{kkd} i_{kq} - k_d L_{akq} i_q$$

The resulting inductances in the above expression of the rotor flux linkages after substitution of the ***dq*** currents are constant and independent of the i_0 current component since the zero sequence components of armature current do not produce net flux across the air gap. However, the problem which results from the ***dq0*** transformation is that mutual inductances between stator and rotor quantities are not reciprocal. This problem is solved by the appropriate choice of the per unit system for the rotor quantities. The widely-used approach is called the L_{ad}-base reciprocal per unit system [3]. The approach allows the per unit quantities to be chosen such that the per unit mutual inductances between different windings are reciprocal and that all per unit mutual inductances between stator and rotor circuits in each axis are equal [3]. In order to achieve reciprocity, the same volt-ampere base must be used for the rotor and stator circuits, and the base current in any rotor circuit is defined as that which induces in each phase a per unit voltage equal to per unit, L_{ad}. The resulting per unit rotor voltage equations and considering two ***q***-axis amortisseur circuits represented by the by subscripts 1***q*** and 2***q*** are:

$$\begin{aligned} e_{fd} &= p\psi_{fd} + R_{fd}i_{fd} \\ 0 &= p\psi_{1d} + R_{1d}i_{1d} \\ 0 &= p\psi_{1q} + R_{1q}i_{1q} \\ 0 &= p\psi_{2q} + R_{2q}i_{2q} \end{aligned} \tag{2.60}$$

The electrical dynamic performance with respect to the generator torque is derived from its instantaneous stator three-phase power output and the mechanical rotor speed. The instantaneous three-phase power output of the stator in the ***abc*** reference frame is given by:

$$P_t = e_a i_a + e_b i_b + e_c i_c \tag{2.61}$$

By applying the ***dq0*** transformation (2.56) the instantaneous power (i.e. in the ***dq0*** components) is given by:

$$P_t = \frac{3}{2}\left(e_d i_d + e_q i_q + 2e_0 i_0\right) \tag{2.62}$$

Under steady state condition, the 0-axis component is zero (i.e. $e_0 = i_0 = 0$) which simplifies the instantaneous power to:

$$P_t = \frac{3}{2}\left(e_d i_d + e_q i_q\right) \tag{2.63}$$

The electrical torque generated in the air gap can be obtained by dividing the power transferred across the air gap (i.e. power corresponding to the speed voltages) by the rotor speed in mechanical radians per second. Firstly, the power corresponding to the speed is determined by expressing the voltage components in the instantaneous power, Eq. (2.62) in terms of flux linkage and currents in the ***qd0*** components using the stator voltage equations Eq. (2.58) as follows:

$$P_t = \frac{3}{2}\left(\left[p\psi_d - \psi_q p\theta - R_a i_d\right]i_d + \left[p\psi_q + \psi_d p\theta - R_a i_q\right]i_q + \left[2p\psi_0 i_0 - 2R_a i_0 i_0\right]\right)$$

$$P_t = \frac{3}{2}\left(p\psi_d i_d + p\psi_q i_q + 2p\psi_0 i_0 + \omega_r\left[\psi_d i_q - \psi_q i_d\right] - R_a\left[i_q^2 + i_d^2 + 2i_0 i_0\right]\right)$$

The air-gap torque, T_e is therefore given by:

$$T_e = \frac{3}{2}\left(\left[\psi_d i_q - \psi_q i_d\right]\right)\frac{\omega_r}{\omega_m}$$

The base torque can be determined from the stator base quantities provided earlier, such that the normalised air-gap torque is:

$$T_e = \left(\left[\psi_d i_q - \psi_q i_d\right]\right) \tag{2.64}$$

The generator mechanical part is modelled considering the rotational inertia characteristic describing the effect of unbalance between the electromagnetic torque and the mechanical torque of the machine. Similarly, these equations are expressed in per unit form by applying the base quantities. When there is an unbalance between the electromechanical torque and the mechanical torque acting on the rotor, the net effect is either acceleration or deceleration of the rotor. This relationship is captured through Eq.(2.65)

$$J\frac{d\omega_m}{dt} = T_m - T_e \tag{2.65}$$

-where J is the combined generator and turbine inertia, in kg.m^2, ω_m is the angular velocity of the rotor, in mech.rad/s; t is time, s and T_m is the mechanical torque in N.m and T_e is the electromechanical torque in N.m.

Eq. (2.65) is normalized in terms of per unit inertia constant ***H*** defined as the kinetic energy in watt-seconds at rated speed divided by the volt-ampere base of the machine. The inertia constant is given by:

$$H = \frac{1}{2}\frac{J\omega_{0m}^2}{VA_{base}} \tag{2.66}$$

-where ω_{0m} is the rated angular velocity in mechanical radians per second.

The per unit form of the equation of motion of the generator is obtained by expressing the moment of inertia ***J*** in terms of the inertia constant ***H*** in Eq. (2.66) and substituting it in Eq. (2.65). The resulting equation of motion per unit is given by:

$$2H\frac{d\overline{\omega_r}}{dt} = T_m - T_e \tag{2.67}$$

-where $\overline{\omega_r} = \frac{\omega_r}{\omega_0}$ with ω_0 is angular velocity of the rotor and the other variables maintain the same meaning with the torques in per unit. The angular position of the rotor with respect to the synchronously rotating reference in electrical radians can be given by δ. At time $t = 0$, the rotor angular position will be $\delta = \delta_0$.

$$\delta = \omega_r t - \omega_0 t + \delta_0 \tag{2.68}$$

The first derivative and second derivative of Eq. (2.68) are given by (2.69) and (2.70) respectively:

$$\frac{d\delta}{dt} = \omega_r - \omega_0 = \triangle\, \omega_r \tag{2.69}$$

$$\frac{d^2\delta}{dt^2} = \frac{d\omega_r}{dt} = \frac{d}{dt} \triangle \omega_r \tag{2.70}$$

Using the relationship, $\overline{\omega_r} = \frac{\omega_r}{\omega_0}$ the second derivative expression can be written as:

$$\frac{d^2\delta}{dt^2} = \omega_0 \frac{d\overline{\omega_r}}{dt} = \omega_0 \frac{d}{dt} \triangle \overline{\omega_r} \tag{2.71}$$

In terms of the rotor angle position, the equation of motion can be expressed as:

$$\frac{2H}{\omega_0} \frac{d^2\delta}{dt^2} = T_m - T_e \tag{2.72}$$

A component of damping torque, not accounted for in calculation of electromechanical torque, is often included by adding a term proportional to speed deviation in the equation of motion [3] as follows:

$$\frac{2H}{\omega_0} \frac{d^2\delta}{dt^2} = T_m - T_e - K_D \triangle \overline{\omega_r} \tag{2.73}$$

-where K_D is a component of damping torque.

Eq. (2.73) is known as the swing equation which describes the swings in rotor angle during disturbances. As described earlier in the previous chapter, the state-space representation requires the component models to be expressed as a set of first order differential equations. The swing equation expressed as two first order differential equations, becomes:

$$\frac{d\overline{\omega_r}}{dt} = \frac{1}{2H} (T_m - T_e - K_D \triangle \overline{\omega_r}) \tag{2.74}$$

$$\frac{d\delta}{dt} = \omega_0 \triangle \overline{\omega_r} \tag{2.75}$$

In the above equations, time t is in seconds, rotor angle δ is in electrical radians and $\omega_0 = 2\pi f$ is in electrical radians per second.

Saturation

Saturation is the property of iron material reached when an increase in applied external magnetic field does not increase the magnetization of the material further. The effects of the stator and rotor iron saturation are vital in the modelling of synchronous generators. The saturation of the synchronous generator inductances must be included when modelling synchronous generators for power system stability studies [3]. Saturation influences the location of the eigenvalues and hence the small-signal stability. The overall effect of the saturation is lowering the generator reactances and this can limit the performance of the generator because of high air gap line voltage. The saturation parameters are determined from the generator's open-circuit saturation curve. Figure 2.6 is a typical open-circuit saturation characteristic adapted from reference [27] which relates the generator terminal voltage and its field current.

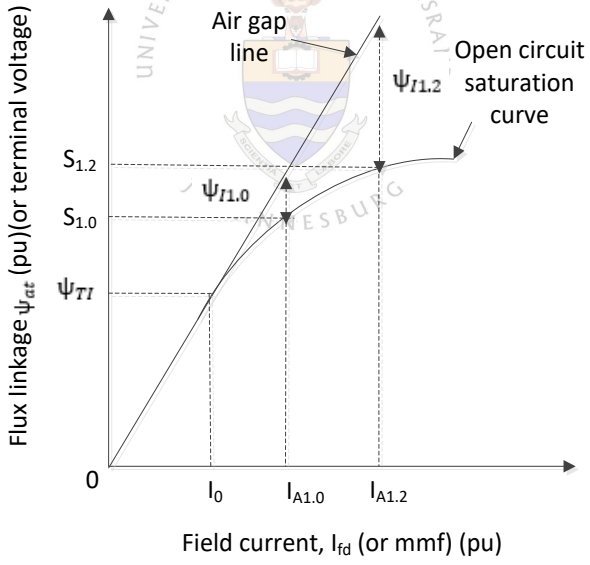

Figure 2.6: Synchronous generator open-circuit characteristic

At lower voltages, and hence low levels of flux, the reluctance of the stator and rotor magnetic circuit is only the air gap - this is described by the linear curve tangent to the lower part of the curve labelled the air gap line. In the linear portion of the open-circuit curve, the terminal voltage and flux are proportional to the field current. At higher voltages, as the flux increases, stator iron saturates and additional field current is required to drive the magnetic flux due to higher reluctance of the magnetic circuit - this result in the curve labelled open-circuit saturation

curve shown in Figure 2.6. There are two different methods which can be used to specify the degree of saturation of synchronous machines. Referring to Figure 2.6, ψ_{TI} defines the point at which the saturation begins and ψ_I defines the deviation of the open-circuit characteristic from the air gap line. The saturation degree, deviation of the open circuit characteristic from air gap line, can be mathematical expressed using an exponential function given by:

$$\psi_I = A_{sat} e^{B_{sat}(\psi_{at} - \psi_{T1})} \tag{2.76}$$

-where A_{sat} and B_{sat} are constants provided depending on the saturation characteristic.

The method used to specify the saturation characteristics in power system simulation packages, such as DIgSilent PowerFactory package used in this investigation, specifies two points on the open-circuit saturation curve - the excitation currents, $I_{A1.0}$ and $I_{A1.2}$ (as labelled in Figure 2.6) which correspond to the 1 p.u and 1.2 p.u stator voltages respectively under no-load conditions. The currents are derived from the following equations:

UNIVERSITY OF THE WITWATERSRAND JOHANNESBURG

$$I_{A1.0} = \frac{1 + \psi_{I1.0}}{L_{adu}} \tag{2.77}$$

$$I_{A1.2} = \frac{1 + \psi_{I1.2}}{L_{adu}} \tag{2.78}$$

-where L_{adu} is the unsaturated value of the equivalent stator and rotor circuit mutual inductance which is a given parameter and respective saturation degrees for the two points are determined using Eq. (2.67) as:

$$\psi_{I1.0} = A_{sat} e^{B_{sat}(1 - \psi_{T1})} \tag{2.79}$$

$$\psi_{I1.2} = A_{sat} e^{B_{sat}(1.2 - \psi_{T1})} \tag{2.80}$$

The saturation parameter values are determined using Eq. (2.81) and Eq. (2.82), where $I_0 = 1/L_{adu}$

$$S_{1.0} = \frac{I_{A\,1.0}}{I_0} - 1 \tag{2.81}$$

$$S_{1.2} = \frac{I_{A\,1.2}}{1.2I_0} - 1 \tag{2.82}$$

2.4.2 Electrical Load

The load characteristics and behaviour significantly influence the power system dynamics and performance. The stable operation of electric power systems is dependent on continuously matching the synchronous generator's power with the load [3]. A load model represents the mathematical relation between the bus voltage (magnitude and frequency) and power (active and reactive) or current flowing into the bus load. Load models are represented as either static or dynamic models [3]. Static load models express the active and reactive powers at any instant of time as algebraic functions of the bus voltage magnitude and frequency at the same instant [28]. The active and reactive powers are considered separately showing the load dependency on the voltage and frequency in algebraic polynomial or exponential form. The relationships between the load voltage dependency on the load active power and reactive power in polynomial form are given by Eq. (2.83) and Eq. (2.84) respectively. The load model parameters are coefficients ***p1*** to ***p3*** and ***q1*** to ***q3*** which define the portion of each component and ***P0***, ***V0*** and ***Q0*** are the nominal system operating conditions.

UNIVERSITY OF THE WITWATERSRAND JOHANNESBURG

$$P = P_o\left[p_1\left(\frac{V}{V_0}\right)^2 + p_2\left(\frac{V}{V_0}\right) + p_3\right] \tag{2.83}$$

$$Q = Q_o\left[q_1\left(\frac{V}{V_0}\right)^2 + q_2\left(\frac{V}{V_0}\right) + q_3\right] \tag{2.84}$$

This load model is referred to as the ZIP model since it is the sum of constant impedance (Z), constant current (I) and constant power (P) [28]. For a constant impedance load the power varies with the voltage magnitude squared whereas for the constant current load model the power varies directly with the voltage magnitude. For the constant power load model, the load is independent of voltage magnitude changes. The exponential load model representing the power relationship to voltage is of the form given by Eq. (2.85) and Eq. (2.86).

$$P = P_o\left(\frac{V}{V_0}\right)^a \tag{2.85}$$

$$Q = Q_o \left(\frac{V}{V_0}\right)^b \tag{2.86}$$

The parameters for this model are the exponents ***a*** and ***b*** which determine the different load models. For exponent values of 0, 1, or 2 the exponential model represents constant power, constant current or constant impedance characteristics respectively. A frequency dependent load is represented by multiplying a polynomial or exponential load model by a factor and is of the form Eq. (2.87) and Eq. (2.88).

$$P = P_o \left(\frac{V}{V_0}\right)^{\alpha} (1 + K_{pf}\Delta f) \tag{2.87}$$

$$Q = Q_o \left(\frac{V}{V_0}\right)^{\beta} (1 + K_{qf}\Delta f) \tag{2.88}$$

-where K_{pf} and K_{qf} are the real and reactive power frequency dependency factors respectively and Δf is the frequency deviation.

The static load models described may be adequate in system analysis even though most of the system loads are dynamic in nature, for example induction motors which require the dynamic load model representation. Dynamic load models express the active and reactive powers at any instant of time as difference or differential equations of voltage magnitude and frequency at past and present instants of time [28]. This load model type is preferred when performing power system analysis which includes the effects of the pertinent load features such as induction motor inertia. This dynamic load model is rather complex and time consuming [3]. Therefore, the static load model is adopted.

2.4.3 Transmission Lines

The electric power produced by synchronous generators is transmitted to consumers through transmission lines. In South Africa, the voltage levels are classified into two classes: - transmission and distribution. Transmission lines voltages are 220 kV and above whereas the voltage levels 132 kV and below are classified as distribution voltages. Transmission lines are characterized by four parameters namely, the series resistance due to conductor resistivity, shunt conductance due to the leakage currents between phases and ground, series inductance due to the magnetic field surrounding the conductor and shunt capacitance due to the electric field between conductors.

Overhead lines are used for transmission purposes over long distances. For the purposes of modelling, the transmission lines are classified into short lines, medium lines or long lines. Short lines lengths do not exceed 80 km whereas medium lines range from 80 km to 200 km

and a transmission line is a long line if the length is greater than 200 km [3]. For modelling purposes, short transmission lines have negligible shunt capacitance and may be represented by their series impedance (i.e. series resistance and series inductance). Medium lines may be represented using the nominal π-model equivalent circuit which is shown in Figure 2.7.

The nominal π-model equivalent circuit considers the series and shunt parameters of the transmission line. For long lines, the distributed effects of the transmission parameters are vital. As a result, long lines may be represented by cascaded sections of shorter lines or may be represented by the equivalent π-model equivalent circuit. This representation requires more detail of the transmission line and is complex. Therefore, in this dissertation, the nominal π-model equivalent model was used in this investigation.

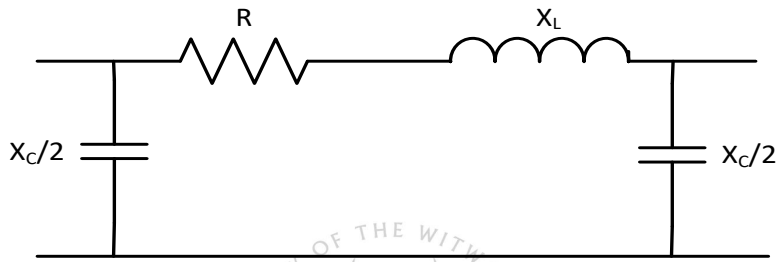

Figure 2.7: π-model for medium length lines

2.4.4 Power Transformers

For efficient transmission, the generator voltages are required to be stepped up to higher voltages using power transformers. Transformers are also required for stepping down voltages to the consumer's level. Transformers can either be three phase units or three single-phase units. The three single-phase units are used for large extra-high voltage transmission systems due to economic and design related reasons. The two winding transformers are used in conventional voltage transformation used by synchronous generators and WTs in power systems. Figure 2.8 shows a single phase equivalent circuit of a three-phase two-winding transformer where subscripts HV and LV on the parameters represent the HV and LV sides of the transformer respectively. $R_{Cu,\ HV,\ LV}$ are the high and low voltage side winding resistances, $X_{HV,LV}$ are the high and low voltage side leakage reactances respectively, X_M is the magnetizing reactance, R_{Fe} is the shunt resistance [29]. $N_{1,\ 2}$ are for the transformer's HV and LV windings.

An ideal transformer is usually used to explain basic transformer theory and for the development of the equivalent circuits. The following are assumed for an ideal transformer [30]:

- Windings have zero resistance; therefore, the I^2R losses in the windings are zero;

- Core permeability is infinite corresponding to zero core reluctance;
- No leakage flux such that the entire flux is confined to the core and link both windings; and
- There are no core losses.

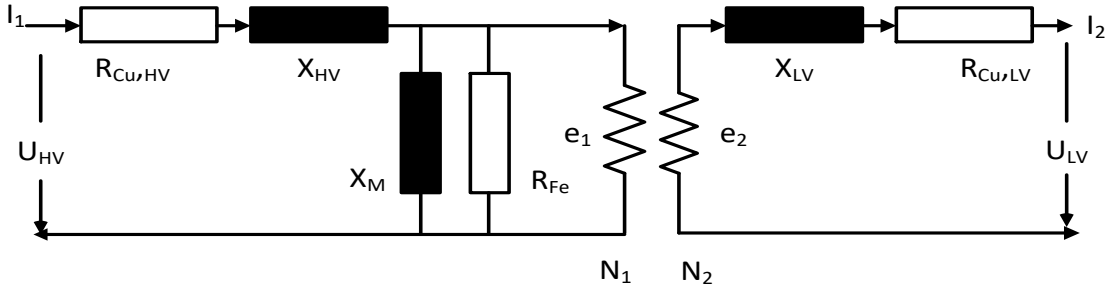

Figure 2.8: Single phase equivalent circuit of a three-phase two winding transformer

For an ideal transformer, the magnetomotive force due to a current flow is given by Eq. (2.89) where subscripts 1 and 2 represent the HV and LV sides of the transformer, *N* represents the number of turns in the respective windings and ***I*** is current flowing in the respective winding.

$$N_1 I_1 = N_2 I_2 \tag{2.89}$$

When the voltage (U_{HV}) is applied to winding 1 an induced voltage (e_1) is created across the primary winding (N_1) due to the rate of change of flux. Using Faraday's law, the induced voltage is given by Eq.(2.90)

$$e_1 = N_1 \frac{d\psi}{dt} \tag{2.90}$$

In a similar manner, another voltage (e_2) is developed across the seconding winding (N_2) due to the flux which is given by Eq. (2.91).

$$e_2 = N_2 \frac{d\psi}{dt} \tag{2.91}$$

Dividing Eq.(2.90) and Eq.(2.91) yields an equation showing the voltage transformation equation given by Eq.(2.92).

$$\frac{e_1}{e_2} = a = \frac{N_1}{N_2} \tag{2.92}$$

For transformer modelling, the transformer power rating in MVA, voltage rating, series reactance and resistance need to be specified among other parameters.

2.4.5 Capacitors

Voltage stability has been defined earlier as the ability of a power system to maintain steady voltages at all buses in the system after being subjected to a disturbance from a given initial operating condition. Voltage stability is vital to the efficient and reliable operation of the power system and it is concerned with the control of voltage and reactive power [3]. The objectives in maintaining voltage stable power systems are to maintain the equipment terminal voltages within acceptable limits, maximise utilization of transmission systems and minimization of reactive power flow to reduce the system losses. Voltage control in power systems is achieved by special devices dispersed throughout the power system. The devices are either shunt or series connected. In this dissertation, only shunt capacitors were used. Shunt capacitors provide passive compensation by supplying reactive power [3]. They contribute to voltage control by modifying the network characteristics. When shunt connected, they are either permanently connected or can be mechanically switched. Shunt capacitors can either be used for power factor correction and in transmission system to boost local voltages. The objective of power factor correction is to provide reactive power close to the point where is it is being consumed. For transmission systems, as used in this dissertation, shunt capacitors compensate for XI^2 losses and ensure satisfactory voltage levels during heavy loading conditions. For this purpose, the shunt capacitors are connected directly to a high voltage bus.

2.5. Study System Configuration - Two-Area-Multi-Machine (TAMM) System

Figure 2.9 shows the test power system, comprising the key network components described in the previous section, which was used in this investigation. The test power system consists of two interconnected areas through two long parallel transmission lines operating at 230 kV, four synchronous generators (two in each area), two loads (one in each area) and two shunt capacitors (one in each area). This test system was adopted from reference [3] and is widely known as the Two-Area-Multi-Machine (TAMM) system. Each area consisted of two round-rotor generators modelled using the 6th order generator model. The saturation characteristics of the generators were calculated using the guidelines provided in Section 2.4.1 with the parameters in Table 2.1. The generators were rated at 20 kV, 900 MVA each and had identical generator parameters except for the inertia constants which were 6.5 and 6.175 seconds for area 1 and area 2 respectively. Each generator represents closely coupled synchronous generators. The generator data is given in Table 2.1.

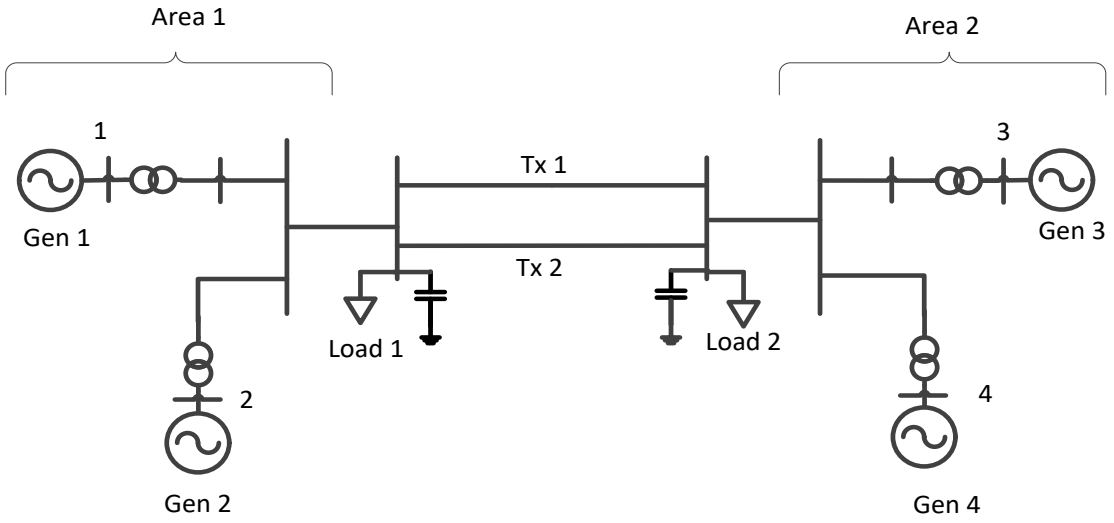

Figure 2.9: Two-Area-Multi-Machine (TAMM) test system

Table 2.1: Generator data

$X_d = 1.8$	$X_q = 1.7$	$X_l = 0.2$	$X'_d = 0.3$	$X'_q = 0.55$
$X''_d = 0.25$	$X''_q = 0.25$	$R_a = 0.025$	$T'_{d0} = 8\ s$	$T'_{q0} = 0.4\ s$
$T''_{d0} = 0.03\ s$	$T''_{q0} = 0.05\ s$	$A_{Sat} = 0.015$	$B_{Sat} = 9.6$	$\psi_{T1} = 0.9$
$H = 6.5$ (for Gen 01 and 02)		$H = 6.175$ (for Gen 03 and 04)		$K_D = 0$

All the synchornous generators were equipped with the IEEE AC4A excitation system shown in Figure 2.10. A high gain, K_a of 200 which is the overall gain of the excitation system (exciter and AVR) was deliberately chosen to introduce negative damping and to be able to see the impact of wind power. The excitation system shown consist of a terminal voltage transducer before the summing junction used for voltage sensing which has been adopted in this investigation with a time constant (T_R) of 0.01s. The filter delay and the derivative time constants (T_B and T_C) of the excitation system are used for tuning the excitation system response and are frequently small enough to be neglected [9]. In this study, the time constants are neglected by setting them to zero with the exciter current compensation factor (K_c). Table 2.2 provides parameters of the IEEE AC4 excitation system obtained from references [3] and [7] used in this investigation.

Table 2.2: IEEE AC4 excitation system parameters

$T_r = 0.01\ s$	$T_b = 0$	$T_c = 0$	$K_a = 200$	$T_a = 0.05\ s$
$K_c = 0$	$V_{imin} = -20\ p.u$	$V_{rmin} = -7\ p.u$	$V_{imax} = 20\ p.u$	$V_{rmax} = 7\ p.u$

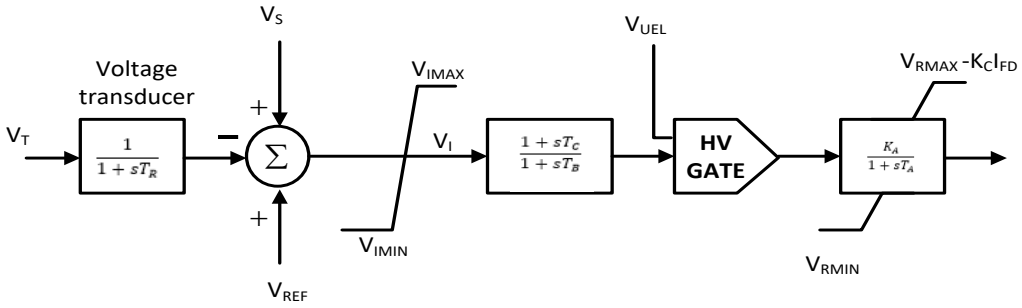

Figure 2.10: Block diagram of the IEEE AC4 excitation system

The transmission lines were modelled using the nominal π-model equivalent transmission line. The parameters of the lines used in per unit on 100 MVA, 230 kV base are:

$$r = 0.0001\ pu/km \qquad x_L = 0.001\ p.u/km \qquad b_C = 0.00175\ p.u/km$$

The transformers were modelled with a positive sequence reactance of 0.15 p.u. Constant impedance load models were used in each area such that the power flow from area 1 to area 2 was approximately 400 MW. The load in area 1 was 967 MW whilst in area 2 it was set to 1 767 MW both at 0.99 power factor. Shunt capacitors of 300 MVAr in area 1 and 450 MVAr in area 2 were included at the load buses. For this study, generator Gen 03 of area 2 was modelled as the reference machine. The other generators Gen 01, Gen 02 and Gen 04 were set to supply active power of about 700 MW. The IEEG1 governor models whose parameters are given in Appendix A were obtained from [3] and [7] were used in the simulations. The TAMM system as described above was built in DIgSilent PowerFactory.

2.6. Summary

In summary, this chapter has reviewed and presented a detailed theoretical analytical technique of the power system's small-small signal stability problem, the concept of PSS and the various types of PSSs with their practical advantages and disadvantages. The chapter has also presented the theoretical concept of the PSS and the conventional control method approach (lead-lag design and root locus technique) which is the current practice to design the PSS settings. In addition, the chapter has examined the modelling of power system components relevant to this investigation (synchronous generators, electrical loads, transmission lines and capacitors). This chapter has presented the test system, which consisted of two power system areas, comprised of identical generators, with similar ratings, to be used for this study.

CHAPTER 3 : TYPE 4 WIND TURBINE GENERATOR (WTG)

A Wind Power Plant (WPP) or a wind farm consists of several Wind Turbines Generators (WTGs) used to collectively generate electrical power from the wind kinetic energy. For power system grid impact studies, aggregated WPP models should be used rather than a full WPP. The aim of this chapter is to develop a WPP model, based on the IEC 61400-27-1 Type 4 WTG model, to be used for the investigation of the impact of wind power on the inter-area and local modes of power systems. Firstly, an introduction to WTGs is presented discussing types of WTGs namely fixed-speed WTGs and variable-speed WTGs. This is followed by a detailed discussion of the IEC 61400-27-1 Type 4 WTG model used in this investigation. The chapter then presents an aggregated WPP model developed based on the guidelines in the literature. The WPP model was built, simulated and analysed in DIgSilent PowerFactory software package.

3.1. An Introduction to Wind Turbine Generators (WTGs)

Figure 3.1 shows a typical onshore wind farm using horizontal-axis Wind Turbines (WTs) adapted from [31]. In general, WTs consist of rotor blades that capture the wind kinetic energy and convert it to shaft power.



Figure 3.1: Typical wind farm or Wind Power Plant [31]

The nacelle, which is found at the top of the WT tower, houses the main shaft, gearbox, generator, brakes and bearing, cooling system and yaw mechanisms. At the WT base is a pad-mount transformer which is used for transforming the lower generating voltage of the WTG to medium voltage level suitable for connection to the power system grid at distribution voltage level. Before connection to the power system grid, several medium voltage cables run from each WTG to collect the generated power. The medium voltage may further be stepped up to a higher voltage level at the point of connection [32]. At the point of connection, WPPs can operate in either voltage control mode, reactive power control mode or power factor control mode through the main controller, as further described.

As wind energy technologies evolved, the WTGs developed from fixed-speed WTGs to variable-speed WTGs found in modern WPPs. This classification is based on the WTGs capability to operate over a range of wind speed. Fixed-speed WPPs operate in a limited range of wind speed, in which an increase in the wind speed results in a slight increase of the rotor speed above the synchronous speed and hence varying slip based on the induction machine torque-speed relationship. The fixed-speed WPPs uses Squirrel Cage Induction Generators (SCIGs) and constitute many of the old WPPs. On the other hand, the variable-speed WTGs vary their rotor blade speed as a function of wind speed to extract maximum power in a wide range of the rotor speed above and below the synchronous speed. In addition, variable-speed WTGs can independently control the active and reactive power between the WTG and the power system grid. Although the WTGs can be classified into either fixed-speed WTGs and variable-speed WTGs, as the main categories, they can be further classified into four distinct types namely:

- Type 1 fixed-speed Wind Turbine Generator (WTG);
- Type 2 variable-speed Wind Turbine Generator (WTG);
- Type 3 variable-speed Wind Turbine Generator (WTG); and
- Type 4 variable-speed Wind Turbine Generator (WTG).

3.1.1 Fixed-Speed Wind Turbine Generators (WTG)

Figure 3.2 shows the configuration of the Type 1 fixed-speed WTGs which use SCIGs. As illustrated in Figure 3.2, the WT Rotor (WTR) blades are connected to the SCIG rotor, labelled IG in Figure 3.2, through a gearbox (GB). The gearbox converts the low speed WTR blades to the speed required to turn the SCIG. From the gearbox, the SCIG stator terminals connect to a pad mounted step-up transformer, labelled TR in Figure 3.2, which feeds into the collector cable system. This arrangement results in a direct connection between the Type 1 WTG WPPs and the electric power system grid. Given this, Type 1 WTG's speed is determined by the electric power system grid frequency. Since the grid frequency is maintained within a small frequency band, Type 1 WTG speed can vary from 1 to 2% above the synchronous speed [33]. This slight speed variation is achieved through the SCIG rotor winding resistance. For this reason, Type 1 WTGs are referred to as

fixed-speed WTGs. Pitch control is seldom used in Type 1 WTGs to limit the generator output power to its nominal value during high wind speeds.

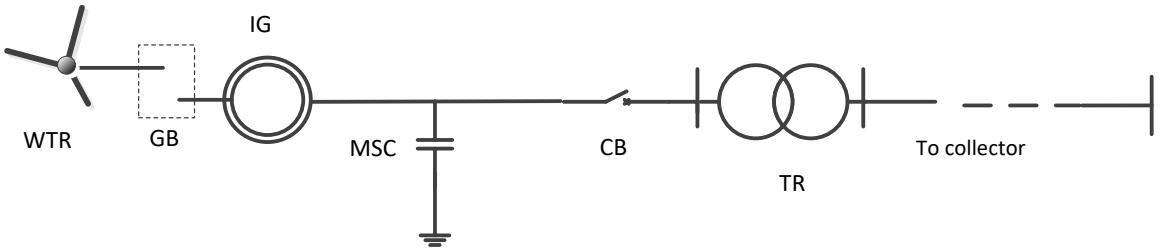

Figure 3.2: Type 1 fixed-speed WTG configuration

The major advantages of fixed-speed WTGs are that their structure is simple, robust and low cost. However, reactive power compensation using Mechanically Switched Capacitors (MSC) is required to offset the WTGs' inductive characteristics. The configuration of the capacitor banks required for reactive power compensation is depicted in Figure 3.2 whose power ratings are determined at the WPP no load condition [34]. Another drawback associated with Type 1 WTGs is significant output power fluctuations due to their fixed speed nature.

3.1.2 Variable-Speed Wind Turbine Generators (WTGs)

Type 2 variable-speed WTG configuration and characteristics are similar to Type 1 fixed-speed WTGs. The only difference is the induction generators used for Type 2 WTGs have Variable Rotor Resistance (VRR) which is indicated in Figure 3.3. The rotor resistance allows the rotor speed to vary within a limited range of up to 10% of the synchronous speed. As a result, Type 2 WTG WPPs are classified as variable-speed. Like Type 1 WTGs, reactive power compensation is required during start-up of the induction generators. The limitations associated with Type 2 WTGs are similar to those of Type 1 WTGs - losses due to the variable rotor resistance.

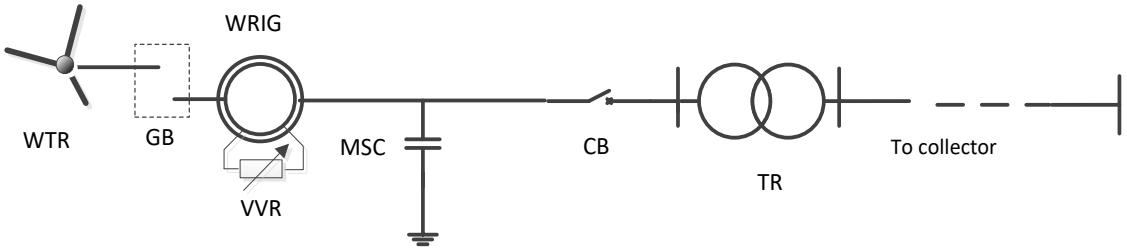

Figure 3.3: Type 2 variable-speed WTG configuration

Due to rapid technological advancements, newer WPPs are variable-speed WTGs using Doubly Fed Induction Generators (DFIGs) or synchronous generators with power electronic converters namely Type 3 WTGs and Type 4 WTGs. Figure 3.4 shows the configuration of

the Type 3 WTG which uses DFIGs and a partially rated power converter connected through the rotor windings. The grid-side converter consists of two back-to-back AC-DC voltage source converters. The power converter allows independent control of the active and reactive power between the WTG and the power system grid. In that respect the reactive power compensation drawbacks associated with Type 1 WTGs and Type 2 WTGs are resolved by the power converter. The power converter also matches the DFIG rotor mechanical and the power system grid frequencies regardless of the wind speed. These converters are rated at 20% to 30% of the WTG MVA rating since only a fraction of the total power passes through the power converter [32]. The application of the power converters results in Type 3 WTGs being more expensive than Type 1 and Type 2 WTGs. Type 3 WTGs rotors operate at ±20% to ±30% of the synchronous speed.

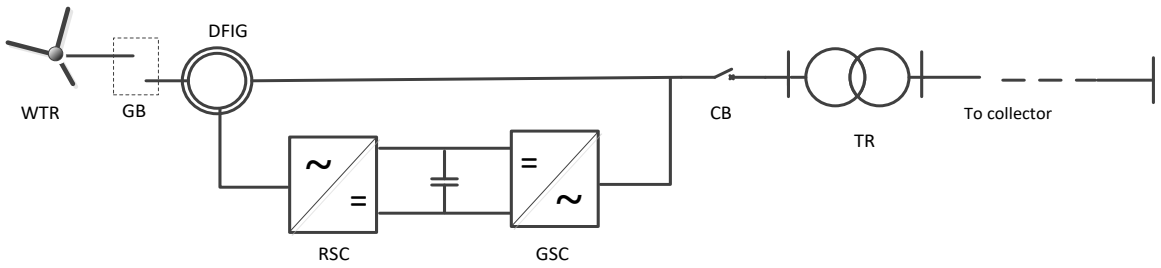

Figure 3.4: Type 3 variable-speed WTG configuration

The major difficulty associated with the Type 3 WTGs is the protection against over-currents and high DC voltages during external network faults [35]. To resolve this, the second generation of Type 3 WTGs use a crowbar that short circuits the rotor winding which effectively converts the Type 3 WTG into a conventional induction generator during external network faults. Switched resistors can be connected across the converter DC-link to avoid total disconnection during external network faults [36].

Type 4 WTGs are gaining prominence in the power grids. Figure 3.5 depicts the configuration of the Type 4 WTG which consists of an optional gearbox and a fully-rated power converter interfacing the WTG with the power system grid. This type of variable speed-WTG can use synchronous generators (SG) or induction generators.

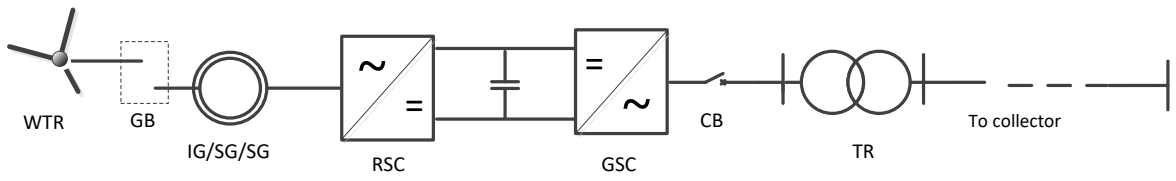

Figure 3.5: Type 4 variable-speed WTG configuration

Some other Type 4 WTGs use direct drive synchronous generators without gear box. The fully-rated power converter consists of the Rotor Side Converter (RSC) which interfaces with the generator rotor to the Grid Side Converter (GSC) before connection through the Circuit Breaker (CB) to the pad-mount transformer (TR). The speed of Type 4 WTG can vary independently of the power system grid frequency. In addition, another advantage of Type 4 WTGs is that the power converters enable independent control of the reactive and active power.

3.2. Wind Turbine Generator (WTG) Generic Models

The Western Electricity Coordinating Council (WECC) first developed generic WTG models based on the General Electric 1.5 MW and 3.6 MW WTGs [37]. The reason for the development of these generic WTG models was that manufacturer specific WTG models are highly confidential and require non-disclosure agreements to be signed prior to acquiring them which restricts the availability of the WTG models in the public domain. Because of continuous developments in wind power technologies, there has been collaborative work to further improve the WECC generic models. Recently, the IEC 61400-27-1(2015) was developed in agreement with various WTG manufacturers to model the behaviour of their WTGs in a generic, simple and accurate way. These WTG models can emulate a wide range of WTGs on the market upon appropriate parameter setting substitution. IEC 61400-27-1 WTG models are for fundamental frequency positive sequence responses and are suitable for [36]:

UNIVERSITY OF THE WITWATERSRAND JOHANNESBURG

i. Balanced short-circuits on the transmission grid external to the WPPs, for voltage recovery studies;

ii. WPP grid frequency disturbances;

iii. **Electromechanical oscillation modes of synchronous generators;** and

iv. Reference value changes in the WTG control, e.g. voltage, reactive/active power

Since this study is focused on the power system small-signal stability which is concerned with electromechanical oscillations, item (iii), this implies that the IEC 61400-27-1 WTG models can be adopted for this investigation. The IEC 61400-27-1 WTG models are implemented in DIgSilent PowerFactory as templates with default settings adjusted per the manufacturer's design to emulate a specific WTG model [13].

3.3. IEC 61400-27-1 Type 4 Wind Turbine Generator (WTG) model

As described earlier, the WPP consist of several WTGs collectively generating electric power from the wind kinetic energy. From a modelling point of view, the interface between the WT model, electric power system grid model and WPP model is shown in Figure 3.6. At the point of connection, the WPP controller coordinates the individual WT controllers to achieve the WPP requirements by regulating the terminal behaviour of the WPP by dispatching commands for the active and reactive power or voltage control to the individual WT generators. The WT model accounts for the dynamic features required to generate the electrical power from the wind energy.

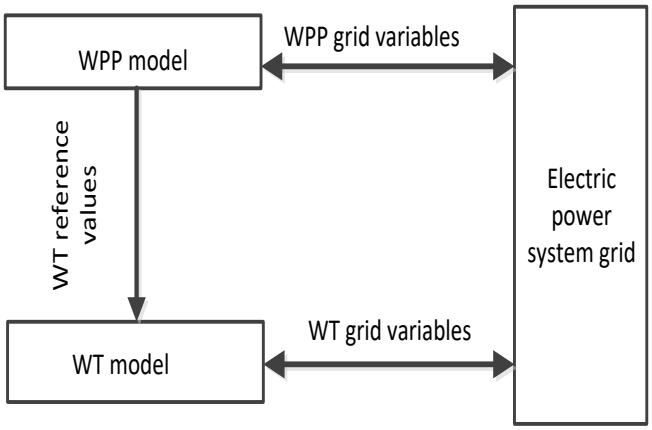

Figure 3.6: Interface between the WT model, grid model and WPP model

The Type 4 WTG model implemented by IEC 61400-27-1 consists of the WTG aerodynamic model, the mechanical model, the generator model, the electrical equipment model, the grid protection and control module. The IEC 61400-27-1 defines two Type 4 WTG models:

- Type 4A without the mechanical model: a model neglecting the aerodynamic and mechanical parts and thus not capable of simulating any power oscillations; and
- Type 4B with the mechanical model: a model including a two-mass mechanical model to replicate the power oscillations but assuming constant aerodynamic torque.

Type 4B was adopted based on the recommendations provided in reference [36] to include the WT mechanical model for power system stability studies. In addition, reference [38] supports that the constant aerodynamic torque is acceptable for power system simulation studies and that non-constant aerodynamic torque are used for energy yield analysis. In this dissertation, this Type 4B is referred to as the Type 4.

The modular structure for the IEC 61400-27-1 Type 4 WT model used is shown in Figure 3.7 where P_{WTref} is the WT active power reference and x_{WTref} is either the WT reactive power reference or delta voltage reference, depending on the WTG control mode dependent on the actual grid status, for which the System Operator issues specific commands on these reference parameters based on the grid requirements. Based on these reference parameters the WTs respond accordingly to meet the requirements of the power grid. The following subsections introduce the basic principles of the aerodynamic model and extend this to the constant aerodynamic torque model implemented with the Type 4 WTG model which is used in this dissertation, explain in detail the WT mechanical model, generator model, the electrical equipment model, the grid protection and the control module in accordance to the IEC 61400-27-1.

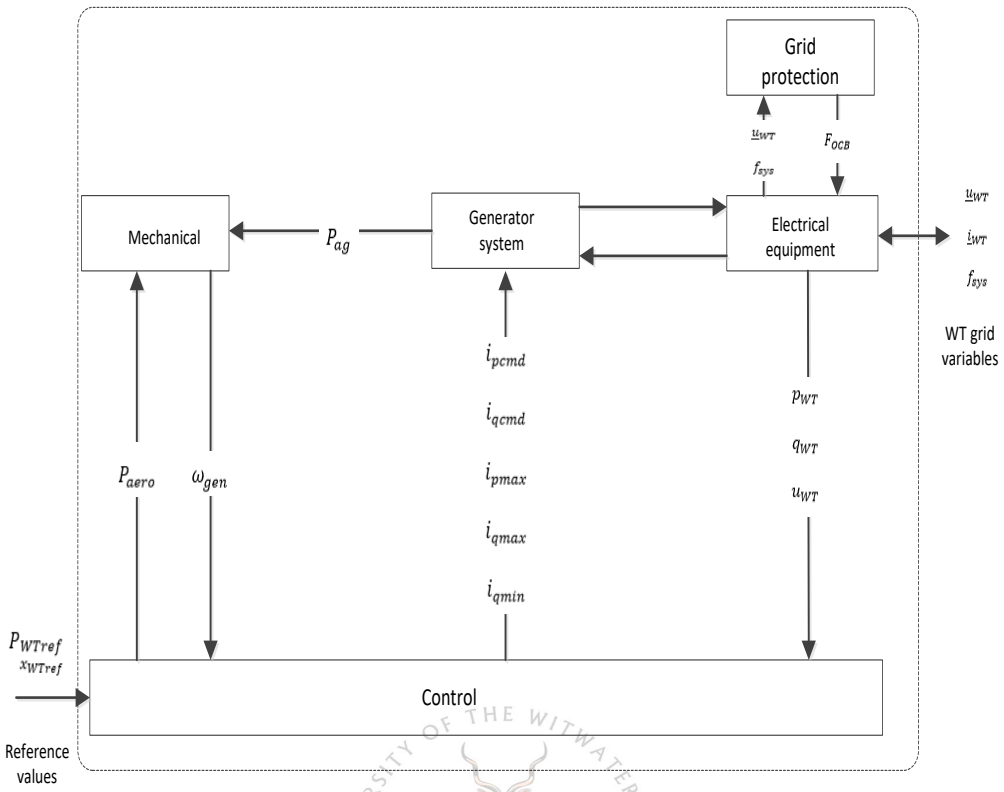

Figure 3.7: Modular structure of the IEC 61400-27-1, Type 4B (herein referred to as Type 4 WT)

3.3.1 Aerodynamic Model

The aerodynamic model determines the aerodynamic power P_{aero}, extracted from the wind energy which is given by Eq. (3.1):

$$P_{aero} = \frac{d}{dt}E_w \tag{3.1}$$

- where; $\frac{d}{dt}$ is the rate of change and E_w is the kinetic energy of a mass of air (in Joules), *m* (in kg) moving at a speed *V* (in m/s) given by Eq. (3.2):

$$E_w = \frac{1}{2}mV^2 \tag{3.2}$$

In air flow analysis, it is further convenient to consider the mass of air, *m* in a cylinder with length *V* meter and radius of the WT rotor, R_{WTR}. Since the wind speed is *V* m/s, the mass contained in the cylinder is the amount of mass that will pass through the WT rotor per second. It is therefore, convenient to use mass per second $\dot{m}$ as the amount of matter contained in a cylinder of air. This is such that the aerodynamic power P_{aero}, Eq. (3.1) can be expressed as:

$$P_{aero} = \frac{d}{dt}E_w = \frac{1}{2}\frac{d}{dt}mV^2 = \frac{1}{2}\dot{m}V^2 \quad (3.3)$$

- where, $\dot{m}$ is mass per second given by $\dot{m} = \rho AV$; where ρ is air density and A is cross sectional area swept by the WT rotor.

As the wind speed, V increases, the pitch angle, β of the WT rotor is varied at high speeds to protect the WT from damage and reduce the power generated. At lower speeds the objective in varying the pitch angle, β is to maximize the efficiency of the WT by optimizing the tip speed ratio, λ which is defined by Eq. (3.4):

$$\lambda = \frac{v_{tip}}{V} \quad (3.4)$$

- where v_{tip} is the WT rotor tip speed (in m/s) and V is wind speed (in m/s). The WT rotor tip speed, v_{tip} is calculated from:

$$v_{tip} = R_{WTR}\Omega_{WTR}$$

where Ω_{WTR} is the WT rotational speed (in rad/s).

The resultant aerodynamic power, P_{aero} extracted from wind energy is dependent on the WT rotor pitch angle, β and the tip speed ratio, λ. The aerodynamic coefficient C_p which is the function of the blade pitch angle β and the tip speed ratio, λ is introduced in the aerodynamic power expression to consider the effect of the WT efficiency. The resultant aerodynamic power, P_{aero} is calculated by Eq. (3.5):

$$P_{aero} = \frac{1}{2}\rho\pi R_{WTR}^2 V^3 C_p(\lambda, \beta) \quad (3.5)$$

- where: ρ is the air density (in kg/m^3),

  R_{WTR} is the WT rotor radius (in m)

  V is the wind speed (in m/s)

  C_p is the function of blade pitch angle β (in rad) and tip speed ratio, λ.

The aerodynamic power is input signal to the mechanical model which is explained in the following section. As discussed earlier, the constant aerodynamic torque model is suitable for this investigation. Figure 3.8 shows the constant aerodynamic torque model used with the IEC 61400-27-1 Type 4 WTG where τ_{init} is the initial aerodynamic torque which is automatically set from the load flow solution [36].

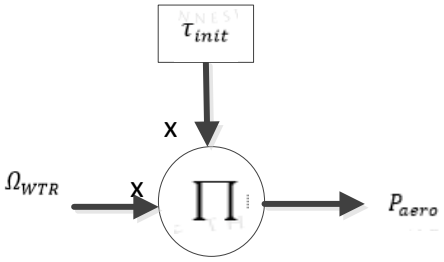

Figure 3.8: Block diagram of a constant aerodynamic torque model

3.3.2 Mechanical Model

The mechanical model consists of the two masses of the WT rotor and generator represented using their inertias linked with a shaft modelled as a spring and damper. The model replicates WT power oscillations and torsional shaft oscillations excited in the mechanical system due to torque imbalances. Figure 3.9 below shows the mechanical model block diagram implementation. The two-mass model has two inputs which are aerodynamic power, P_{aero} and generator air gap power, P_{ag} with the WT rotor speed, Ω_{WTR} and generator rotational speed ω_{gen} as output signals.

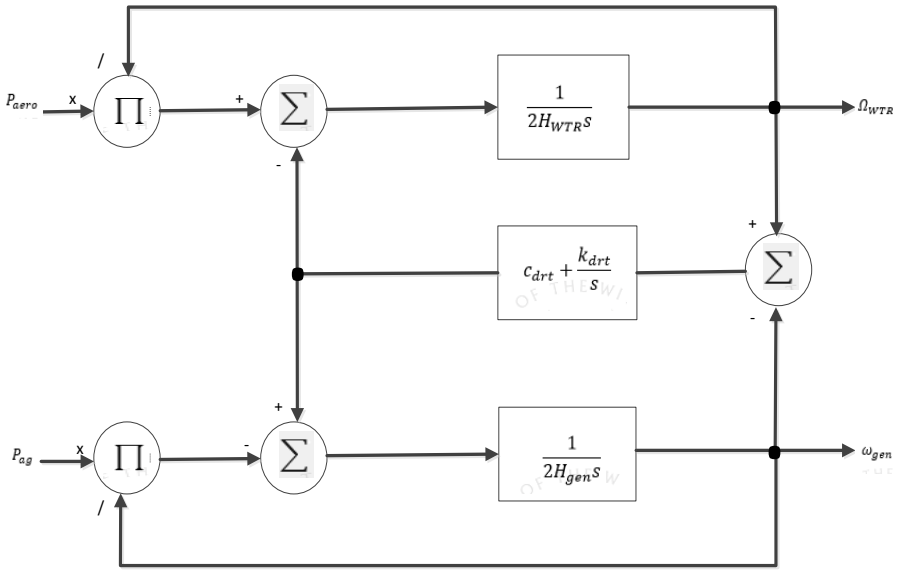

Figure 3.9: Block diagram for two-mass model [36]

Table 3.1 provides the two-mass model variables definition and their parameters adopted from the IEC 61400-27-1 Type 4 WTG model. The interaction between the two masses result in the torsional oscillation mode and has significant impact on the WTG dynamic behaviour. According to [36] these torsional modes due to the WT are in the range of 0.2 Hz to 4 Hz and can be calculated from the two mass model parameters in Table 3.1 using Eq. (3.7) where the variables have the same meaning as provided in Table 3.1.

$$f = \frac{1}{2\pi}\sqrt{\frac{k_{sh}\left(H_{WTR} + H_{gen}\right)}{2H_{WTR}H_{gen}}} \tag{3.6}$$

Table 3.1: Parameters for the two-mass mechanical model

Description	Value
Inertia constant of the wind turbine rotor, H_{WTR}	5 s
Inertia constant of generator, H_{gen}	0.7 s
Drive train damping, c_{drt}	1
Drive train stiffness, K_{drt}	80

The WPP model inertia is 5.7 s which is determined from the sum of inertia constants of the wind turbine rotor and generator provided in Table 3.1. Due to the presence of the power converter the WPP inertia is decoupled from the power system grid and the inertia will not have any contribution towards the entire power system behaviour [10].

UNIVERSITY OF THE WITWATERSRAND JOHANNESBURG

3.3.3 Generator System

IEC 61400-27-1 standard does not specify the generator model for WTs. However, standard generator models in the simulation tool should be used. Since Type 4 WTG are interfaced with the power system grid via fully-rated power converters their generators are decoupled from the grid. As such the WTGs behaviour as seen from the grid is determined by power converters [39]. For this reason, static generator models are used to represent Type 4 WTGs and other non-rotating generator system such as photovoltaic generators, reactive power compensators, fuels cells and storage devices. The static generator represents a generator without the physical dynamics. A static generator uses a voltage and current source model for steady state and dynamic simulation respectively. Table 3.2 shows the Type 4 WTG model generator settings where, I_n is the nominal current of the generator (in A).

Table 3.2: Type 4 WT generator settings

Description	Parameter
Time constant, Tg	0.01 s
Minimum reactive current ramp rate, diqmin	-100 I_n/s
Maximum active current ramp rate, dipmax	1 I_n/s
Maximum reactive current ramp rate, diqmax	100 I_n/s

3.3.4 Grid Protection Model

The WT grid protection system is characterised by over-voltages or under-voltages and over-frequencies or under-frequencies protection. WTs are expected to operate within the specified voltage and frequency limits at the same time remain connected to the power system grid. WT protection system is used to make sure that the voltages and frequencies related to the WTs are within the required limits. The WT protection system is derived from the WT fault-ride-through characteristics specified through allowable voltage level dips and durations. Typical WT fault-ride through characteristics are defined by two piecewise curves -the Low Voltage Ride Through (LVRT) and High Voltage Ride Through (HVRT). Figure 3.10 shows the WT LVRT and HVRT characteristics which was used in this dissertation.

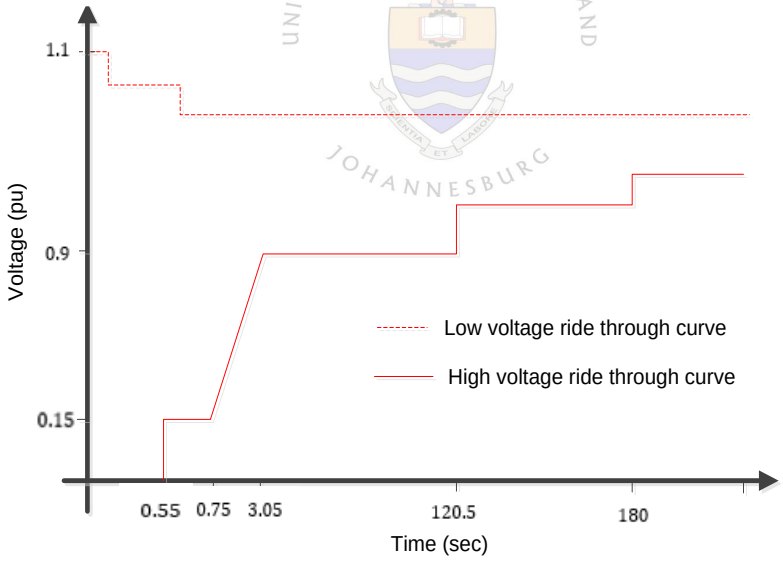

Figure 3.10: WT fault-ride through characteristics

The requirement with reference to Figure 3.10 is that the WT should operate within the LVRT and HVRT curves without disconnecting following any disturbances such as faults. The voltage limits were set at 0.9 p.u and 1.1 p.u for under-voltage and over-voltage respectively whereas the under- frequency and over-frequency thresholds were at 0.95 p.u and 1.04 p.u respectively.

3.3.5 Control Block Model

For WPPs, the control system is executed at two levels:- at WPP level and at WT unit level. At WPP level, the WPP controller communicates with the individual WT unit controllers to achieve the point of connection requirements as required by the System Operators. Figure 3.11 shows the IEC 61400-27-1 Type 4-WT modular control structure which consists of P control model, Q control model, Current limitation and Q limitation models whose functions are explained in the following subsections.

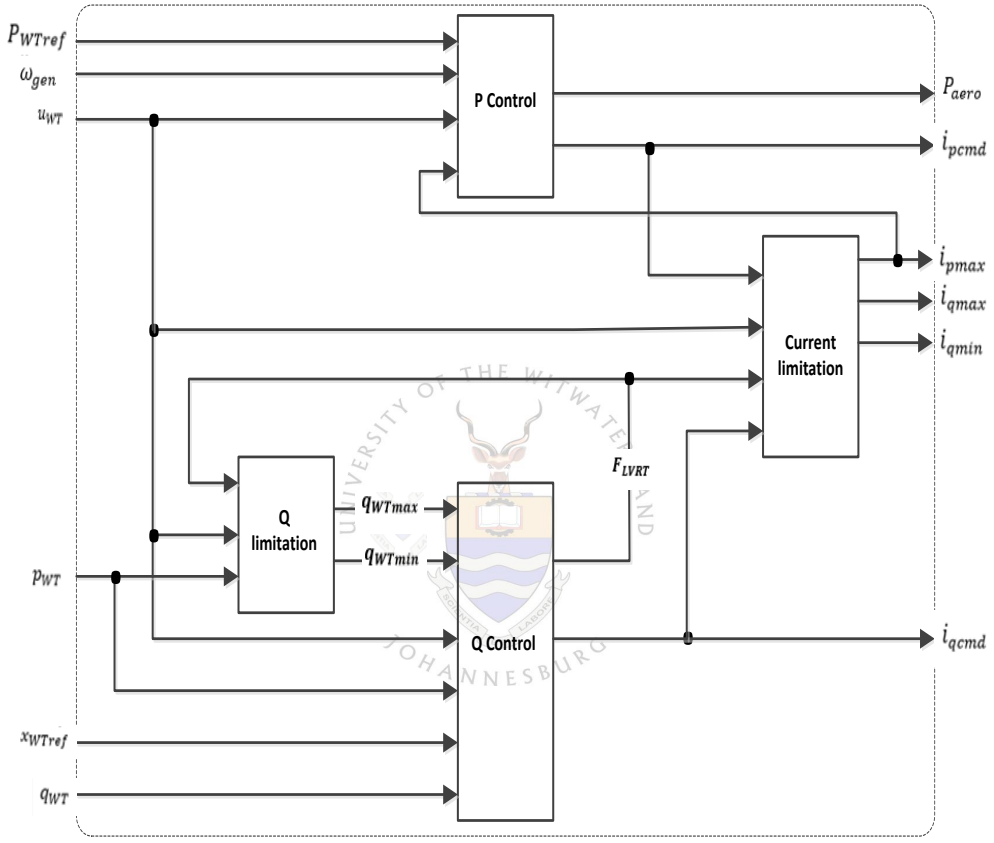

Figure 3.11: Type 4 WT control block structure [36]

P Control model

In Figure 3.11, P_{WTref} is the WT active power reference which is specified by the system operator based on power system grid requirements and u_{WT} is the WT's terminal voltage. P_{WTref}, u_{WT} and the generator rotational speed ω_{gen} are external inputs to the WT P control model to determine the WT aerodynamic power, P_{aero} and the active current command sent as set point inputs to the mechanical system and generator system respectively. To achieve this, the P control requires the allowable maximum active power current, i_{pmax} as an input, which is determined from the current limitation block. Figure 3.12 shows the block diagram implementation of the P control where T_{ufilt} is

the voltage measurement filter time constant, T_{pord} is the time constant in power order lag of a first order filter with maximum WT power ramp rate, dp_{maxp} limitation detection and T_{paero} is the time constant in aerodynamic power response.

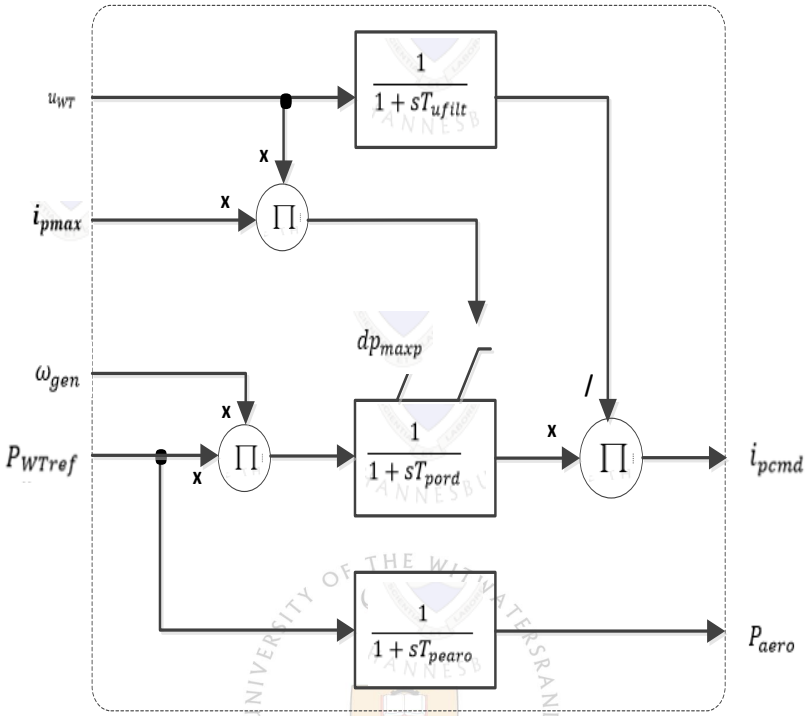

Figure 3.12: Block diagram implementation of the P control model

Table 3.3 provides the parameters and settings used for this P control.

Table 3.3: P control settings

Description	Parameter
Time constant in power order lag, T_{pord}	0.01 s
Voltage measurement filter time constant, T_{ufilt}	0.01 s
Time constant in aerodynamic power response, T_{paero}	0.5 s
Maximum wind turbine power ramp rate, dp_{maxp}	1 I_n/s

Q Control model

Figure 3.13 shows the block diagram implementation of the Q-control model which consists of two Proportional plus Integral (PI) controllers. The Q-control uses several inputs to determine the WT's LVRT flag signal and reactive current command are sent as input to the current limitation and Q-limitation functions, and to the WT's generator system model respectively. The inputs of the Q-control model are the WT's

maximum reactive power, q_{WTmax} and the WT's minimum reactive power, q_{WTmin}, which are determined from the Q-limitation function based on the LVRT flag signal, F_{LVRT} the WT's terminal voltage, u_{WT} and the WT's terminal active power, p_{WT}. The other input of the Q-control is represented by the variable x_{WTref} which can either be the WT reactive power reference or delta voltage reference depending on the WT control mode which is specified by the system operator based on the power grid requirements. The WTs operational modes can either be voltage control whereby all the WTs collectively control the point of connection voltage, power factor whereby the WTs maintain a constant power factor at the point of connection by controlling the reactive power production proportional to the active power or reactive power control whereby the WTs maintain a constant reactive power at the point of connection by supplying or absorbing the reactive power accordingly independent of the active power and the voltage. The IEC 61400-27-1 Q-control model uses only the right PI controller in Figure 3.13 while both the PI controllers are used for reactive power and power factor-control modes [14]. In addition, the IEC 61400-27-1 WT's Q control model supports the reactive power control mode, voltage control mode, power factor control mode, open loop reactive power control, and open loop power factor control. In reactive power control, the WPP controller maintains constant reactive power at the point of connection by supplying or absorbing the reactive power accordingly independent of the active power and voltage. In voltage control the WPP controls the voltage at the point of connection while in power factor control mode the WPP maintains a constant power factor at the point of connection by controlling the reactive power proportional to the active power. The open loop reactive power control and power factor control modes involve the passing the point of connection set points directly to the WT inverters. Each control mode is activated using the settings as provided in Table 3.4 in the blocks labelled M_{qG} in Figure 3.13.

Table 3.4: Q control mode and associated settings (M_{qG}) [36]

Description	Mode setting (M_{qG})
Voltage control	0
Reactive power control	1
Open loop reactive power control	2
Power factor control	3
Open loop power factor control	4

The variables p_{WT} and q_{WT} represent the WT's terminal active power and reactive power respectively measured from the WT terminals. x_{WTref}, u_{WT}, p_{WT} and q_{WT} are external input parameters required to determine the LVRT flag signal, F_{LVRT} through the delay function and reactive current command which are the Q-control outputs. The delay function provides the LVRT flag signal based on the comparison of the WT terminal voltage, u_{WT} and specified voltage threshold for LVRT detection, u_{dip} in one of the three stages described in Table 3.5.

Table 3.5: Description of F_{LVRT} flag signal values

Description	Mode setting
Normal operation ($u_{WT} > u_{dip}$) where u_{qdip} is the voltage threshold for LVRT detection	0
During fault ($u_{WT} \leq u_{dip}$)	1
Post fault stays in stage 2 with ($u_{WT} > u_{dip}$) for ($t = T_{post}$)	2

The LVRT flag signal is sent as an input to the current limitation and Q-limitation functions while the reactive current command is sent as an input to the WT's generator system model respectively. IEC 61400-27-1 WT's Q control model supports three different LVRT modes where each control mode can be selected in the blocks labelled **M_{qLVRT}** in Figure 3.13 using settings provided in Table 3.6. During a fault or post fault (i.e. LVRT flag signal is 1 or 2 respectively according to Table 3.5), a freeze signal is sent to the PI controllers otherwise the PI controller functions as desired under normal operating condition (i.e. LVRT flag signal is 0 according to Table 3.5).

Table 3.6: Low-voltage ride through modes and associated settings (M_{qLVRT}) [36]

Description	Mode setting (M_{qLVRT})
Voltage dependent reactive power injection	0
Reactive current injection controlled as the pre-fault value plus an additional voltage dependent reactive current injection	1
Reactive current injection controlled as the pre-fault value plus an additional voltage dependent reactive current injection during fault, and as the pre-fault value plus an additional constant reactive current injection post fault	2

The Q-control model includes a voltage droop block which is used to determine the voltage at a remote point, for example at the voltage at the high voltage side of the pad mount transformer [36]. The voltage drop is calculated considering the series impedance $(r + jx)$ from the WT terminals to the desired point. This voltage droop function is calculated by Eq. (3.7).

$$u = \sqrt{\left(u_{WT} - r_{droop}\frac{P_{WT}}{u_{WT}} - x_{droop}\frac{q_{WT}}{u_{WT}}\right)^2 + \left(x_{droop}\frac{P_{WT}}{u_{WT}} - r_{droop}\frac{q_{WT}}{u_{WT}}\right)^2} \quad (3.7)$$

-where r_{droop} and x_{droop} are the series resistance and reactance from the WT terminal to the remote point.

Table 3.7 provides the settings of the Type 4 WT Q-control model adopted in this dissertation. IEC 61400-27-1 Type 4 WT default Q-control settings were adopted in this dissertation however the WT was set to operate in voltage control mode. This was based on conclusions and recommendations in [40] that when WT's are operated in voltage control the system becomes stiffer which results in a less damped system.

Table 3.7: WT Q-control model settings

Description	**Parameter**
Reactive power PI controller integration gain, Klq	5
Q-Control mode, MqG 0 = U, 1= Q, 2 = QOL, 3= PF, 4= OLPF	-
Voltage PI controller integration gain, Klu	25
Reactive power PI controller proportional gain KPq	1 V_n/P_n
Voltage PI controller proportional gain KPu	1 I_n/V_n
User defined bias in voltage reference uref0	0 V_n
Time constant in reactive power order lag Tqord	0.1 s
Power measurement filter time constant Tpfiltq	0.01 s
Resistive component voltage droop impedance rdroop	0
Inductive component of voltage droop impedance xdroop	0
Voltage measurement filter time constant Tufiltq	0.01 s
Voltage threshold for LVRT detection in Q-control uqdip	0.9 V_n
Length of time period where post fault reactive power is injected Tpost	0.1 s
Voltage dead band lower limit udb1	0.9 V_n
Voltage dead band upper limit udb2	1.1 V_n
Post fault reactive current injection iqpost	0 I_n
Voltage scaling factor for LVRT current Kqv	2 I_n/V_n
LVRT Q-Control modes, M_{qUVRT} [0/1/2]	-
Minimum voltage in voltage PI controller integral term umin	0.01 V_n
Minimum reactive current injection iqmin	-1 I_n
Maximum voltage in voltage PI controller integral term umax	1.1 V_n
Maximum reactive current injection iqmax	1 I_n
Maximum reactive current injection during dip iqh1	1 I_n

UNIVERSITY OF THE WITWATERSRAND JOHANNESBURG

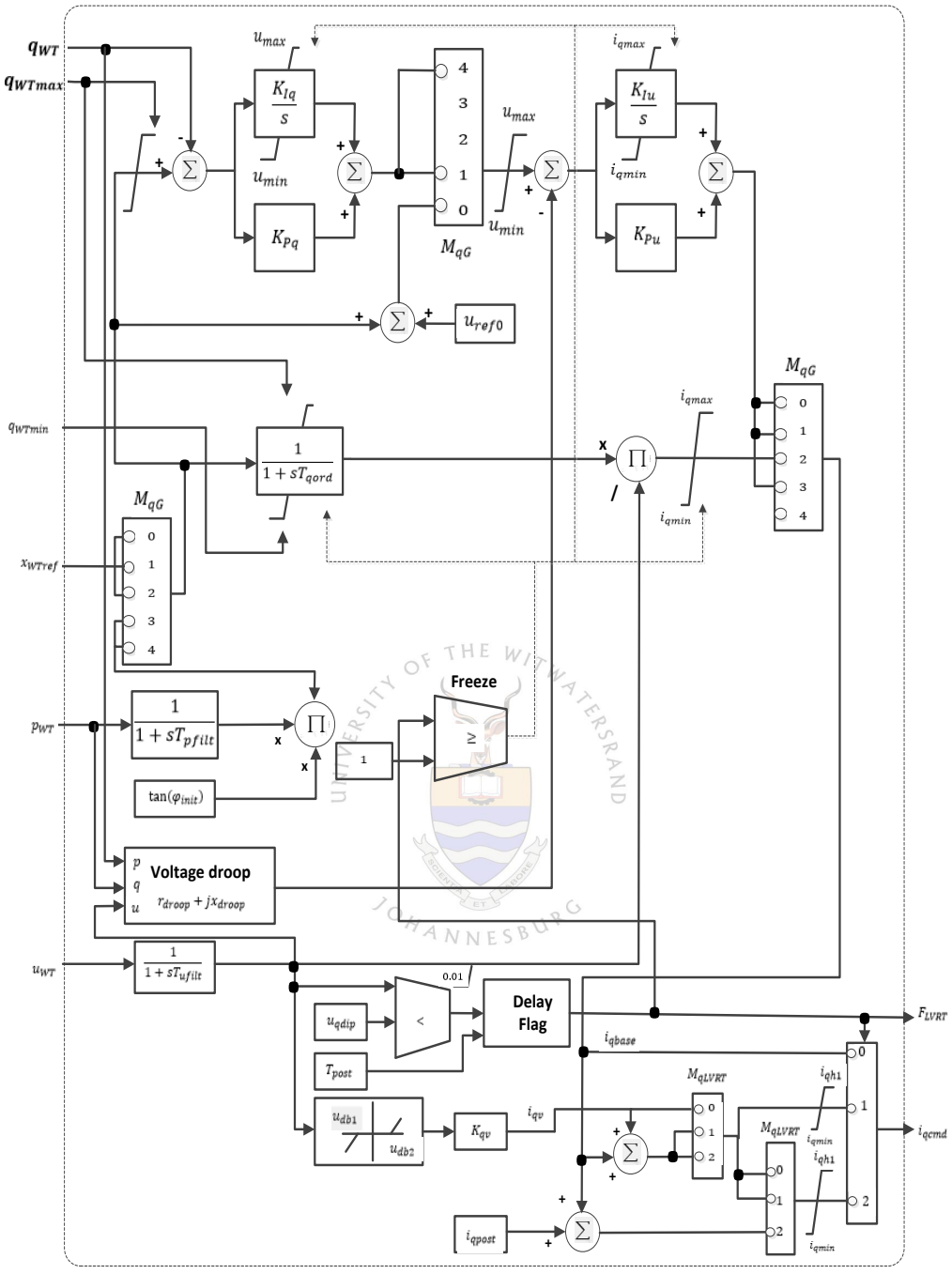

Figure 3.13: Block diagram implementation of the Q Control model

Current limitation model

The current limitation model combines the individual WT physical and control limits. The current limiter settings include look-up tables for the WT's voltage and maximum active, and reactive currents. Figure 3.14 shows the block diagram implementation of the current limitation model. The current limitation model uses four input signals to determine the WT's maximum continuous active current, i_{pmax} and the WT's maximum, i_{qmax} and minimum reactive current i_{qmin} which are sent as input signal to the generator system. The input signals are the WT terminal voltage, u_{WT}, the Q-control LVRT flag signal, F_{LVRT}, the WT active current command signal i_{pcmd} from the P control model and the WT reactive current command signal from the Q-control model, i_{qcmd}. In Figure 3.14 the generator rotational speed, ω_{gen} input is not used for Type 4 and this is ensured by setting the M_{DFSLim} = 1 [36]. Table 3.8 shows the current limiter model settings which were used in this dissertation and the corresponding look-up tables for WT voltage and maximum active, and reactive currents are provided in Table 3.9.

Table 3.8: Current limiter settings

Description	Parameter
Maximum continuous current at WT terminals	1.1 I_n
Maximum current during voltage dip at the WT terminals	1.2 I_n
Stator current limitation M_{DFSLIM} (0: total current, 1: stator current for Type 4)	1
Prioritisation of Q-control during LVRT (0: active power; 1: reactive power)	1
Lookup table for voltage dependency of active current limits	see Table 3.9
Lookup table for voltage dependency of reactive current limits	see Table 3.9
Voltage measurement filter time constant	0.01 s
WT voltage in the operation point where zero reactive current can be delivered	2
Partial derivative of reactive current limit vs. voltage	2

Table 3.9: WT voltage and maximum active and reactive current settings

Ipmax (p.u)	WT voltage (p.u)	Iqmax (p.u)
1	0	1
1	1	1
1	2	1

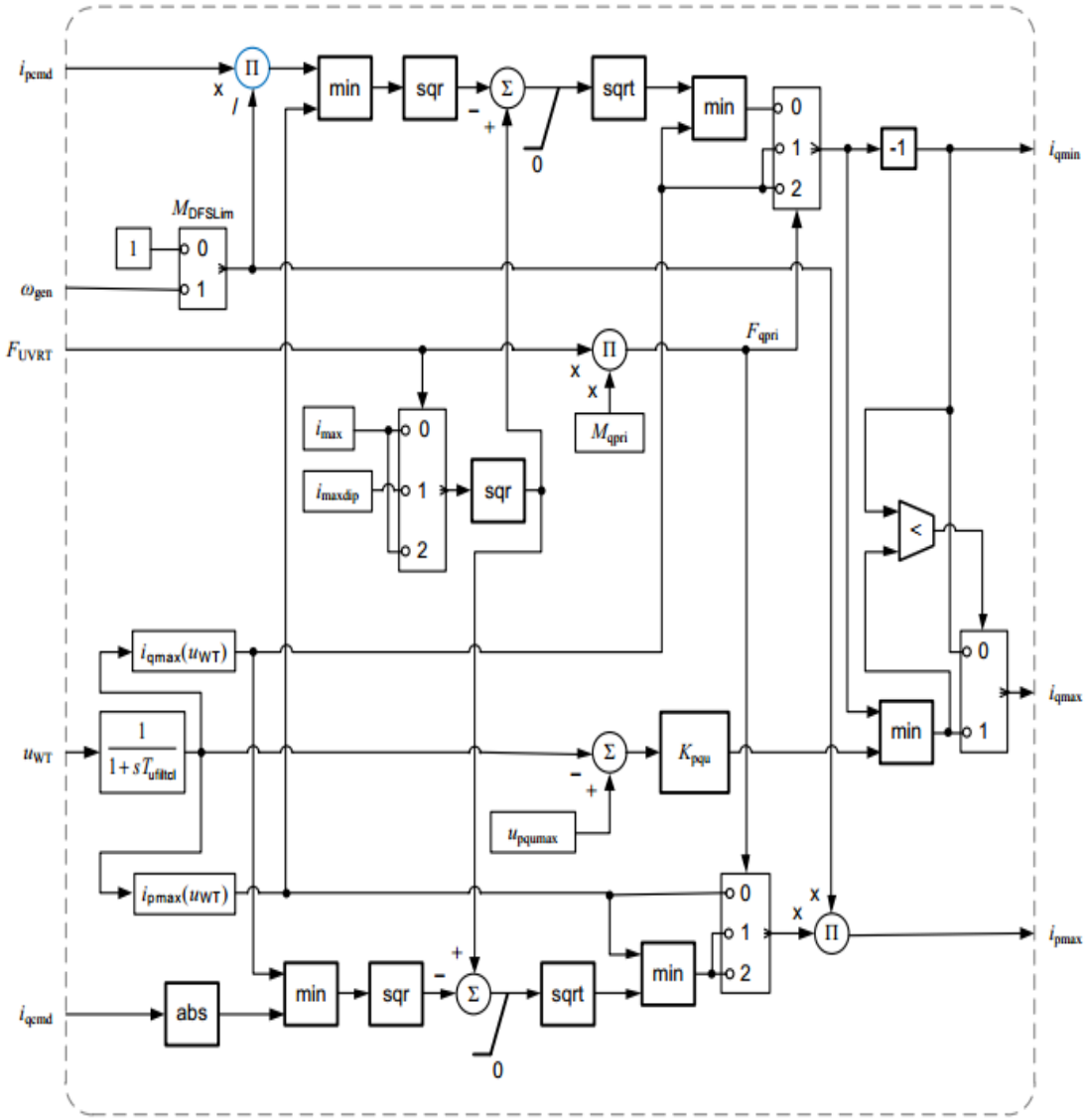

Figure 3.14: Block diagram implementation of the current limitation model

Q limitation model

The Q-limitation model is implemented as the QP and QU limitation models for IEC 61400-27-1 Type 4 WT generic models. The Q-limiter model determines the WT's maximum reactive power, q_{WTmax} and the WT's minimum reactive power, q_{WTmin} which are used as input to the Q-control model. The Q-limitation function is based on the LVRT flag signal, F_{LVRT} the WT's terminal voltage, u_{WT} and the WT's terminal active power, p_{WT} inputs. Figure 3.15 is the Q-limitation model block diagram implementation. Table 3.10 provides the settings of the Q-limiter model while Table 3.11 and Table 3.12 provides the reactive power capability of the Type 4 WT used for this study.

Table 3.10: Q-limitation (or QP and QP limitation) model

Description	Parameter
Voltage measurement filter time constant for Q capacity	0.01
Power measurement filter time constant for Q capacity	0.01
Lookup table for active power dependency of reactive power maximum limit	see Table 3.11
Lookup table for active power dependency of reactive power minimum limit	see Table 3.11
Lookup table for voltage dependency of reactive power maximum limit	see Table 3.12
Lookup table for voltage dependency of reactive power minimum limit	see Table 3.12

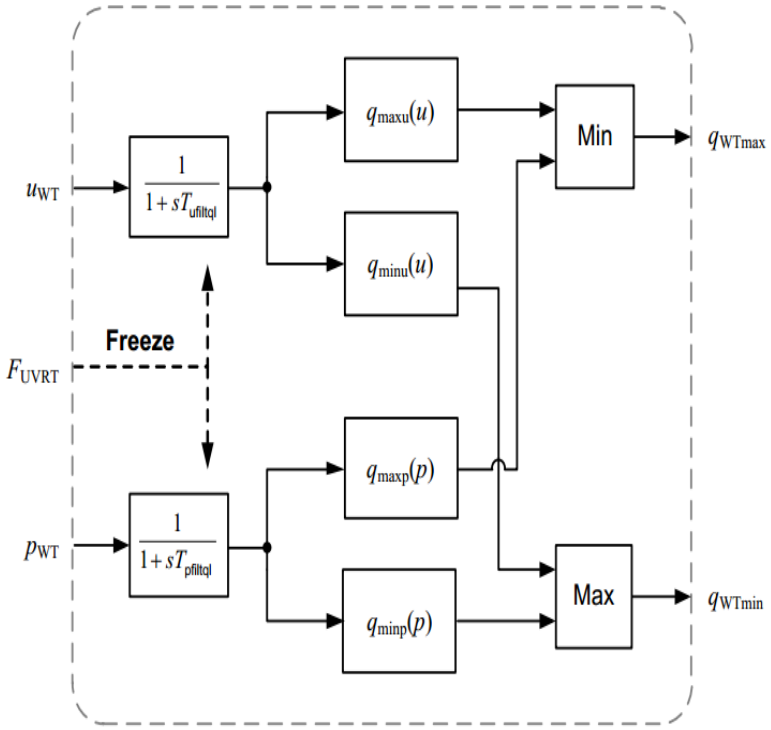

Figure 3.15: Block diagram implementation for QP and QU limitation model

Table 3.11: WT power dependency of reactive power

Qmin (p.u)	WT power (p.u)	Qmax (p.u)
0	0	0
-0.33	0.3	0.33
-0.33	1	0.33

Table 3.12: WT voltage dependency of reactive power

Qmin (p.u)	WT voltage (p.u)	Qmax (p.u)
0	0	0
-0.33	0.8	0.33
-0.33	0.9	0.33

3.4. Aggregation of Wind Power Plants (WPPs)

In [12] the WECC provided recommendations for the WPP aggregation approach to be used when modelling WPPs to investigate the impact of wind power on the electric power system. WECC recommends the use of the single-machine equivalent representation in Figure 3.16 to model the WPPs where the equivalent WTG is a single WTG but specified with the total number of all the WTG of the WPP being in parallel.

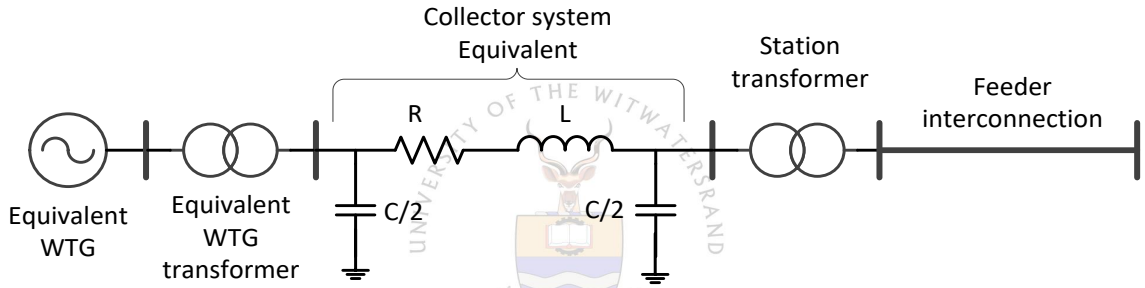

Figure 3.16: Single-machine equivalent WPP model layout

The equivalent WTG system represents the total generating capacity of all the WTGs of the WPP and the associated power factor correction capacitors. The equivalent aggregated WPP capacity is equal to specified number of parallel WTGs times the single generator MVA rating. The equivalent WTG step-up transformer represents the aggregated effect of all the WPP's WTG step-up transformers. The total number of the WPP's WTG step-up transformers is specified as the total number of the WTG step-up transformers in parallel. This lumped equivalent WTG transformer rating is determined by the product of the single transformer rating and number of transformers used. The WPP collector system consist of relatively long medium voltage cables represented as the equivalent collector system in Figure 3.16. The equivalent collector system represents the aggregate effect of the WPP collector system while approximating the full WPP power losses and voltage drops [12]. A method developed in [41] can be used to derive the equivalent impedance, Z_{eq} and equivalent susceptance, B_{eq} of the WPP collector cable system through Eq. (3.8) and Eq. (3.9) respectively.

$$Z_{eq} = R_{eq} + jX_{eq} = \frac{\sum_{i=1}^{I}(R_i + jX_i)\, n_i^2}{N^2} \tag{3.8}$$

$$B_{eq} = \sum_{i=1}^{I} B_i \tag{3.9}$$

-where I is the total number of branches of the WPP collector cable, $R_i + jX_i$ is the impedance for the i_{th} branch, n_i is the number of WTGs seen downstream of the i_{th} branch; and N is the total number of WTGs.

The WPP station transformers, WPP reactive power compensation and the feeder interconnector must be modelled explicitly. Using a single-machine representation of the WPP as explained earlier rather than a detailed WPP model implies that the internal behaviour within the WPP is neglected. However, this has several advantages of reduced simulation times than a complete WPP model when performing grid impact studies. This representation is also considered adequate for positive-sequence dynamic simulations.

3.5. Development of the Aggregated Wind Power Plant (WPP) Model

The guidelines for modelling aggregated Wind Power Plants (WPP) from reference [12] were adopted in this dissertation to develop a WPP model. An aggregated WPP representation is derived from a full WPP as discussed in the previous section. Realistic aggregated WPPs and the equivalent collector system data provided in reference [12] were adopted and used to develop a 100 MW WPP. The WPP size and the collector system parameters given on 100 MVA and the collector system voltage base in Table 3.13 from reference [12] were adopted. With reference to Section 2.4.3 and the equivalent collector system data provided in Table 3.13 the collector system is represented using the medium transmission line modelled using the nominal π-model equivalent circuit which includes the series and shunt parameters.

Table 3.13: Sample of equivalent collector system parameters [12]

WPP size (MW)	Collector system voltage (kV)	Equivalent collector cable parameters		
		R (p.u)	X (p.u)	B (p.u)
100	34.5	0.017	0.014	0.030

In DIgSilent PowerFactory, the WPP aggregation is achieved by specifying the total number of the WTGs and pad mount transformers of the WPP within the static generator and transformer models respectively. This results in the single static generator rating being multiplied by the specified number of the WTGs WPP to obtain the total installed WPP capacity. The IEC 61400-27-1 Type 4 WTG model template

consist of the static generator rated at 2 MVA with a unity power factor and a stator terminal voltage of 0.69 kV connected to a 0.69/34.5 kV 2.1 MVA transformer. The number of parallel machines and parallel transformers was set to 50 to model a 100 MW WPP with a capacity of 100 MVA with the default settings. The transformer was connected to a single 34.5 kV equivalent cable collector system whose parameters are provided in Table 3.13 and then connected to a 34.5/230 kV station transformer. IEC 61400-27-1 does not specify the station transformer size and rating as these parameters are dependent on the WPP capacity. In this dissertation, the station transformer was modelled as a 105 MVA, 34.5/230 kV transformer with 10% positive sequence impedance. The WPP model was built and simulated using the DIgSilent PowerFactory to investigate its load flow, dynamic behaviour and small-signal stability characteristics. For accurate results and convergence during simulation the models work with integration time steps up to a quarter cycle of the power frequency. As such, the minimum allowable time constants of the model are two times the integration time step (i.e. 0.01sec) [36]. In addition, power converters of variable-speed WTs are modelled using switches whose operating frequencies are in the kHz range thus smaller simulation time steps are required. Figure 3.17 shows the simulated single line diagram of the developed WPP using the equivalent collector system parameters in Table 3.13.

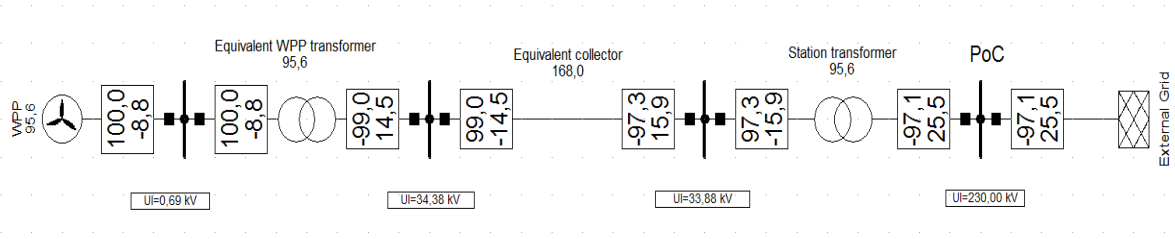

Figure 3.17: Simulated WPP model in DIgSilent PowerFactory

In Figure 3.17, PoC represents the point of connection at which the WPP will be connected to the study system for the evaluation of the impact of wind generation. Figure 3.17 shows the voltage levels, component loading and the power flows of the developed WPP model. The power losses of the WPP model are around 3% which is considered acceptable according to reference [41]. The reactive power is adjusted according to the WTG reactive power capability to maintain the voltage at the WPP point of connection.

The WPP model voltage dynamic behaviour which tests for the voltage ride through capabilities relates to the voltage stability of wind farms. This test was not performed in detail since it was not the focus of this investigation. However, the dynamic behaviour of the WPP developed is worth investigating since this will be considered when the WPPs are integrated to the test in the following chapter. This was done using a 3-phase fault without any fault impedance at the point of connection to determine the WPP behaviour during transient conditions. The fault was cleared after 150 milliseconds. This is a typical fault condition which is applied when investigating the capability of WPPs' voltage ride through based on the South African Renewable Energy Grid Code [5]. The WPP is expected not to trip because of the applied fault but to recover to its initial operating point when the fault is cleared. Figure 3.18 shows the WPP's point of connection terminal voltage, active power and reactive power responses to the 3-phase fault. From Figure 3.18, the pre-fault WPP's point of connection voltage was 1 p.u which drops

to zero when the fault was applied and recovers to its initial value when the fault was cleared with a small overshoot. During the fault, the WPP active power reduced from 97.1 MW to zero and recovers to its initial value before the fault inception. From Figure 3.18, the reactive power increases during the fault, as the active power decreases, to support the WPP voltage at the point of connection. With reference to these dynamic simulation results, the developed WPP model performs as required during fault conditions.

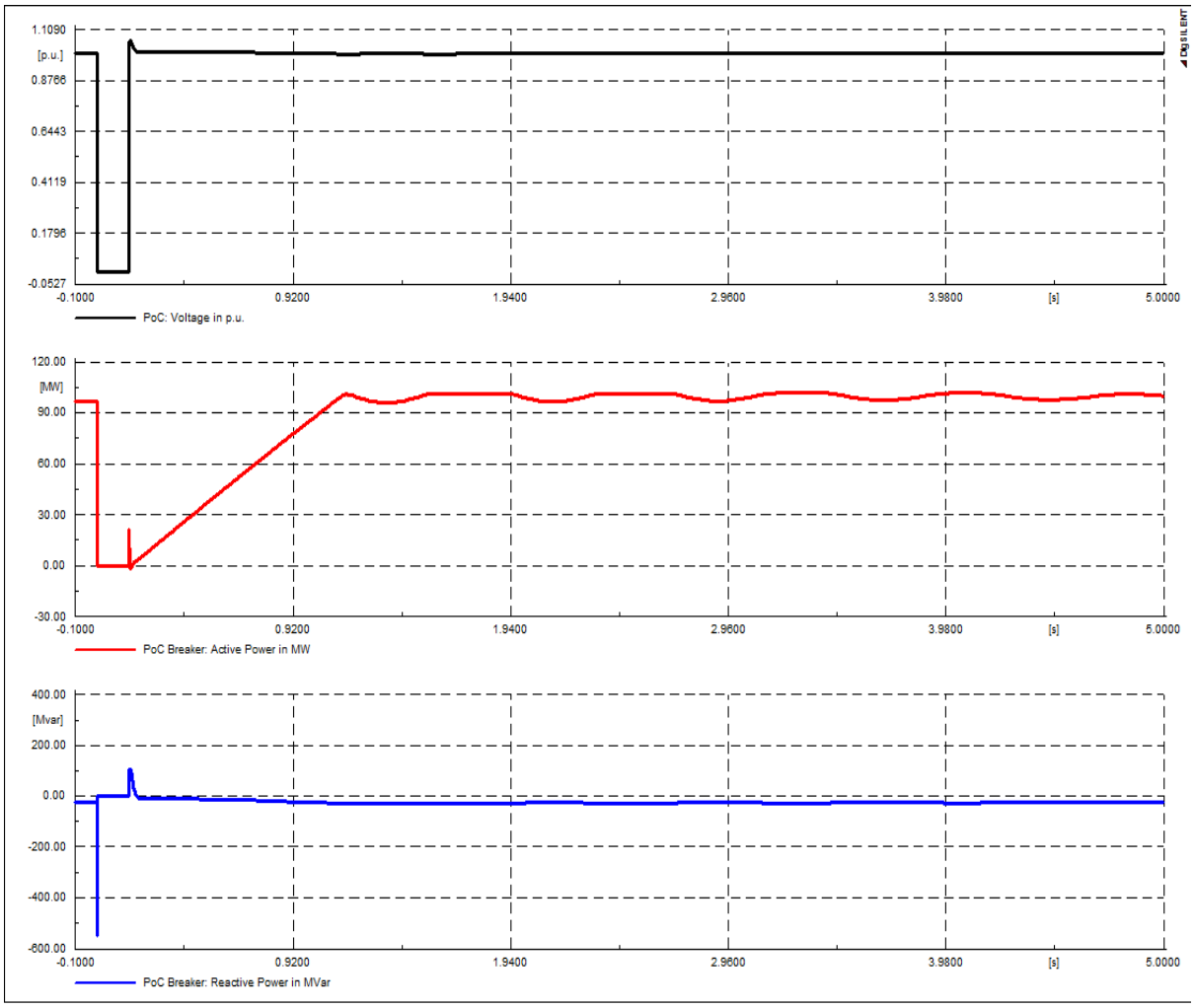

Figure 3.18: WPP point of connection terminal voltage, active power and reactive power responses

The small-signal analysis of the developed WPP model was conducted to determine the oscillation mode characteristic of the developed WPP before it was integrated to the test power system. Figure 3.19 shows the WPP model eigenvalue plot obtained from the small-signal analysis. The eigenvalue analysis shows that the WPP had two oscillatory modes at 1.29 Hz and 6.1 Hz with eigenvalues at -0.412 ± j 8.112 and -90.124 ± j 38.17 respectively. The system participation factor was used to further explore these modes. The system participation factor revealed that the 1.29 Hz mode is a torsional mode due to the interaction of the generator and WT rotor modelling constituting the mechanical two mass model as described in Section 3.3.2.

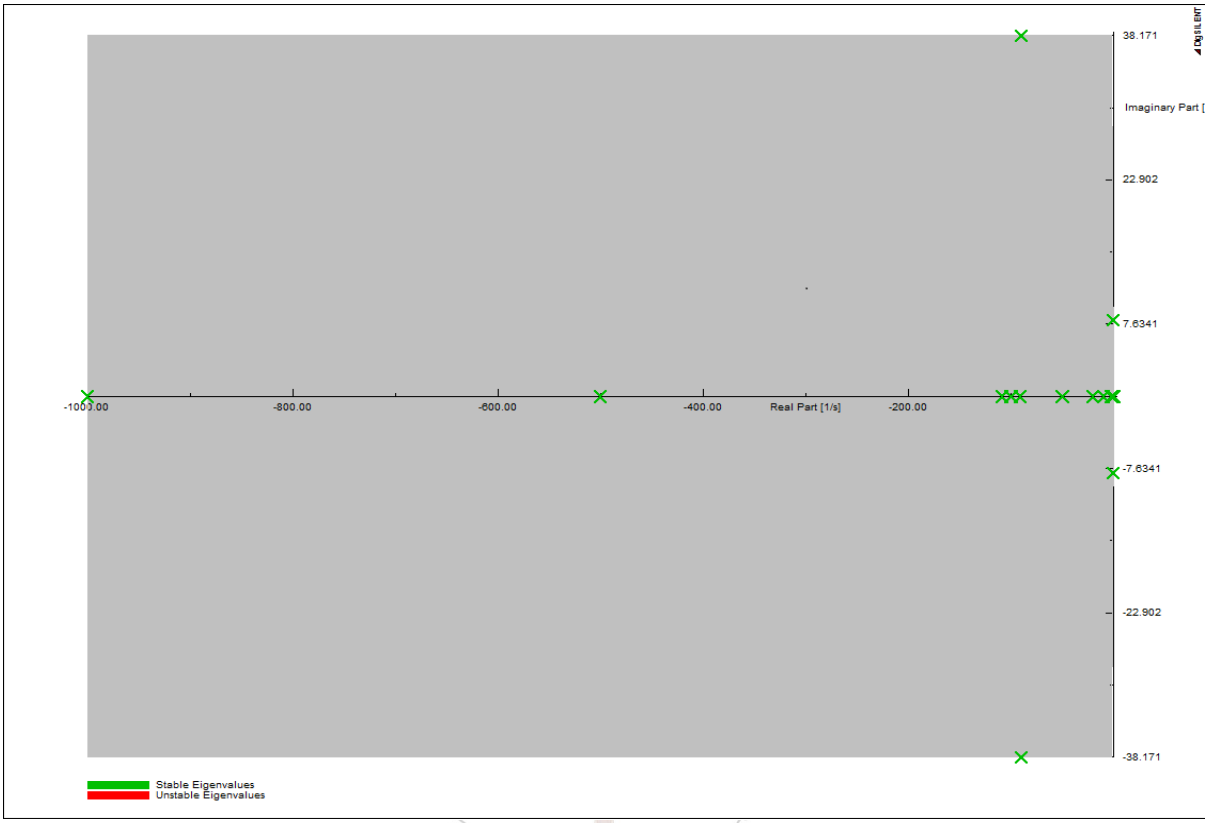

Figure 3.19: WPP model eigenvalue plot

Using Eq. (3.6) and the two mass model parameters in Table 3.1 the torsional oscillation mode frequency was verified as:

$$f = \frac{1}{2\pi}\sqrt{\frac{k_{sh}\left(H_{WTR} + H_{gen}\right)}{2H_{WTR}H_{gen}}} = \frac{1}{2\pi}\sqrt{\frac{80 \times (5 + 0.7)}{2 \times 5 \times 0.7}} \approx 1.29\ Hz$$

The 6.1 Hz mode, which was well damped at about 92%, according to the system participation factors corresponded to the WPP controllers. Different WPPs capacities of 100 MW were realized by increasing the number of parallel machines, pad-mount transformer, and equivalent collector cable system and station transformers. It important to note that the realized WPP MVA ratings were equal to the WPP MW outputs since the WTG used were rated at unity power factor. Similar dynamic behaviour and small-signal characteristics were observed between the 100 MW WPP and various realized WPP models. This is expected since the dynamic model does not change as the capacity increases.

3.6. Summary

This chapter has developed and presented an aggregated 100 MW WPP, based on the IEC 6400-27-1 Type 4 variable-speed WTG model, to be used for investigating the impact of wind generation on the inter-area and local oscillation modes of power systems. The model has

been developed from the aggregated WPP size and equivalent collector system parameters of a 100 MVA WPP from reference [12]. The model was set to operate in voltage control mode while the other default parameter settings provided in DIgSilent PowerFactory were adopted. The WPP was built and simulated using DIgSilent PowerFactory to investigate its load flow, dynamic behaviour and small-signal characteristics. The WPP model load flow, dynamic response to a three-phase fault and small-signal analysis were performed. The load flow results indicate the active power losses were within 3% which is acceptable in accordance to [12]. The model is able to withstand a three-phase fault for 150 milliseconds in accordance with the South African Grid Code for Renewable Power Plants without tripping. During the fault, the WPP could supply reactive power to support its voltage at the point of connection when the active power is zero. The small-signal analysis of the WPP revealed the torsional oscillation modes at 1.29 Hz due to the interaction of the generator and the WT rotor. The torsional oscillation mode was verified using the empirical formula. Another oscillation mode at 6.1 Hz resulting from the WPP controllers was observed during the small-signal analysis. It can be considered that the developed WPP represented a realistic wind farm which can be used for this work. The model is used to realize different WPP capacities of 100 MW by increasing the number of parallel machines, pad-mount transformer, and the equivalent collector cable system and station transformers to be used in the studies in the following chapters.

CHAPTER 4 : POWER SYSTEM STABILIZER (PSS) DESIGN

This investigation considered the design and implementation of PSSs for the Two Area Multi-Machine (TAMM) system before investigating the impact of wind power on the inter-area and local oscillation modes. This chapter focuses on the design and testing of PSSs. Firstly, the focus is on the application of small-signal analysis demonstrating the effect of the synchronous generator excitation control system and the requirements of PSSs. The small-signal stability analysis considered two generator control strategies namely; manual excitation control and closed-loop (or automatic) excitation control. The chapter proceeds with the design of PSSs using conventional control design methods (phase-lead, eigenvalue analysis and root-locus technique). In addition, the performance of the designed PSSs is evaluated under different operating conditions to establish the PSSs adequacy in providing damping before integrating additional wind power sources.

4.1. Small-Signal Analysis of the Two-Area-Multi-Machine (TAMM) System

The Two-Area-Multi-Machine (TAMM) system is used in this investigation as a test system to analyse the power system oscillation modes firstly without the designed PSSs with and without additional sources of wind power generation. Figure 4.1 shows the single-line diagram of the TAMM system. The TAMM system small-signal stability was firstly analysed with the synchronous generators operating in manual excitation control and with automatic excitation control to demonstrate the effect of the excitation control system.

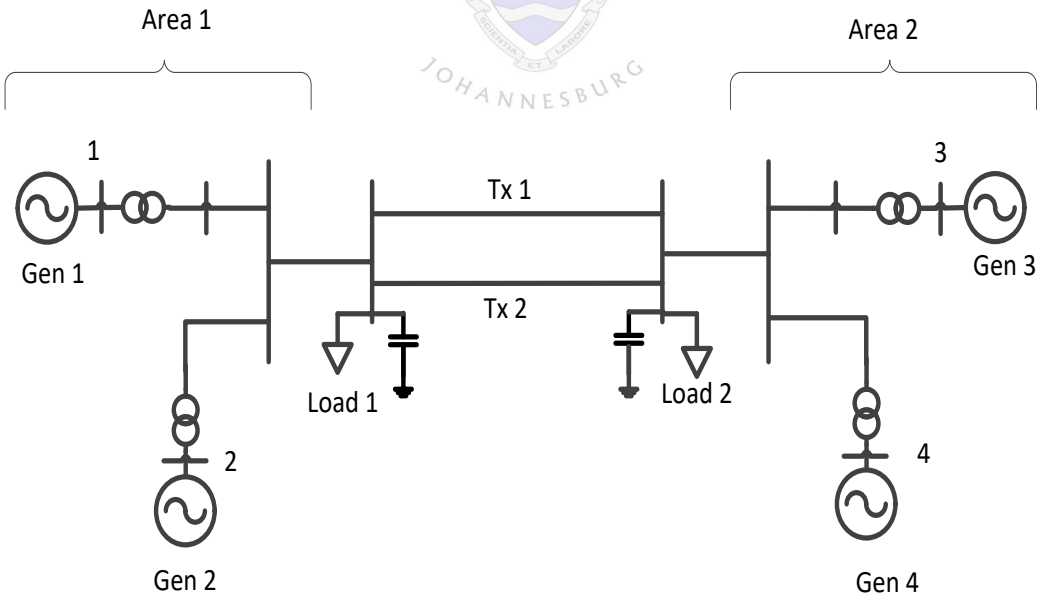

Figure 4.1: Two-Area-Multi-Machine (TAMM) test system

4.1.1 Synchronous generator operating with manual control

The modal analysis results of the TAMM system when the synchronous generators were operating with manual excitation control revealed three stable modes (two local and an inter-area oscillation modes). Table 4.1 provides the modal analysis results showing the dominant modes eigenvalues, frequencies and damping ratios when the generators were operating in manual excitation control mode. Table 4.2 provides the mode shapes (magnitude and angle) which determines the characteristics of the oscillation modes. From the mode shapes in Table 4.2, Mode 1 is an inter-area mode whereby generators Gen 01 and Gen 02 of area 1 are oscillating against generators Gen 03 and Gen 04 of area 2. This is shown by the ***REV*** angles of generators Gen 01 and Gen 02 which are out of phase with the ***REV*** angles of generators Gen 03 and Gen 04 as provided in Table 4.2. In addition, the frequency 0.54 Hz of Mode 1 falls within the frequency range (0.25 Hz to 0.8 Hz) of the inter-area modes as described in Chapter 1 and further supports that Mode 1 is an inter-area oscillation mode. From Table 4.1, the TAMM system is stable since all the eigenvalues of the modes have negative real parts. The inter-area mode eigenvalues are complex with a negative real part which indicates that the modes reside in the left half of the complex plane hence the inter-area mode is stable. However, its corresponding damping ratio is 4.1% which is below the minimum damping criterion of 5% according to reference [7]. This implies that although the inter-area mode is stable its damping ratio must be improved.

Table 4.1: Small-signal stability analysis with manual excitation control

	Mode 1	**Mode 2**	**Mode 3**
Eigenvalue	-0.139 ± j 3.410	-0.626 ± j 6.673	-0.636 ± j 6.895
Frequency in Hz	0.54 Hz	1.06 Hz	1.10 Hz
Damping ratio (ζ)	0.041	0.093	0.091
Damping ratio (%) ($\zeta \times 100$)	4.1%	9.3%	9.1%

Table 4.2: Mode shapes with manual excitation control

Generator	**Mode 1**		**Mode 2**		**Mode 3**	
	$\lvert REV \rvert$	$\angle REV$	$\lvert REV \rvert$	$\angle REV$	$\lvert REV \rvert$	$\angle REV$
Gen 01	0.002	112.40	0.013	95.84	0.000	96.05
Gen 02	0.001	122.82	0.016	-86.73	0.000	-29.58
Gen 03	0.847	-91.67	0.002	109.37	0.387	-82.52
Gen 04	0.007	-92.28	0.002	-69.97	0.577	93.64

From the mode shapes in Table 4.2, Mode 2 is the local mode involving generators Gen 01 and Gen 02 of area 1 oscillating against each other. This is also shown by the ***REV*** angles of the generators which are out of phase as shown in Table 4.2. Moreover, the frequency 1.06 Hz of Mode 2 falls within the typical frequency range of the local modes 0.8 Hz to 2 Hz which further supports that Mode 2 is a local mode.

The eigenvalues of this local mode are also complex with a negative real part which indicates that the corresponding mode is stable. Its corresponding damping ratio is 9.3% which is above the minimum damping ratio requirement of 5%. Similarly, Mode 3 is area 2 local mode whereby generators Gen 03 and Gen 04 are swinging against each other as shown by their ***REV*** angles in Table 4.2 which are out of phase. The frequency 1.10 Hz of Mode 3 is within the typical frequency range of the local modes which corroborates that Mode 3 is a local mode which was stable with a damping ratio of 9.1%.

It must be noted that the small-signal stability analysis of this TAMM system in its original form from reference [3] as studied here has been presented in various literature. The results obtained in this dissertation with the generators operating in manual excitation control show some differences from the results in reference [3] although the overall system small-signal stability characteristics are similar (stable system with two local modes and one inter-area modes). The differences can be attributed to the use of different software.

4.1.2 Synchronous generators operating with automatic excitation control

Table 4.3 shows the eigenvalue results obtained when the generators were operating with automatic excitation control using the IEEE AC4 excitation system model in Figure 2.10. From Table 4.3, the results reveal that the number of modes when the generators are operating with automatic excitation control remain the same however their characteristics are significantly changed. This is expected since the total number of generators remained the same while the associated generator controls are changed. However, the introduction of the automatic excitation control reduced the inter-area and local mode damping and eventually caused the inter-area mode to be unstable. The inter-area mode eigenvalues shifted into the right-half of the complex plane and this was associated with an increase in the frequency from 0.54 Hz to 0.61 Hz and a negative damping ratio of 1.22% from positive damping ratio of 4.1%.

UNIVERSITY OF THE WITWATERSRAND JOHANNESBURG

Table 4.3: Small-signal stability analysis with automatic excitation control on the generators

	Inter-area mode	Area 1 local mode	Area 2 local mode
Eigenvalue	0.047 ± j 3.816	-0.637 ± j 7.015	-0.638 ± j 7.229
Frequency in Hz	0.61 Hz	1.12 Hz	1.15 Hz
Damping ratio (ζ)	0.0122	0.0949	0.0879
Damping ratio (%) ($\zeta \times 100$)	-1.2%	9.0%	8.8%

The local mode frequencies and damping ratios also changed with the introduction of the automatic excitation control on the generators. The frequencies of the area 1 and area 2 local modes exhibited slight increase from 1.06 Hz to 1.12 Hz and 1.10 Hz to 1.15 Hz respectively. The introduction of the automatic excitation control on the generators resulted in the local modes damping ratio decreasing. The impact of the high gain and fast response excitation system have indicated an adverse effect on the power system small-signal stability. These findings concur with the work of de-Mello and Concordia in [18]. Based on these eigenvalue results, it is further confirmed that the generators with

higher inertias contribute to low mode frequencies. This is supported by generators Gen 01 and Gen 02 of area 1 with inertia constants of 6.5 s oscillating at 1.12 Hz while generators Gen 03 and Gen 04 of area 2 with inertia constants of 6.175 s were oscillating at 1.15 Hz.

4.1.3 Time Domain Simulation

In order to support and validate the small-signal analysis results of the TAMM with the generators operating with automatic excitation control, time domain studies using small disturbances were performed while observing the response of the system control outputs and variables. It is expected that the system variables exhibit the oscillation modes as reviewed in the previous section. Figure 4.2 shows the power flow response in the transmission line connecting the two areas after applying a 3% step change in area 1 active load. A 3% step change was chosen for this purpose so that the excitation system limiters were not activated as this would result in a non-linear condition for which the results would not be comparable to the modal analysis results. Figure 4.2 shows the inter-area power flow over transmission line 1 which exhibited a growing oscillation mode.

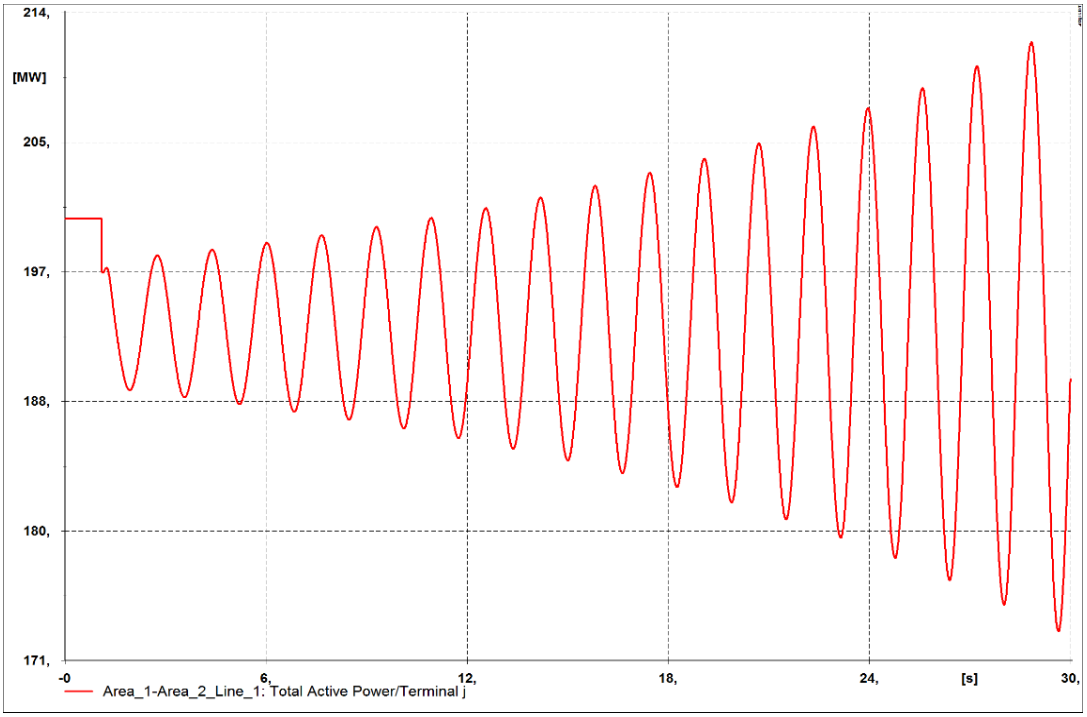

Figure 4.2: Inter-area power flow over transmission line 1

The Fast Fourier Transform (FFT) was used to determine the frequency component present in the inter-area active power flow. The inter-area power flow FFT analysis is shown in Figure 4.3 which indicates a 0.61 Hz frequency component corresponding to the inter-area mode as determined through the modal analysis. Based on the linear modal analysis results presented in the previous section and the non-linear time domain response with the application of the FFT, there is a correlation between the two approaches with respect to the identification of the oscillation mode.

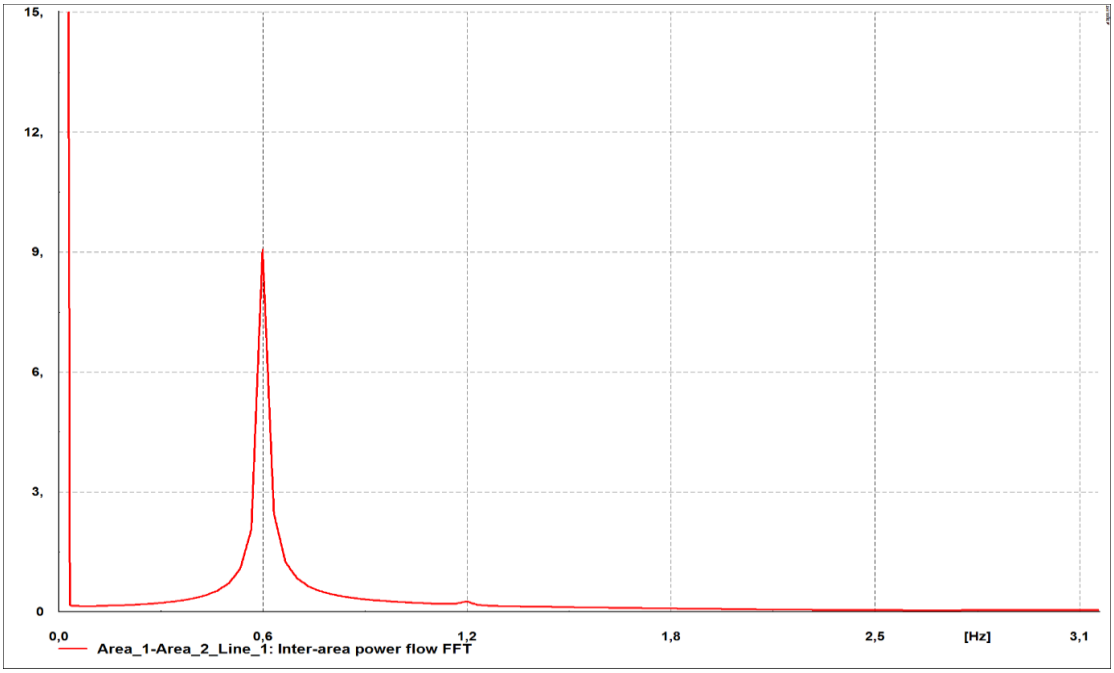

Figure 4.3: Inter-area power flow Fast Fourier Transform (FFT)

In addition, a 3-phase fault on transmission line 1 (Tx 1, see Figure 4.1) connecting the two areas was applied at 1.5 second and cleared by disconnecting the transmission line after 500 milliseconds. The response of the generator speeds is shown in Figure 4.4 which further indicates that generators Gen 01 and Gen 02 of area 1 are oscillating against generators Gen 03 and Gen 04 of area 2 since their speeds are out-of-phase as revealed by the modal-analysis results.

UNIVERSITY OF JOHANNESBURG

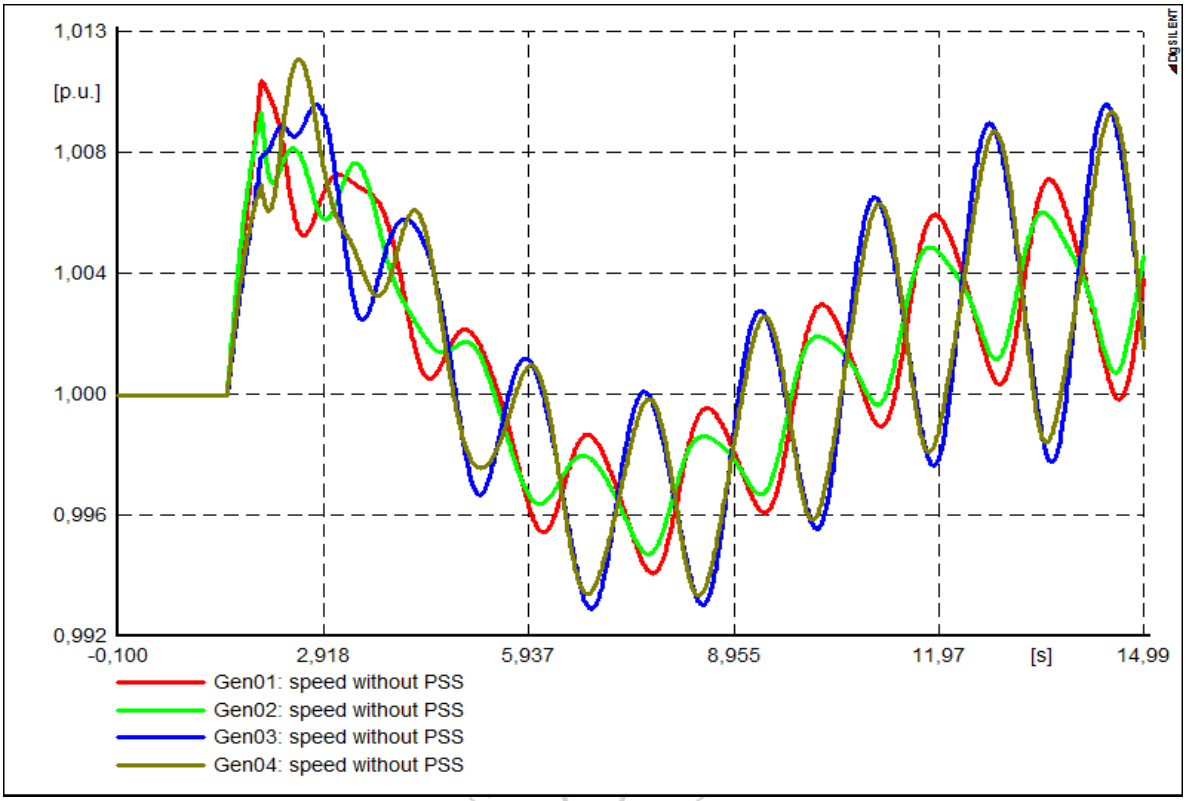

Figure 4.4: Rotor angle speed of the generators without the PSSs

4.2. Selection of Power System Stabilizers (PSSs) Location

Practical interconnected power systems consist of several synchronous generators and finding the most suitable location for PSSs and determining the generator phase-lag are two distinct steps involved in PSS design [42]. Identification of the power system critical generators is among the initial stages in design and installation of PSSs. The participation factor is a good indication of the importance of a state to the mode and it is particularly useful as a screen for PSS optimal placement [3] [7]. Adding damping to generators with real positive participation factors towards a mode will improve the oscillation mode damping [7]. The generator rotor speed state participation factors are used for the selection of PSS locations. Since the modal analysis results indicated that the inter-area mode is unstable when the generators operate with automatic excitation control, the generator with the highest rotor speed state participation factor will improve the damping of the inter-area mode when the PSS is installed on it. The determined rotor speed state participation factor magnitude towards the inter-area mode are shown in Table 4.4. From Table 4.4, generator Gen 03 of area 2 has the highest participation factor and thus can be equipped with the PSS to improve the power system's small-signal stability. The generator ranking for installing PSSs is also presented in Table 4.4. The ranking indicates that after generator Gen 03, the next possible generator to equip with the PSS is generator Gen 04 of area 2, followed by generator Gen 01 and lastly generator Gen 02 of area 1. The following sections proceed to determine the requirements and the design of PSSs.

Table 4.4: Generator speed participation factors towards the inter-area mode

Generator	$\|PF\|$	Ranking
Gen 01	0.387	3
Gen 02	0.230	4
Gen 03	0.614	1
Gen 04	0.498	2

4.3. Determination of the generator phase-lag

Since generator Gen 03 of area 2 has the highest positive participation factor towards the inter-area mode, additional damping through its excitation system is required to improve the system stability. The first step to achieve this is to determine the amount of phase-lag between the generator electrical torque and the excitation system reference voltage while still connected to the power network. The phase-lag should be determined with the generator inertia increased to infinity to avoid feedback due to change in generator rotor angle [24]. Figure 4.5 shows the determined generator Gen 03 phase-lag between its electrical torque and the excitation system reference voltage with the generator inertia set to infinity while connected to the power network. The generator Gen 03 electrical torque phase-lag was found to be around 20˚ at the inter-area oscillation mode frequency and 38˚ at the frequencies of the local modes. The phase-lag between the generators Gen 01, Gen 02 and Gen 04 electrical torques and their excitation system reference voltages were determined. The generators' phase-lag were found to be around 20˚ at the inter-area mode for generator Gen 01, and 22˚ for generators Gen 02 and Gen 04. In area 1, at the 1.12 Hz local mode the phase-lags for generators Gen 01 and Gen 02 were found to be 36˚ and 38˚ respectively, whereas in area 2, at the 1.15 Hz local mode the phase-lags for generator Gen 04 was 43˚. Table 4.5 provides the determined phase-lags for the oscillation modes. With reference to Figure 4.5, the phase compensation of the PSSs will introduce the necessary phase-shift to cause a phase shift of nearly zero degrees throughout the range of frequencies of interest i.e. from 0.1 Hz to 2 Hz. With the phase shift close to zero degrees, the electrical torque component will be nearly in phase with the generator speed oscillations which is directed to improving the damping of the generator rotor oscillations [19].

Table 4.5: System generator, excitation system and generators phase-lags

Generator	Inter-area mode (0.61 Hz)	Area 1 local mode (1.12 Hz)	Area 2 local mode (1.15 Hz)
Gen 01	-19.28˚	-35.92˚	-
Gen 02	-21.53˚	-37.63˚	-
Gen 03	-19.73˚	-	-37.98˚
Gen 04	-21.75˚	-	-42.51˚

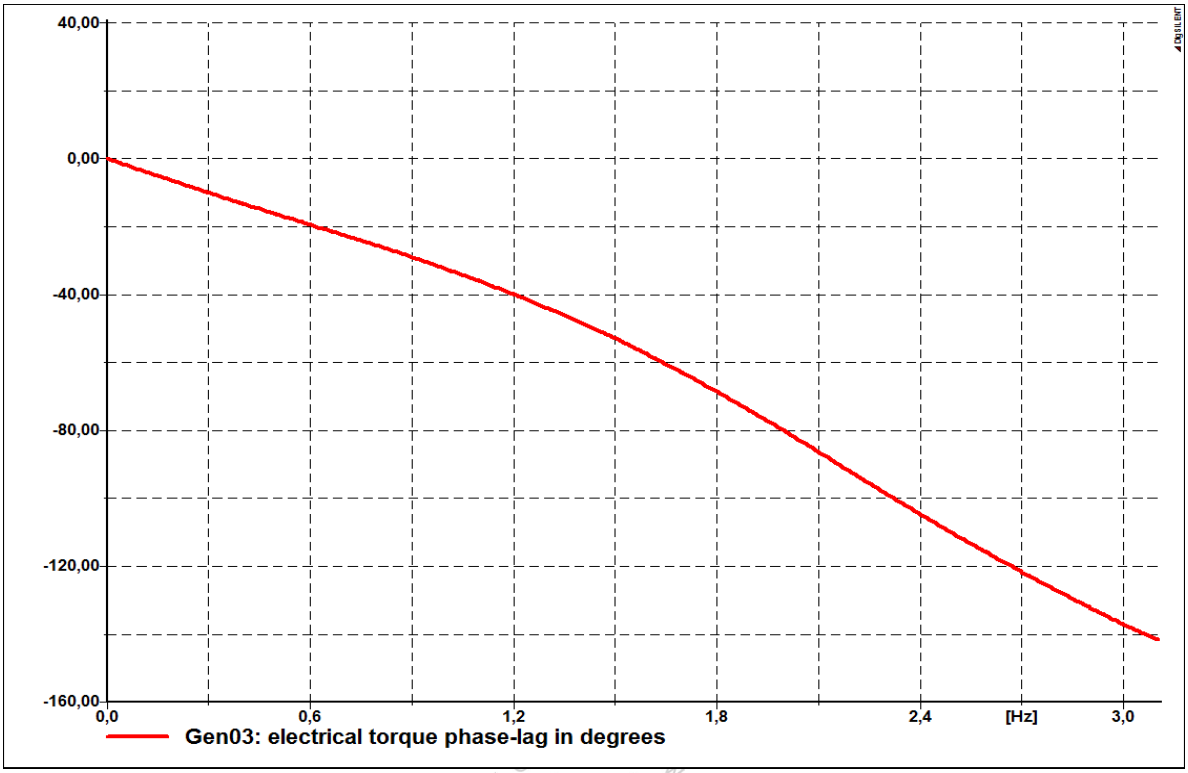

Figure 4.5: Phase-lag between generator (Gen 03) electrical torque and excitation system reference voltage phase-lag

4.4. IEEE Power System Stabilizer (PSS2B) Design

Once the phase-lag between the generator electrical torque and AVR reference voltage has been determined, the PSS settings can be designed. As mentioned earlier, the IEEE PSS2B whose principle of operation was presented in Chapter 2 was adopted in this investigation. Figure 4.6 shows the IEEE PSS2B block diagram implementation which consists of two paths: - rotor-speed path and electrical power path.

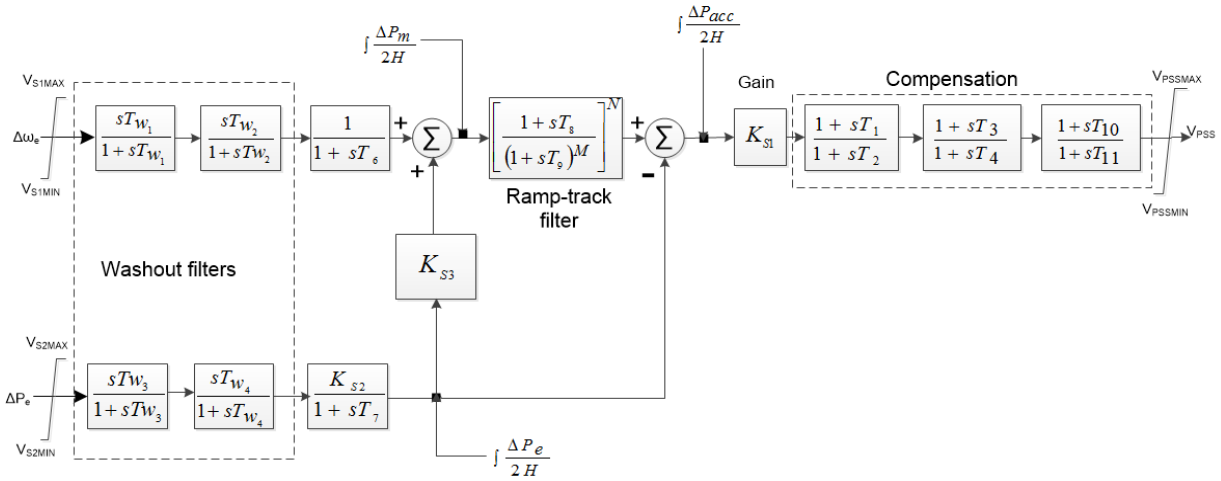

Figure 4.6: IEEE Type PSS2B-dual-input PSS structure

Referring to Figure 4.6, the integral of mechanical power is derived from the change in rotor-speed and electrical power given by Eq. (4.1)

$$\frac{1}{2H}\int \Delta P_m \; dt = \; \Delta\omega + \frac{1}{2H}\int \Delta P_e \; dt \tag{4.1}$$

The torsional (or ramp-track) filter is used to remove the torsional modes in the integral of mechanical power input derived through Eq. (4.1) such that the output of the torsional (or ramp-tracking) filter is given by:

$$G(s)\left(\Delta\omega + \frac{1}{2H}\int \Delta P_e \; dt\right) \tag{4.2}$$

-where $G(s)$ is the transfer function of the torsional (or ramp-tracking) filter

The integral of accelerating power injected into the PSS main path (from the gain and compensation blocks) is then derived by subtracting the integral of electrical power from the output of the ramp-tracking filter to obtain the absolute rotor-speed deviation signal from the integral of accelerating power. This yields Eq. (4.3) as the PSS2B transfer function from the input to the output of the torsional (or ramp-track) filter.

$$\frac{1}{2H}\int \Delta P_{acc} = \; G(s)\left(\Delta\omega + \frac{1}{2H}\int \Delta P_e \; dt\right) - \frac{1}{2H}\int \Delta P_e \; dt \tag{4.3}$$

From practical experience the PSS2B optimal performance occurs when the rotor-speed and electrical power washout filter time constants are matched [20]. To achieve this match common practice is to use two washout filters in each path such that:

(i) For the rotor-speed signal path, T_6 is set to zero (i.e. $T_6 \approx 0$) for $T_{w_1} = T_w = T_{w_2}$; and

(ii) The electrical power path is set such that $T_{w_3} = \; T_7 = T_w \; ; \; T_{w_4} = 0$.

The value of K_{s2} in the electrical power path depends on the generator inertia and is determined through Eq.(4.4).

$$K_{s2} = \frac{T_7}{2H} \tag{4.4}$$

-where H is the inertia constant of the generator (in sec).

To obtain an integral of mechanical power before the ramp-tracking filter, the parameter K_{s3} should be unity. With such settings, the PSS design (washout filter, compensation time constants and gain) can be determined using the single-input speed-based PSS techniques [43].

4.4.1 Washout Filter Time Constants

For local and inter-area oscillation modes, washout filter time constants range from 1 to 2 seconds and 10 to 20 seconds respectively [44] [45]. The time constant values must be large enough to allow the oscillation related signals to pass unaltered without causing large voltage excursions during islanding. Using these guidelines, a 10 second time constant was used in this investigation. The washout filter phase compensation contribution can be determined using Eq.(4.5).

$$H_w(\lambda) = \frac{sT_w}{(1 + sT_w)} \tag{4.5}$$

-where T_w is the washout filter time constant (in sec) and s is the oscillation mode frequency of interest in the Laplace form (in rad/sec).

Figure 4.7 shows the frequency response of a single washout filter and double cascaded washout filters (as for the PSS2B model) for the 10 second selected. The frequency response shows that for a 10 second washout filter time constant the compensation contribution is unity gain with a phase-lead of 0.8113° and 0.7903° at the TAMM system local mode frequencies and 0.99 with phase-lead of 1.51° at the inter-area mode frequency. The overall contribution of washout filters to the PSS compensation is minimal as revealed.

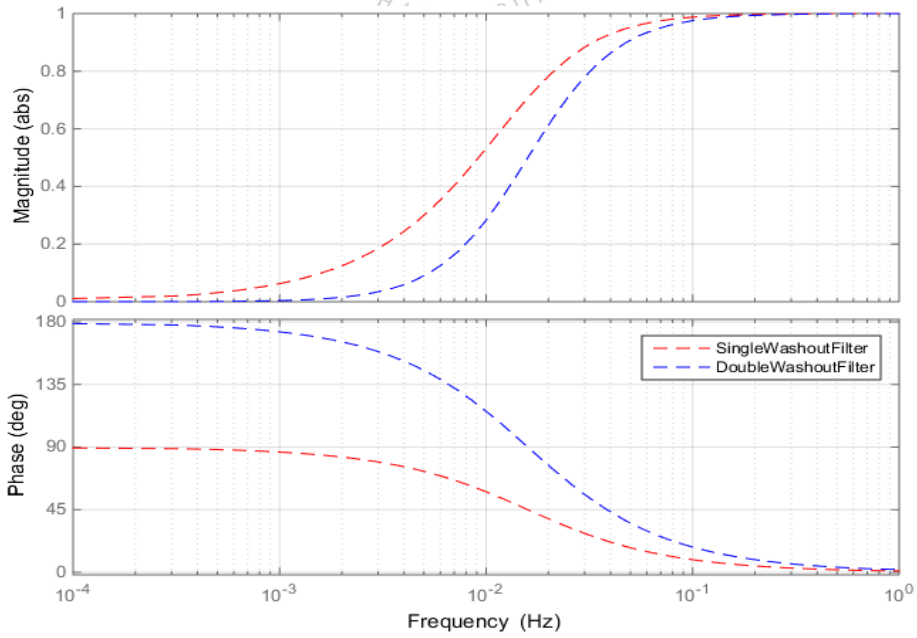

Figure 4.7: Frequency response of a single washout filter and double or cascaded single washout filters

4.4.2 Torsional (or Ramp-Tracking) Filter

Torsional (or ramp-tracking) filters attenuate high-frequency components in the input signal, allow low-frequency mechanical power changes to pass with negligible attenuation and minimize the PSS output deviation that occurs when the mechanical power changes rapidly [20]. The torsional filter transfer function is given by Eq. (4.6), where $T_8 = M \times T_9$ and $T_8 \neq 0$.

$$G(s) = \left[\frac{1 + sT_8}{(1 + sT_9)^M}\right]^N \tag{4.6}$$

The commonly used torsional filter parameters adapted from [8] and [9] are provided in Table 4.6. Figure 4.8 shows the corresponding frequency response of the torsional filter parameters. Table 4.6 also presents the attenuating gains which were determined at the minimum torsional frequency of 4 Hz in accordance to reference [9]. The first set of the torsional filter parameters are used in this study because the settings are recommended in various literature including in [9] and they show adequate attenuation of frequencies above 4 Hz which ensures damping of the typical torsional modes.

ITY OF THE WITWAT

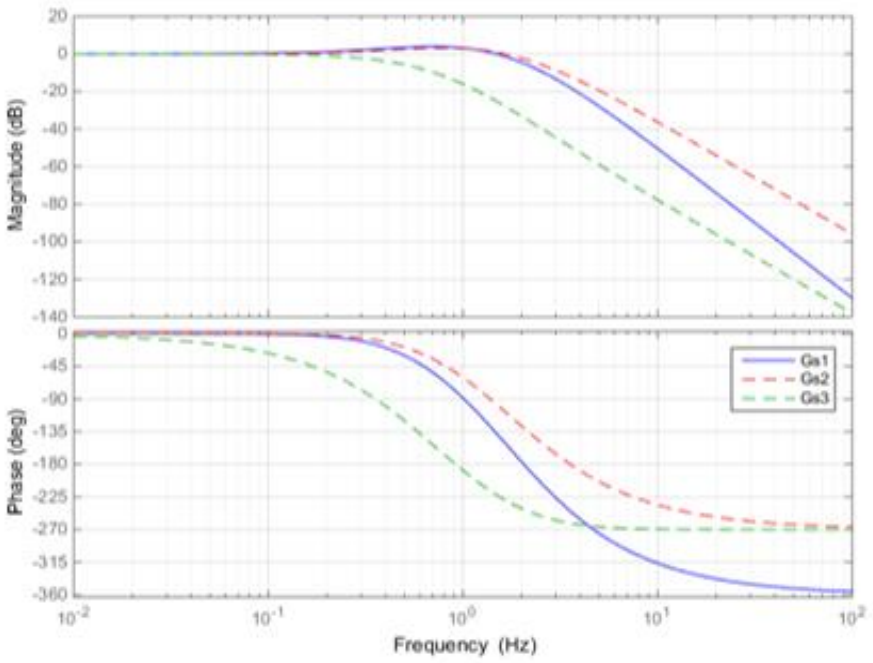

Figure 4.8: Frequency response of typical torsional (or ramp tracking) filters

Table 4.6: Torsional (or ramp tracking) filter typical parameters

Ramp tracking filter (G(s))	M	N	T_8 (seconds)	T_9 (seconds)	Attenuating gain (dB)
G(s)_1	5	1	0.5	0.1	21
G(s)_2	4	1	0.4	0.1	15
G(s)_3	4	1	0.05	0.2	53

4.4.3 Phase Compensation and Gain Design

According to reference [43] the first target in PSS design are local modes and that the PSS gain is optimized to improve the damping of the inter-area modes. This approach was adopted and the number of phase-lead blocks to be used was based on guidelines provided in Chapter 2 that the maximum allowable phase-lead of a single PSS phase-lead block is 55º. It should be noted that the presence of three phase-lead blocks of the PSS2B can be used to shape the overall phase-lead as desired in a system with more than one oscillation mode. In practical power systems, not all generators are equipped with PSSs but for the TAMM system used it was decided to equip all the generators with PSSs. Thus, the PSS phase-compensation was determined considering the individual generators phase-lag given in Section 4.2. An example calculation for the 1.12 Hz local mode targeted by the generator Gen 01 PSS is given below.

Example calculation illustration for the 1.12 Hz local mode targeted by the generator Gen 01 PSS

- The required phase-lead is 35.92˚ and the number of phase-lead compensator blocks to be used is 1.
- Single block compensation is thus, $\emptyset = 25.92$ considering 10˚ under-compensation.
- Using Eq. (2.52), α is determined as:

$$\alpha = \frac{-1 - \sin 25.92}{\sin 25.92 - 1} = 2.553$$

- The phase-lead time constants are determined from using Eq.(2.53) as:

$$T = \frac{1}{2\pi f\sqrt{\alpha}} = \frac{1}{2\pi(1.12\ Hz)\sqrt{2.553}} = 0.0889\ seconds$$

$$\alpha \mathrm{T} = 2.553 \times 0.0889 = 0.2271\ seconds$$

Figure 4.9 shows the phase compensation provided by the PSS is as calculated above. A phase-lead of 25.92˚ is provided at the 1.12 Hz local mode using one phase-lead compensator block.

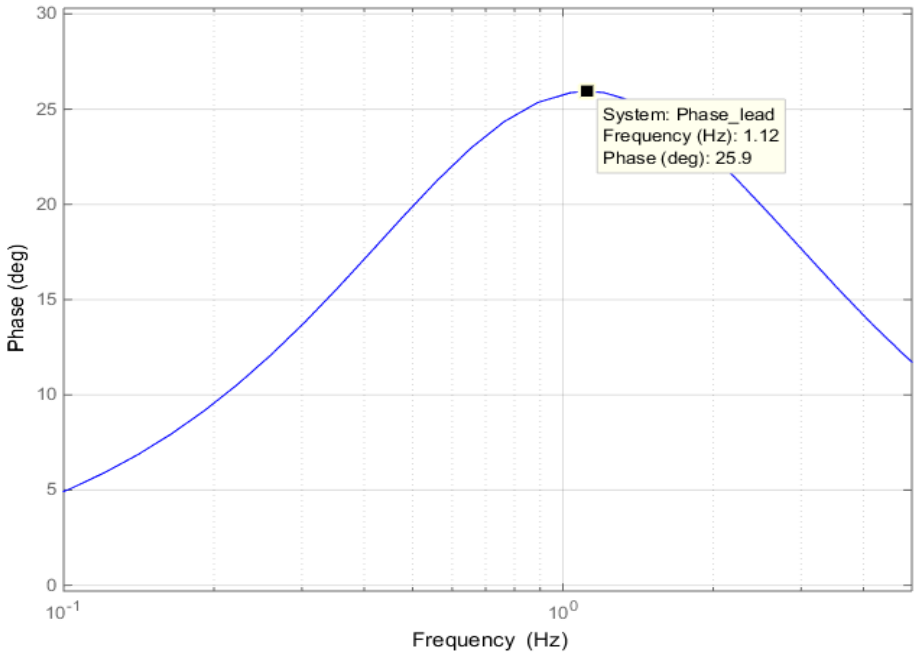

Figure 4.9: Phase compensation of the example designed phase-lead

The root locus technique was used to determine the PSS gains. Figure 4.10 shows the root-locus plots of the TAMM system local modes and inter-area modes obtained during PSS gain selection. Figure 4.10 shows that increasing the PSS gains resulted in the inter-area mode eigenvalue moving from the right-half of the complex plane into the left-half of the complex plane which shows an increase in its damping. It was observed that the mode damping would firstly increases and then decreases with further increase in the PSS gain. The increase in the PSS gains caused the local mode eigenvalue to move away from the complex plane imaginary axis but further increase of PSS gains resulted in the eigenvalues moving towards the origin of the complex plane as shown in Figure 4.10.

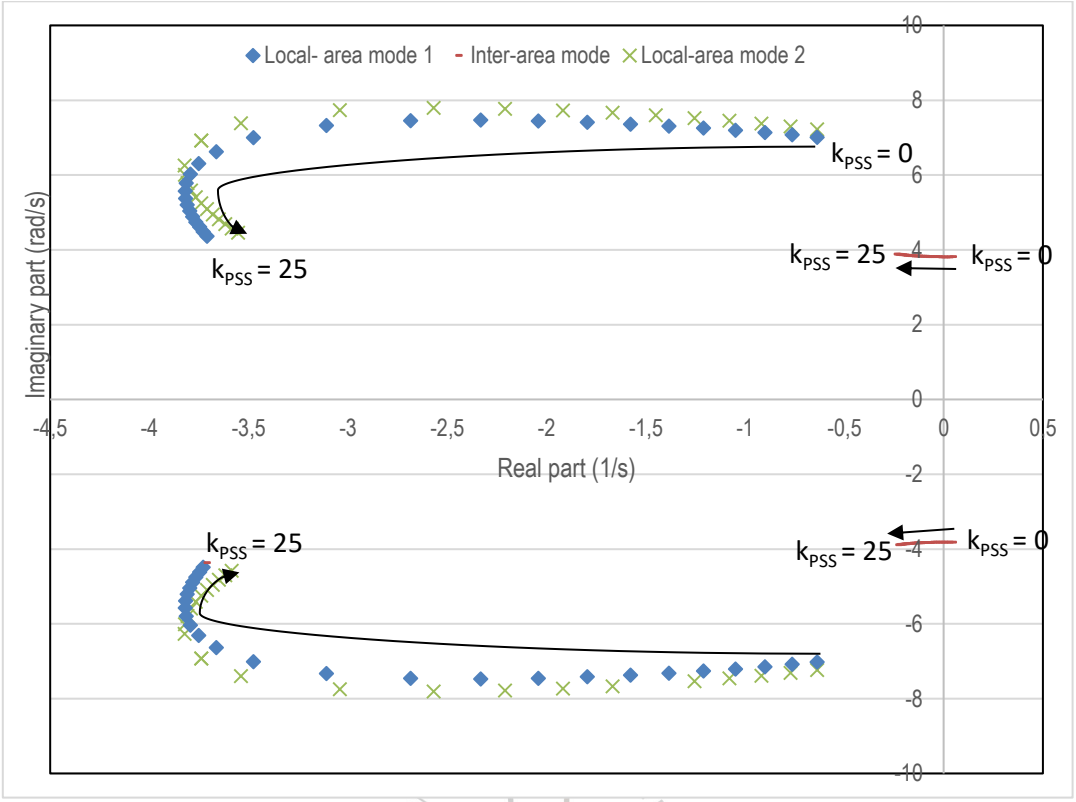

Figure 4.10: System root loci with increasing PSS gain

Ideally, the PSS phase-lead design of the PSSs affects the small-signal synchronising torque while the gain of the PSS has an important effect of increasing the oscillation modes' damping. The oscillation mode damping is revealed through modal analysis. Figure 4.11 shows the inter-area mode and local mode frequencies with increasing PSS gains. Figure 4.11 shows that the inter-area and local oscillation mode frequencies firstly increases with increasing PSS gains and then decreases with increasing PSS gains. This was more noticeable in the local oscillation modes. This noticeable increase in the local mode frequencies can be explained by the fact that since the maximum phase-lead of PSSs were designed at the local mode frequencies the increasing PSS gains will be introducing too much phase-lead at the local modes than at the inter-area mode. The increase in the inter-area and local mode frequencies with increasing PSS gains indicate that the PSSs are introducing damping torque with increasing synchronizing torque whereas decreasing mode frequencies indicates that the PSSs will be providing too much phase-lead which means a decrease in synchronizing torque.

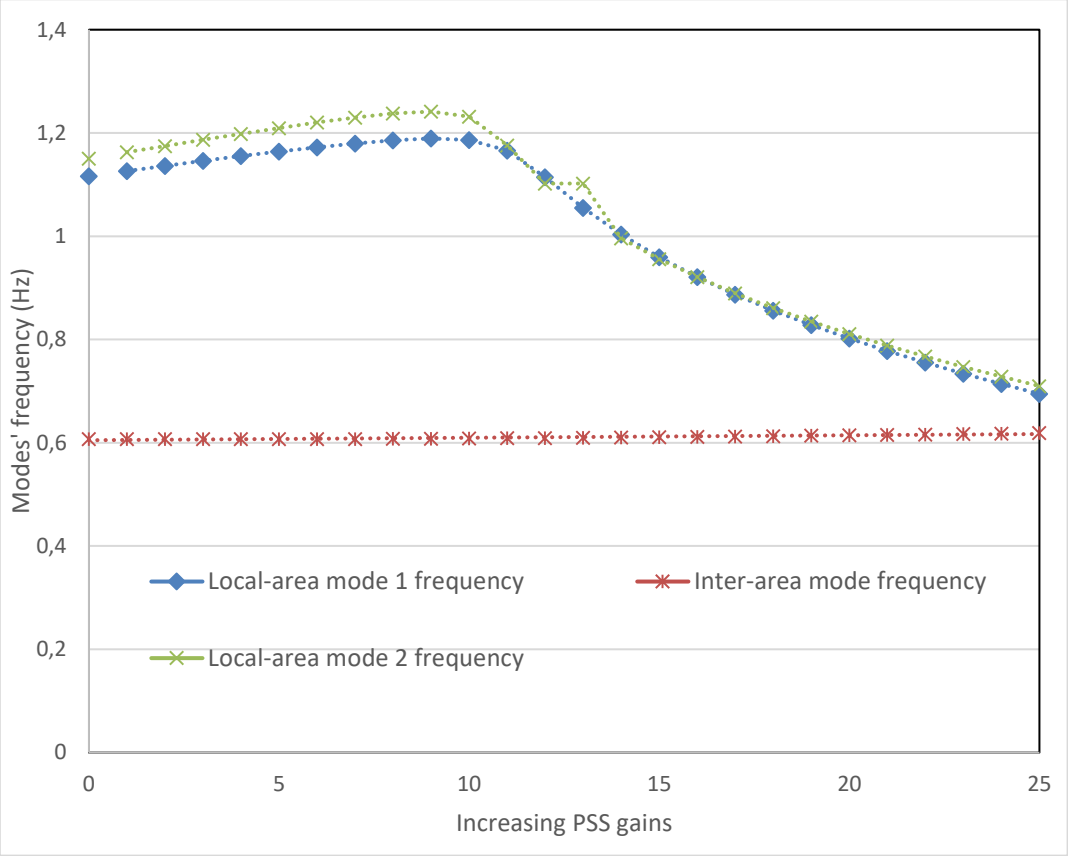

Figure 4.11: System modes' frequency change with increasing PSS gains

Table 4.7 shows the final settings of the PSSs including the selected gains which were used in this investigation. The PSS gains at which instability occurred were also determined through root-locus and were found to be around three-times the selected gains. The PSS positive and negative output limiters were selected at 0.1 and -0.1 respectively based on the guidelines provided in Section 2.3.4. The PSS settings designed were tested under various test system operating conditions to validate their performance.

Table 4.7: Designed PSS2B settings

Parameter	Description	Gen 01 PSS	Gen 02 PSS	Gen 03 PSS	Gen 04 PSS
T_{w1}	Speed washout filter time constant	10	10	10	10
T_{w2}	Speed washout filter time constant	10	10	10	10
T_{w3}	Power washout filter time constant	10	10	10	10
T_{w4}	Power washout filter time constant	0	0	0	0
T_1	Phase lead/lag filter numerator time constant	0.2271	0.2348	0.2302	0.2523
T_2	Phase lead/lag filter denominator time constant	0.0889	0.0860	0.0832	0.0759
T_3	Phase lead/lag filter numerator time constant	-	-	-	-
T_4	Phase lead/lag filter denominator time constant	-	-	-	-
T_6	Speed signal transducer time constant	0	0	0	0
T_7	Power signal transducer time constant	10	10	10	10
T_8	Ramp tracking numerator time constant	0.5	0.5	0.5	0.5
T_9	Ramp tracking denominator time constant	0.1	0.1	0.1	0.1
M	Ramp tracking filter parameter	5	5	5	5
N	Ramp tracking filter parameter	1	1	1	1
T_{10}	Phase lead/lag filter numerator time constant	-	-	-	-
T_{11}	Phase lead/lag filter denominator time constant	-	-	-	-
K_{S1}	PSS gain	12	8.65	11.35	6.2
K_{S2}	Power signal transducer factor	0.7692	0.7692	0.8097	0.8097
K_{S3}	Washouts coupling factor	1	1	1	1
V_{PSSMIN}	PSS minimum output limiter	-0.1	-0.1	-0.1	0.1
V_{PSSMAX}	PSS maximum output limiter	0.1	0.1	0.1	0.1

4.5. Power System Stabilizer (PSS) Performance Evaluation

PSSs are expected to provide desirable damping requirements over various operating conditions. The operating conditions can be simulated by considering different generator output power, loads and change in network topology. Line switching is used to change the total impedance between the generators) [46].

4.1.1. Test Cases

The PSS tuning procedures are dependent on the input signal employed for which the speed-based and power-based input PSSs tuning conditions are similar. The tuning should be examined including the generators operating at full load feeding into a strong transmission system (simulated by line switching) which results in maximum phase-lag. As such, in this study the test cases were derived at full generator output while varying the system loads and by switching the transmission lines connecting the two areas in/out of service. The following four cases were considered for testing the designed PSS settings:

- Case 1 is defined as the nominal operating condition, where the load in area 1 was 967 MW while area 2 load was 1 767 MW.
- Case 2. Area 1 load was changed to 1 167 MW load while area 2 load was changed to 1 467 MW which results in 200 MW being transferred from area 1 to area 2.
- Case 3. Area 1 load is 867 MW while area 2 load was 1 767 MW which results in 500 MW being transferred from area 1 to area 2.
- Case 4. Area 1 load was 1 167 MW while area 1 load was 1 467 MW with one transmission line out of service resulting in 200 MW being transferred from area 1 to area 2 over a single line.

It is important to note that various operating conditions can be derived for testing the designed PSS settings but only the above-mentioned test cases were investigated and are reported. Table 4.8 provides the derived TAMM system test cases operating conditions and resulting power flows between the two interconnected areas. The TAMM system test cases' small-signal stability was analysed with the generators operating in automatic excitation control without the designed PSSs.

Table 4.8: Test cases operating conditions

Case	Active power transferred (MW)	Number of lines in service	Load in area 1 (MW)	Load in area 2 (MW)
1	400	2	967	1 767
2	200	2	1 167	1 467
3	500	2	867	1 767
4	200	1	1 167	1 467

Table 4.9 provides the test cases' small-signal stability results which will be compared when the generators are equipped with the designed PSSs in the subsequent subsections. Table 4.9 presents the eigenvalue, frequency and damping ratio of the inter-area and local oscillation modes for each derived TAMM system test case. The inter-area mode eigenvalue, frequency and damping ratio varied across the derived test cases. The damping ratio of the inter-area mode was below the specified minimum damping ratio of 5% criterion for all the test cases.

The local modes' eigenvalue, frequency and damping ratio also varied over the derived test cases. The change in the inter-area and local modes' characteristic is expected since the operating conditions were changing over the derived test cases. It is important to note that the damping ratios of the local modes were above the specified minimum damping of 5% criterion for all the derived test cases.

Table 4.9: Test cases eigenvalue analysis results used for testing the designed PSSs settings

Case	Inter-area mode	Area 1 local mode	Area 2 local mode
1	0.047 ± j 3.816 (0.610 Hz, -1.221%)	-0.637 ± j 7.015 (1.116 Hz, 9.049%)	-0.638 ± j 7.229 (1.150 Hz, 8.798%)
2	0,019 ± j 4,009 (0.638 Hz, -0.464%)	-0,650 ± j 7,054 (1.123 Hz, 9.173%)	-0,763 ± j 7,253 (1.154 Hz, 10.459%)
3	0.0147 ± j 3.627 (0.577 Hz, -0.406%)	-0.638 ± j 6.989 (1.112 Hz, 9.086%)	-0.768 ± j 7.153 (1.138 Hz, 10.682%)
4	0.022 ± j 2.983 (0.475 Hz, -7.316%)	-0.648 ± j 7.009 (1.116 Hz, 9.209%)	-0.784 ± j 7.208 (1.147 Hz, 10.806%)

4.1.2. Modal Analysis

UNIVERSITY OF THE WITWATERSRAND JOHANNESBURG

The performance of the PSS settings was assessed through modal analysis and time domain disturbances. In this section, the derived test cases' small-signal stability modal analysis results with the designed PSS settings installed on the generators are presented. These results are also compared with the modal analysis results obtained when the PSSs were out of service in order to establish the performance of the designed PSSs.

Table 4.10 gives the inter-area mode characteristics (eigenvalues, frequency and damping ratio) of the TAMM system test cases investigated with the designed PSSs installed on the generators. For the case studies derived from the base two-area network of the test system, the inter-area mode damping ratios were above the minimum damping criterion of 5%. For Case 1, which was defined as the nominal operating condition, with 967 MW of load in area 1 and 1 767 MW in area 2 the designed PSSs increased the inter-area mode damping from -1.22% to 18.47% while the frequency slightly decreased from 0.61 Hz to 0.56 Hz. The decrease in frequency reveals that in addition to introducing the required positive damping the PSSs slightly affects the system synchronizing torque.

Table 4.10: Inter-area oscillation mode damping comparison with the designed PSS settings

Case	Eigenvalue $(\sigma \pm j\omega)$	Frequency (Hz)	Percentage damping ratio $(\zeta \times 100\%)$
1	-0.656 ± j 3.492	0.56	18.47
2	-0.675 ± j 3.713	0.59	17.89
3	-0.554 ± j 3.425	0.55	15.96
4	-0.500 ± j 2.737	0.44	17.96

In Case 2, area 1 load was increased to 1 167 MW from 967 MW and area 2 load was reduced from 1 767 MW to 1 467 MW which resulted in light loaded operating condition with the inter-area power flow of 200 MW, 0.638 Hz inter-area mode with a damping ratio of -0.464%. Case 2 represents lightly loaded operating condition when PSSs are required the most. The implementation of the PSSs increased the inter-area mode damping from -0.464% to 17.89%. With the resulting inter-area mode damping for Case 2, it can be deduced that the designed PSSs are able to provide damping when it is required the most. However, the inter-area mode frequency decreased by 0.048 Hz from 0.638 Hz to 0.59 Hz which implies a slight decrease in the synchronizing torque. In Case 3, the load in area 1 was 867 MW while area 2 load was 1 767 MW. This resulted in 500 MW being exported from area 1 to area 2 with inter-area mode frequency of 0.577 Hz damped at -0.406%. This case simulates the maximum export on a weak transmission line. With PSSs installed on the generators, the inter-area mode damping was satisfactorily increased from -0.406% to 15.96%. For this case, the designed PSSs also increased the inter-area mode damping with slight decrease in the synchronizing torque as revealed by the decrease in the inter-area mode frequency from 0.566 Hz to 0.55 Hz. In Case 4, the operating conditions were characterised by high impedance between the two connected areas which was simulated by taking one transmission line interconnecting the two areas out of service and 1 167 MW of load in area 1 while area 2 load was 1 467 MW. This resulted in an inter-area mode frequency of 0.475 Hz with a damping ratio of -7.316%. For this case, the designed PSSs increased the inter-area mode damping from -7.316% to 17.96%. The PSSs also introduced slight negative synchronizing torque as indicated by a decrease in the inter-area mode frequency of 0.035 Hz from 0.475 Hz to 0.44 Hz. Figure 4.12 shows a comparison of the inter-area mode damping without and with the designed PSS installed on the synchronous generators.

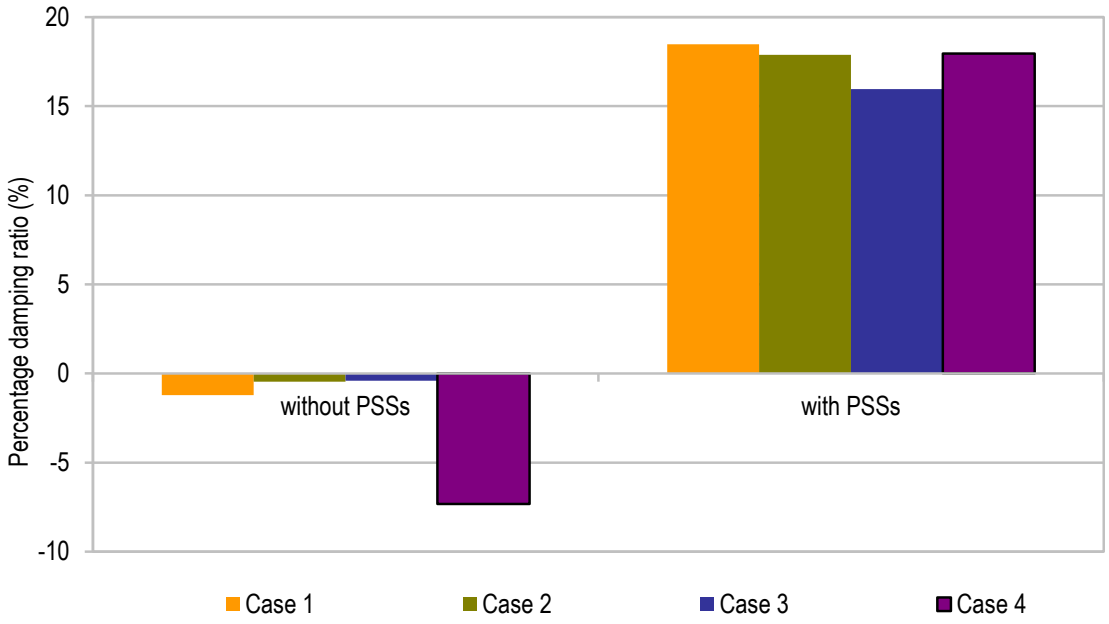

Figure 4.12: Graphical presentation of the inter-area mode damping comparison

As mentioned earlier, the damping ratios of the TAMM system local modes were above the specified minimum damping of 5% criterion for all the derived test cases. This shows that the designed PSSs increased the inter-area mode damping over a wide range of operating conditions. However, the PSSs slightly decreased the synchronizing torque as revealed by the decrease in the inter-area mode frequency. This could be attributed to the phase-lead design which is introducing too much phase-lead. This can be corrected by increasing the under-compensation value and then re-evaluate the modal analysis again. This aspect resulted in conventional PSS design methods being more of an iterative approach which is time consuming.

The installation of the designed PSSs is expected to increase damping over the 0.1 Hz to 2 Hz frequency range. As such an increase in the local mode damping is expected. The following paragraphs discuss the local mode characteristics (eigenvalues, frequencies and damping ratios) of the test cases when the PSSs were installed on the generators. Table 4.11 provides area 1 local mode characteristics (eigenvalues, frequency and damping ratio) of the TAMM system test cases with the designed PSSs installed on the generators. For Case 1, the load in area 1 and area 2 were 967 MW and 1 767 MW respectively, the designed PSSs increased area 1 local mode damping from 9.05% to 64.58% and frequency decreased from 1.12 Hz to 0.787 Hz. The decrease in frequency indicates that the PSSs decrease the synchronizing torque at the area 1 local mode frequency. In Case 2, the load in area 1 was increased to 1 167 MW from 967 MW and area 2 load was reduced from 1 767 MW to 1 467 MW which resulted in a lightly loaded operating condition with the inter-area power flow of 200 MW, 1.123 Hz area 1 local mode with a damping ratio of 9.173%. The introduction of PSSs increased the area 1 local mode damping ratio to 65.63% with a decrease in frequency which indicates that the PSSs are introducing negative synchronizing torque at the area 1 local mode frequency.

Table 4.11: Area 1 local mode damping comparison without and with designed PSSs

Case	Eigenvalue ($\sigma \pm j\omega$)	Frequency (Hz)	Percentage damping ratio ($\zeta \times 100\%$)
1	-4.185 ± j 4.947	0.787	64.58
2	-4.317 ± j 4.963	0.790	65.63
3	-3.859 ± j 5.212	0.830	59.50
4	-4.234 ± j 5.023	0.799	64.45

In Case 3, area 1 load was set to 867 MW while area 2 load was 1 767 MW. This resulted in 500 MW being exported from area 1 to area 2 with area 1 local mode frequency of 1.112 Hz damped at 9.086%. The designed PSSs installed on the generators increased the area 1 local mode to 59.50% and at the same time decreased the synchronizing torque which is shown by a decrease in area 1 local oscillation frequency from 1.112 Hz to 0.830 Hz. In Case 4, the operating conditions were characterised by high system impedance between the two connected areas which was simulated by taking one transmission line connecting the two areas out of service, and the load in area 1 was 1 167 MW while area 2 load was 1 467 MW. This resulted in the area 1 local mode frequency of 1.116 Hz with a damping ratio of 9.21%. For this case, the designed PSSs increased the damping ratio of area 2 local mode to 64.45% and adversely affected the synchronizing torque since the frequency decreased to 0.799%. Figure 4.13 is a comparison of area 1 local oscillation mode damping ratio without and with the designed PSSs installed on the generators.

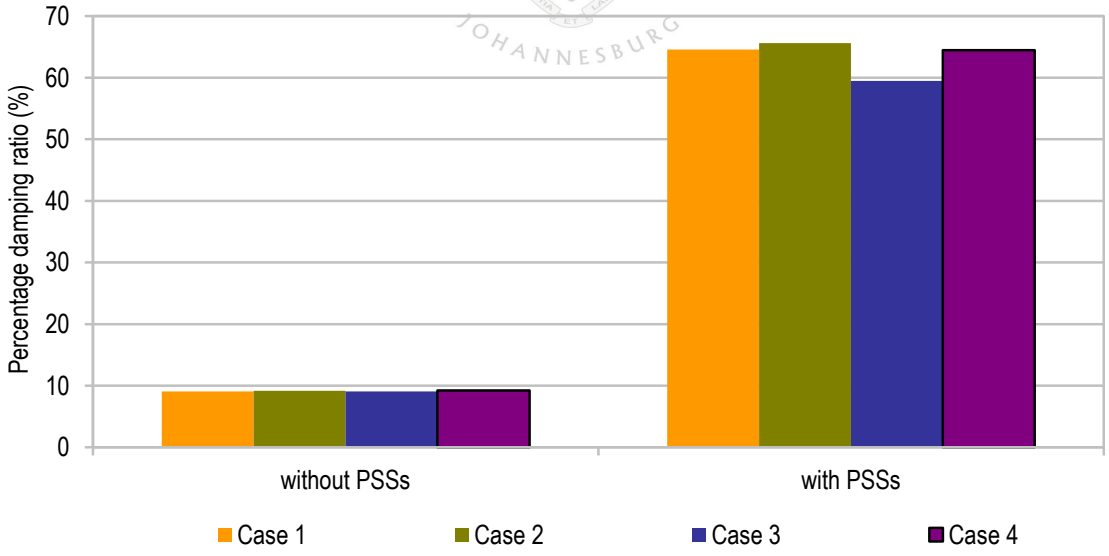

Figure 4.13: Graphical presentation of the area 1 local mode damping comparison

Similarly, the designed PSSs increased area 2 local oscillation mode damping. The detailed characteristics (eigenvalues, frequency and damping ratios) of area 2 local mode are given in Table 4.12. Area 2 local mode damping ratio increased to 63.68%, 66.12%, 61.20% and

64.69% for Case 1 to Case 4 respectively with the following frequencies 0.782 Hz for Case 1, 0.772 Hz for Case 2, 0.801 Hz for Case 3 and 0.784 Hz for Case 4. Figure 4.14 shows the comparison of area 2 local oscillation mode damping without and with the designed PSSs which shows that the damping ratio was increased by the introduction of the PSSs.

Table 4.12: Area 2 local mode damping comparison without and with designed PSSs

Case	Eigenvalue $(\sigma \pm j\omega)$	Frequency (Hz)	Percentage damping ratio (%) $(\zeta \times 100)$
1	-4.060 ± j 4.915	0.782	63.68
2	-4.272 ± j 4.848	0.772	66.12
3	-3.892 ± j 5.030	0.801	61.20
4	-4.176 ± j 4.923	0.784	64.69

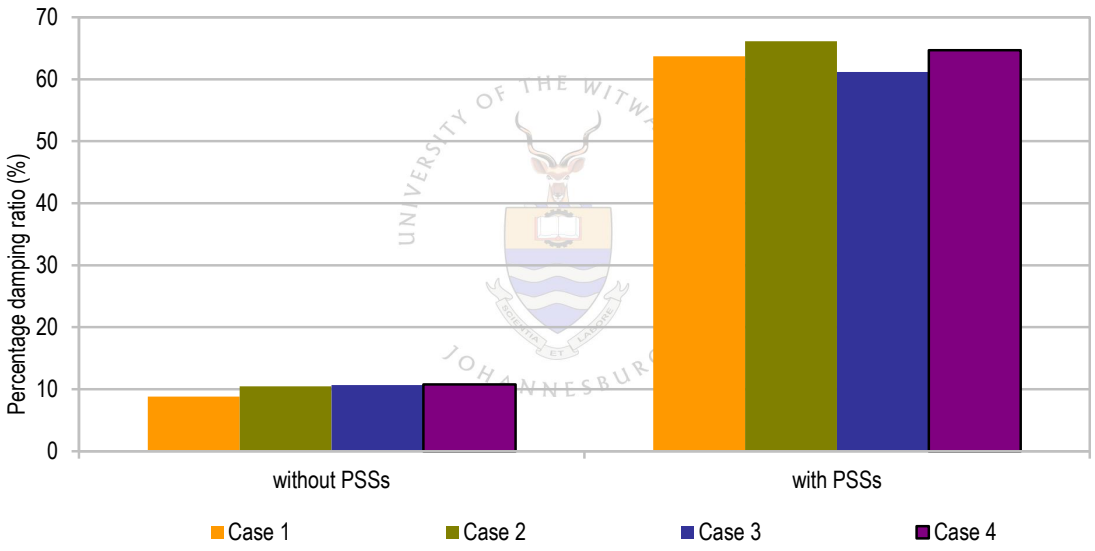

Figure 4.14: Graphical presentation of area 2 local oscillation mode damping comparison

This section has presented and discussed the TAMM system modal analysis results with the designed PSSs installed on generators under a wide range of operating conditions. As expected, the modal analysis results revealed that the implementation of PSSs increases damping of the test system small-signal oscillation (inter-area and local modes) modes. The system modes were adequately damped for the derived operating conditions. However, the analysis of the results further reveal that the designed PSSs slightly introduced negative synchronizing torque which was shown by the small decrease in the mode frequency when the PSSs were installed.

4.1.3. Time Domain Performance Evaluation

The time domain performance evaluation of the TAMM system with the designed PSSs was performed to validate the PSSs performance and complement the modal analysis results presented in the previous section. In the time domain, the PSS performance is assessed by its ability to quickly damp the small-signal oscillations after disturbances so that the system remains stable. In this dissertation, the time domain performance evaluation was achieved through a transient disturbance in the form of a three-phase fault on one of the transmission line (Tx 1 in Figure 2.9). The fault was applied at 1.5 second and cleared by disconnecting the faulted transmission line after 500 milliseconds. It is expected that the system response should not sustain but quickly dampen the oscillation modes when the generators are equipped with PSSs. The time domain simulations were performed for Cases 1 to 4 while observing the generator rotor angles, speed and active power.

For Case 1, Figure 4.15 shows a comparison of the generator rotor angle responses to the three-phase fault for the generators with and without the designed PSSs. Firstly, without the designed PSSs it can be seen that the disturbance can excite the inter-area mode. This is because, from Figure 4.15 the time domain simulations confirm the modal analysis results that without the PSSs the system is unstable (black traces which indicate the growing rotor angles). However, when the three-phase fault is applied, generators Gen 01, Gen 02 and Gen 04 rotor angles firstly increase and because of the PSSs the rotor angles quickly settle to new rotor angle positions when the fault is cleared. This result in the stable response (red traces which indicate that the rotor angles are decreasing and settles) after the disturbances. The pre-fault rotor angle position for Generator Gen 01 was 18.26º which increased to 44.58º when the fault was applied and decreased to 33.2º in the second cycle and settled to around 25º as a new rotor angle position within 8 seconds. Similarly, the rotor angle for generator Gen 02 settled to around 16º as the new rotor angle-position within 8 seconds just after the fault was cleared. Initially, the rotor angle position was 9.2º and increased to 34.30º during the first cycle. Generator Gen 04 initial rotor angle position was about 0.2º before the fault was applied and increased to 4.5º when the fault was applied and settles to a new rotor-angle in about 8 seconds. The generator Gen 03 rotor angle shown in Figure 4.15 is zero degrees as it was modelled as the reference machine. The responses of the generator rotor angles indicate that the designed PSSs can damp the small-signal oscillation modes.

Figure 4.16 shows the corresponding generator speed responses with and without PSSs after the three-phase fault was applied. Similar trends to the rotor-angle position were observed for the generator speeds when the fault was introduced. The generator speeds increased from the fault inception to when the fault was cleared settling to new speed values as opposed to their responses when the generators were not equipped with the PSSs. Before the fault, the generator speeds were at 1 p.u which increased during the fault to about 1.008 p.u for generators Gen 01 and Gen 02 of area 1 and 1.004 p.u for generators Gen 03 and Gen 04 of area 2. From the generator speeds it can be observed that the PSSs performed as expected.

Figure 4.17 shows the generators' active power output responses following the three-phase fault without and with PSSs (black traces represents the generator active power responses without PSSs while the red traces represents the generator active power responses with the PSSs). The generator active power responses indicate that without PSSs installed on the generators the system exhibit some oscillations

whereas when the PSSs are installed the oscillations are dampened and the active power settles when the fault is cleared. The responses indicate that when the fault is applied the generator active powers reduce for the fault duration and then recover to their initial active power outputs when the fault was cleared. However, overshoots in the active power responses were observed before settling to their initial values within 5 seconds after the fault was cleared.

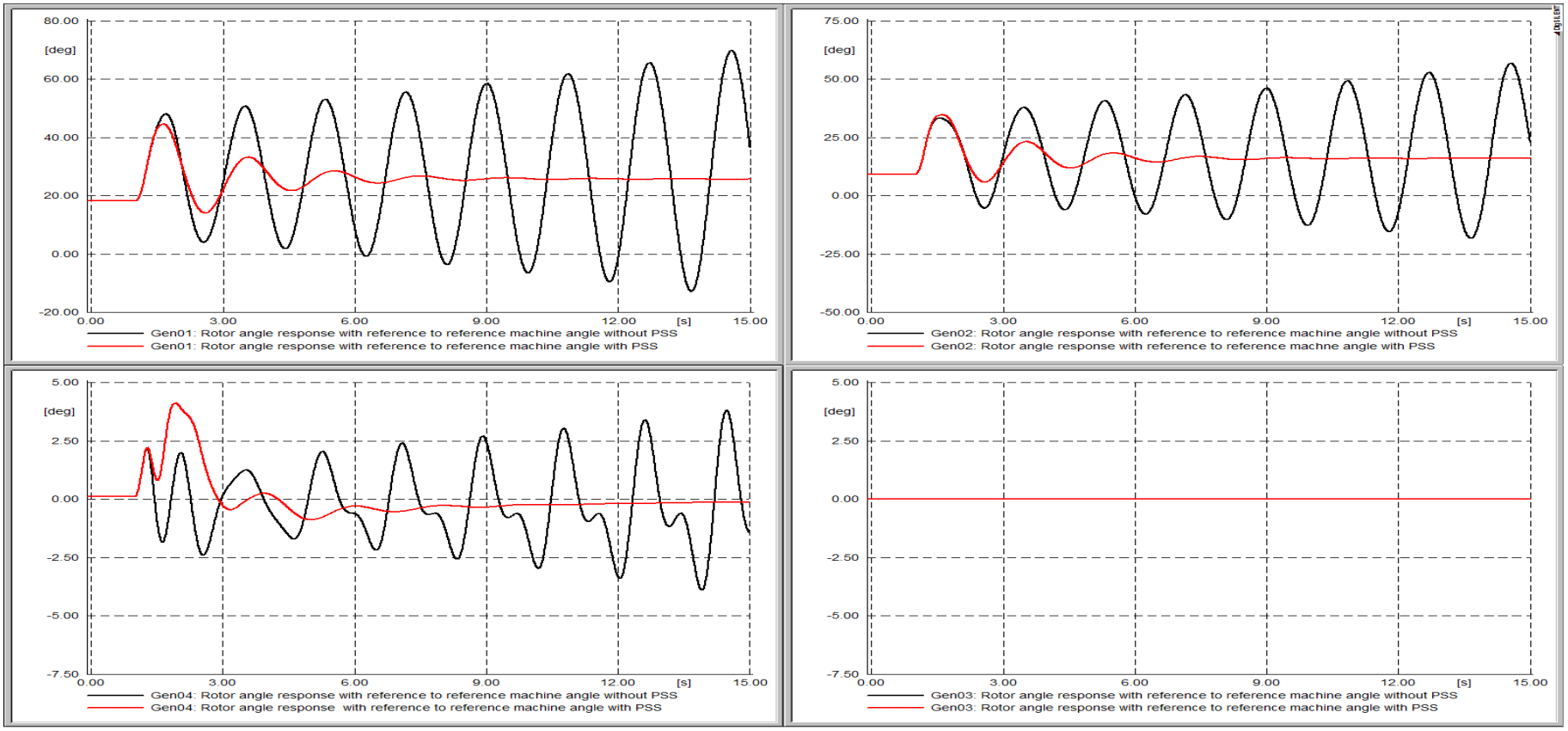

Figure 4.15: Case 1 generator rotor angles response with reference to reference machine (Gen 03) without and with designed PSSs

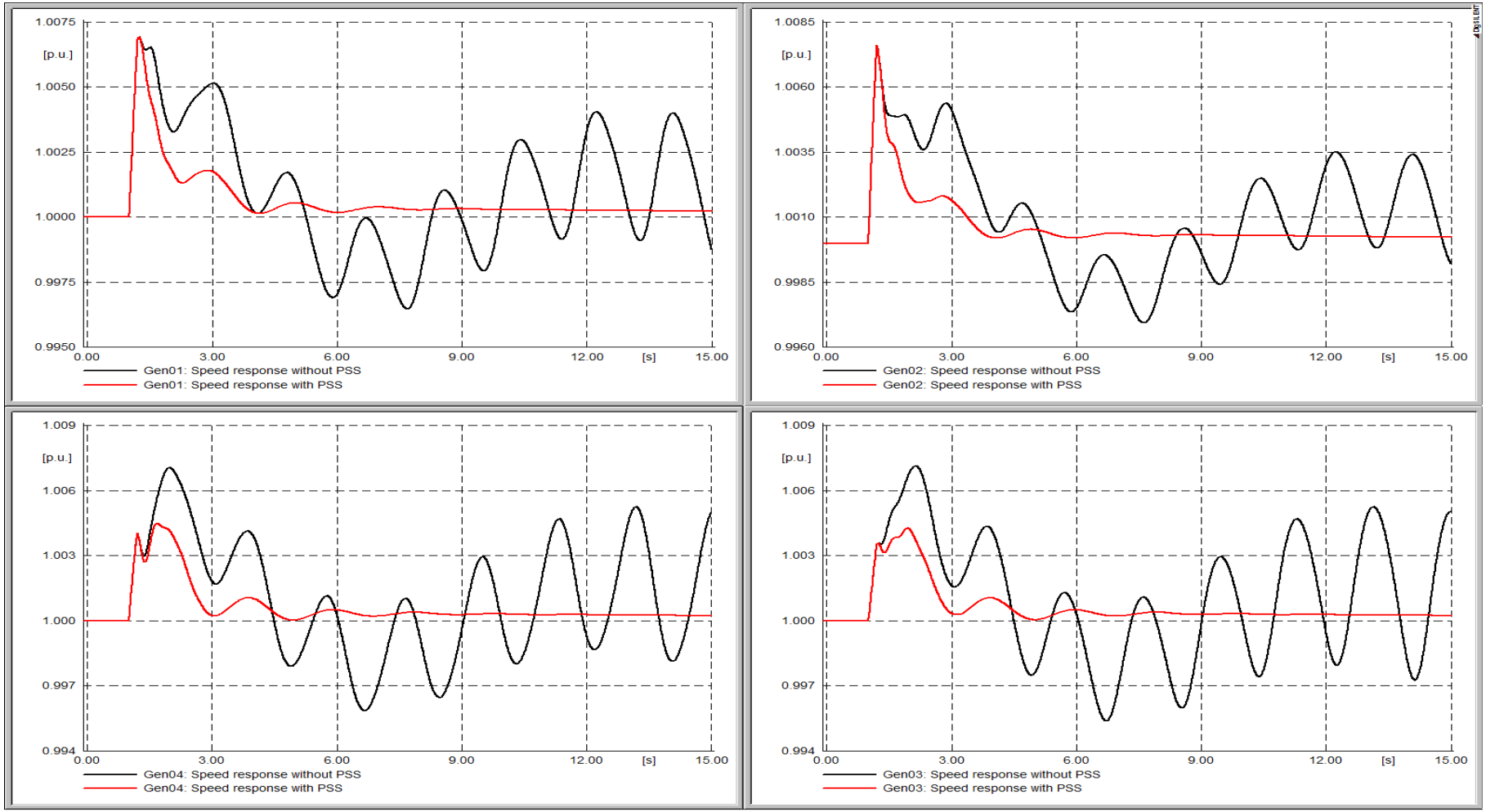

Figure 4.16: Case 1 generator speeds response to the 3-phase fault with and without designed PSSs

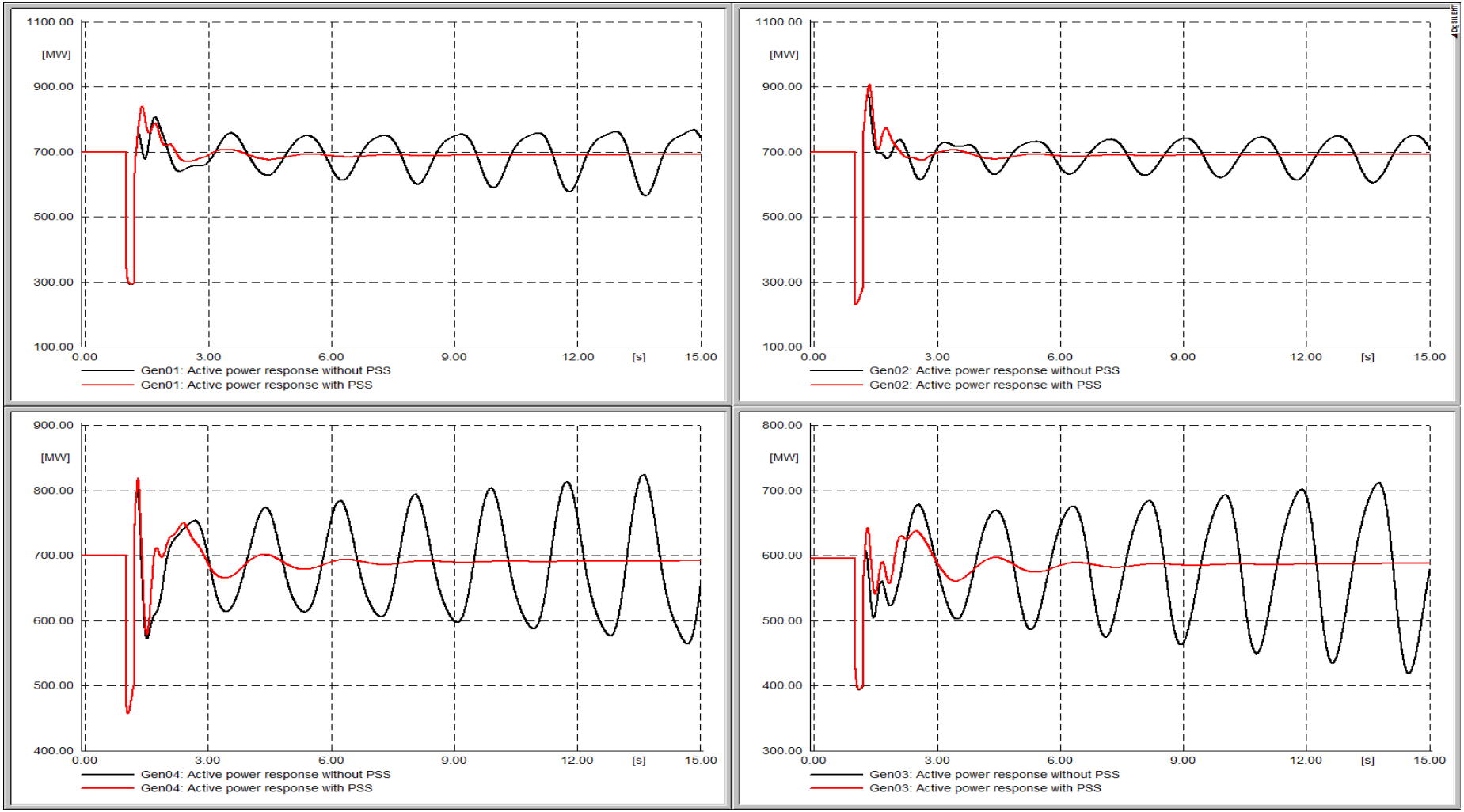

Figure 4.17: Case 1 generators active powers response to the 3-phase fault without and with designed PSSs

Similar trends in the generator rotor angles, speed and active power response with the designed PSSs were observed for Case 2, Case 3 and Case 4. The trends were that the PSSs could provide adequate damping of the small-signal oscillations modes in the time domain as revealed by the modal analysis results. However, the responses of generator rotor angle angles, speed and active power outputs after the three-phase fault inception with the PSSs for Case 3 alone are presented. For Case 3, Figure 4.18 shows a comparison of the generator rotor angle responses to the three-phase-fault for the generators with and without the designed PSSs. Firstly, without the designed PSSs the disturbance can excite the inter-area mode and the responses of the generator rotor angles indicate that the designed PSSs can damp the small-signal oscillation modes. Figure 4.19 further shows the corresponding generator speed responses with and without PSSs after the three-phase fault was applied. For Case 3 as well the generator speeds increased from the fault inception to when the fault was cleared settling to new speed values as opposed to their responses when the generators were not equipped with PSSs. Figure 4.20 also shows the generators' active power output responses following the 3-phase fault with and without PSSs (black traces represents the generator active power responses without PSSs while the red traces represents the generator active power responses with the PSSs). The generator active power responses indicate that the designed PSSs are able to damp the small-signal oscillations and the active power settles when the fault is cleared.

UNIVERSITY OF THE WITWATERSRAND
SCIENTIA ET LABORE
JOHANNESBURG

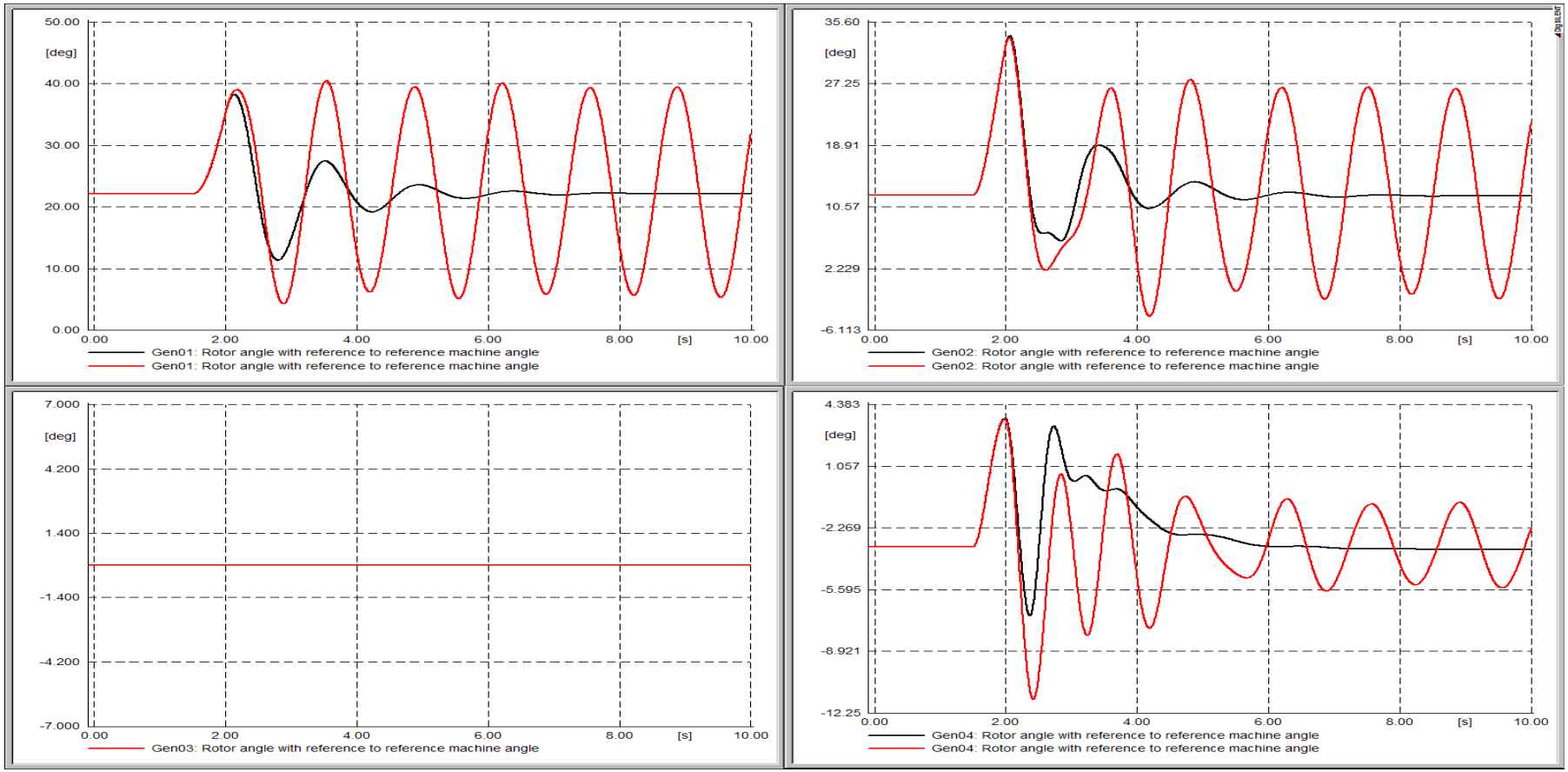

Figure 4.18: Case 3 generator rotor angles response with reference to reference machine (Gen 03) without and with designed PSSs

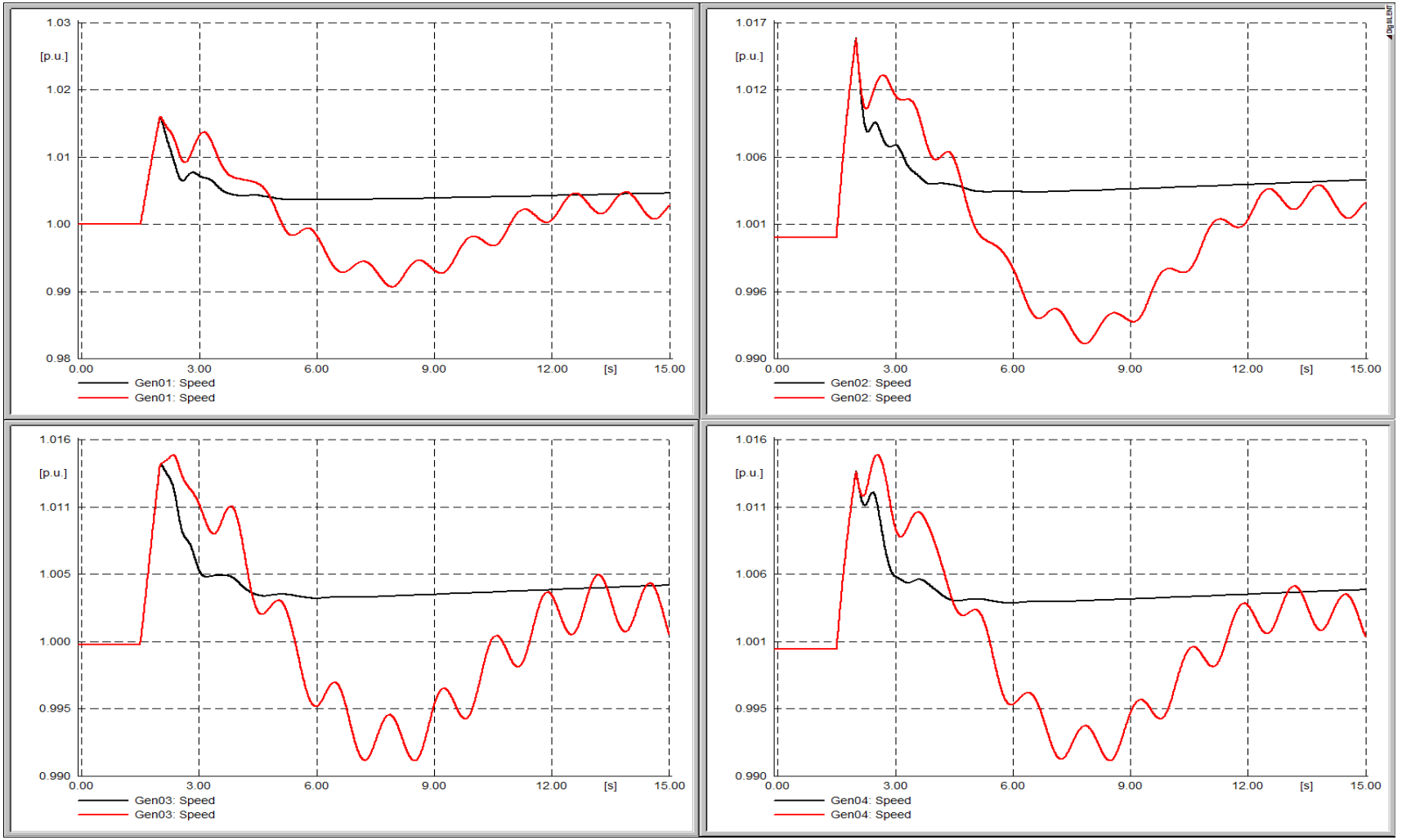

Figure 4.19: Case 3 generator speeds response to the 3-phase fault with and without designed PSSs

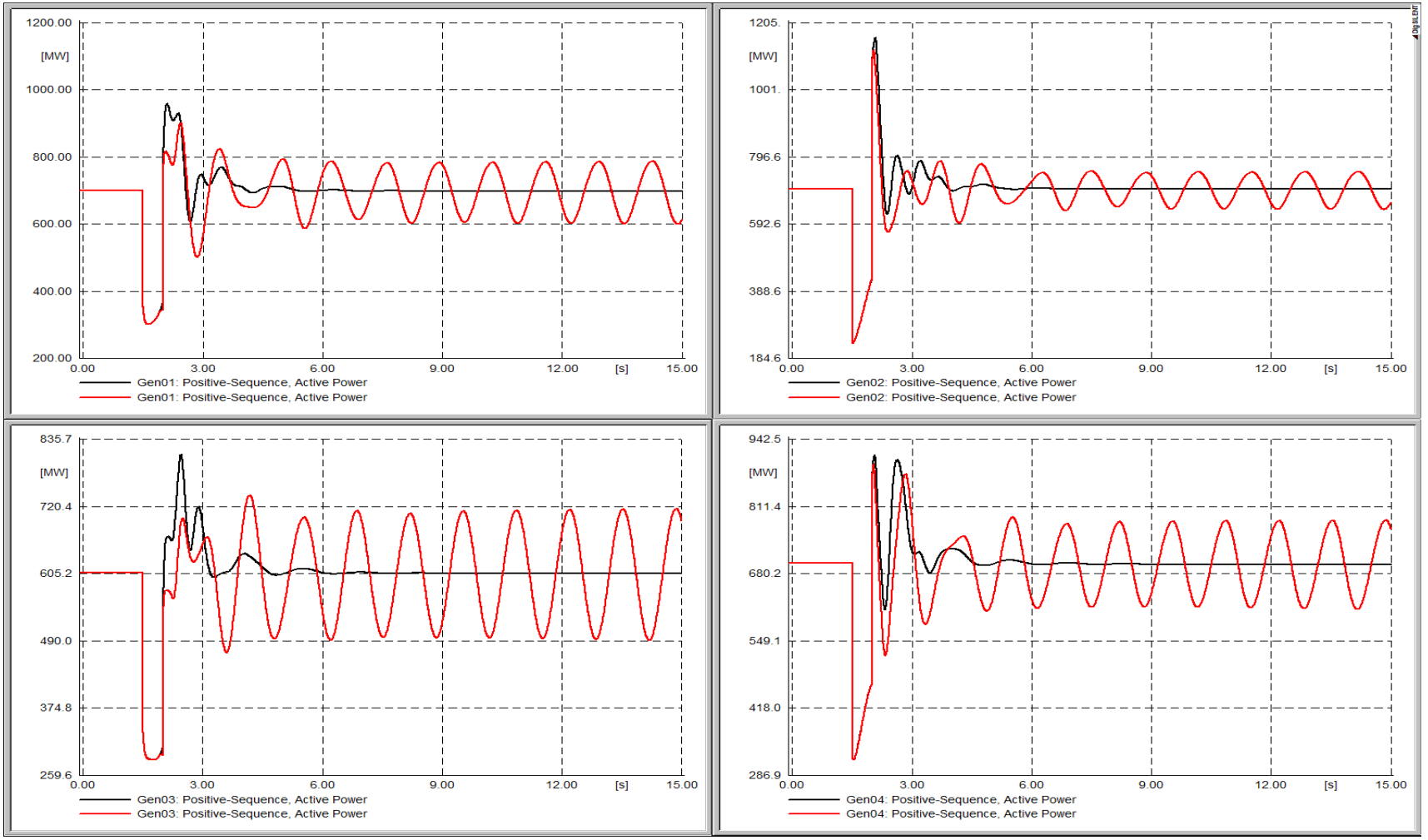

Figure 4.20: Case 3 generator speeds response to the 3-phase fault with and without designed PSSs

4.6. Summary

This chapter has presented the results of the application of small-signal stability analysis to the TAMM test system considering two generator control strategies viz manual excitation control and closed loop, high gain excitation system control (i.e. automatic excitation control). When the generators operated in manual excitation control mode, the system was stable while the inclusion of the high gain closed loop excitation systems resulted in the system becoming unstable. The small-signal analysis results were also corroborated using the FFT technique of the time domain response to small-disturbance. The PSS requirements and their siting selection was done in order to improve the test system small-signal stability. The chapter then provided the conventional design methods of the phase-lead, eigenvalue analysis and the root-locus technique to design PSSs. The designed PSSs could improve the TAMM system's small-signal stability with a slight decrease synchronizing torque. These results demonstrated that PSSs can be used to provide damping to both local and inter-area oscillation modes by optimizing the PSS gain.

UNIVERSITY OF THE WITWATERSRAND JOHANNESBURG
SCIENTIA ET LABORE

CHAPTER 5 : WIND POWER GENERATION IMPACT ON THE SMALL-SIGNAL STABILITY

The aim of this study was to investigate the impact of wind power generation on the inter-area and local oscillation modes of power systems. The previous chapter focused on the design and testing of Power System Stabilizer (PSS) settings for the Two-Area Multi-Machine (TAMM) system. The PSS gains were optimized in order to provide damping to both inter-area and local oscillation modes of the test power system. The focus of this chapter is to present the impact of wind power generation on the inter-area and local modes of the test power system using an aggregated Wind Power Plant (WPP) model developed in Chapter 3. The first part focuses on the impact of wind power generation on the inter-area and local oscillation modes without PSSs installed on the synchronous generators and the final part consider the generators equipped with PSSs designed in the previous chapter.

5.1. Impact of Wind Generation on Inter-Area and Local Oscillation Modes without Power System Stabilizers (PSSs)

Section 4.1 of Chapter 4 performed the small-signal analysis of the TAMM test system configuration shown in Figure 2.9 with the generators operating with automatic excitation control enabled and without PSSs in the absence of any wind power generation sources. Figure 5.1 shows the eigenvalue results obtained when the synchronous generators operated in automatic excitation control mode without PSSs and wind power generation sources. The results showed that the test system is unstable when the generators operated in automatic excitation control mode. This was due to inter-area oscillation mode eigenvalues having a positive real part. As discussed earlier, this was because of the high gain excitation system which was deliberately set higher. Table 5.1 provides the calculated eigenvalue analysis results showing the characteristics of the inter-area and local oscillation modes. The inter-area mode involved generators Gen 01 and Gen 02 of area 1 oscillating against generators Gen 03 and Gen 04 of area 2 at 0.61 Hz with a negative damping ratio of 1.2% which was below the minimum acceptable value of 5%. Generator Gen 03 of area 2 had the highest participation factor towards this inter-area mode. At the same time, generators in the two areas, generators Gen 01 and Gen 02 in area 1 and generators Gen 03 and Gen 04 in area 2 were oscillating against each other at 1.12 Hz and 1.15 Hz respectively. The local modes damping ratios were 9.1% and 8.8% respectively which was above the minimum damping requirement. These eigenvalue results provided a base case against which to compare the cases with wind power generation sources for assessing the impact of wind power on the inter-area and local modes. It was deemed convenient to choose a conventional synchronous generator of the test system to replace with wind power while observing the system's small-signal stability characteristics. To do this, the generators to be replaced were selected based on their participation factor towards the inter-area and local modes as presented earlier in Chapter 4.

Table 5.1: Eigenvalue analysis results without wind power

	Inter-area oscillation mode	**Area 1 local oscillation mode**	**Area 2 local oscillation mode**
Eigenvalue	0.05 ± j3.82	-0.64 ± j7.02	-0.64 ± j7.23
Frequency	0.61 Hz	1.12 Hz	1.15 Hz
Damping ratio	-1.2%	9.1%	8.8%
Generator	**|PF|**	**|PF|**	**|PF|**
Gen 01	0.387	0.766	0.006
Gen 02	0.230	0.880	0.016
Gen 03	0.614	0.029	0.419
Gen 04	0.498	0.012	0.526

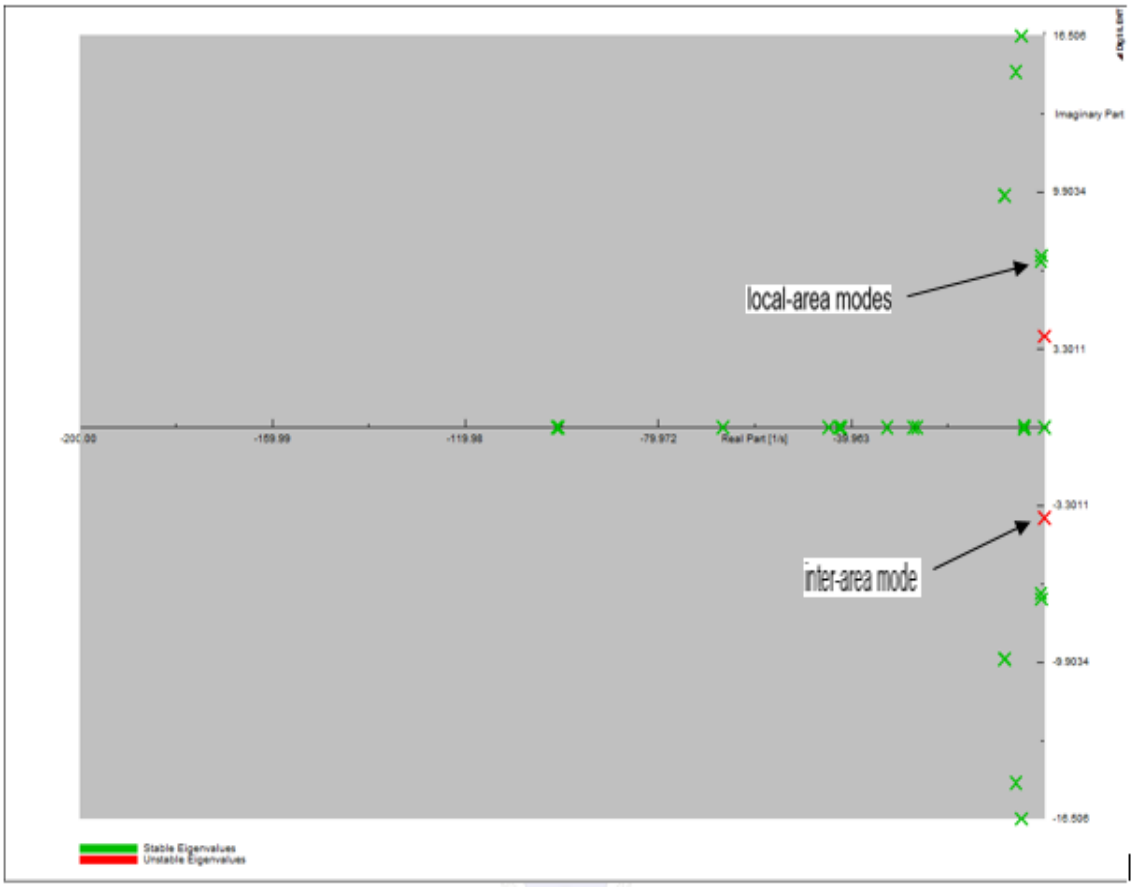

Figure 5.1: Eigenvalue plot of the TAMM system without WPP

When replacing the generators, the approach involved gradually reducing the output dispatch of the selected generators without changing its MVA rating and at the same time compensating the same amount with wind power. As an example, for 100 MW compensation from WPP the number of parallel generators and pad-mount transformers of the WPP model were set to 50 which correspond to a WPP of 100 MW with installed capacity of 100 MVA based on the used Type 4 WTG ratings of 2 MVA with a unity power factor. The number of parallel lines and main transformer representing the collector cable system and station transformer at the WPP point of connection were set at 1. For the 200 MW compensation from WPP the number of parallel generators and pad-mount transformers of the WPP model were set to 100 while the number of parallel lines of the collector cable system and main transformer at the WPP point of connection was increased by 1 which correspond to 200 MW WPP with capacity of 200 MVA. The same approach was done for the required 300 MW to 700 MW of wind power.

5.1.1. Wind Power Replacing Conventional Generation

In this case, the synchronous generator output dispatch was gradually reduced and replaced with wind power generation to investigate the impact of wind power on the inter-area and local modes without PSSs. To determine the impact of wind power generation on the inter-area modes generator Gen 03 of area 2, which had the highest participation factor towards the inter-area mode, output dispatch was gradually decreased while the wind power generation source was introduced to compensate the reduction. The output dispatch of generator Gen 03 was decreased in steps of 100 MW from its initial dispatch of 700 MW to zero while maintaining its MVA rating. The wind power compensating generator Gen 03 active power, and other cases investigated, was provided from the WPP by increasing the number of parallel generators, pad-mount transformers, collector cable and main transformer of the WPP. This was done in a way that the power output corresponds to the reduced active power of the synchronous generator.

UNIVERSITY OF THE WITWATERSRAND JOHANNESBURG

Figure 5.2 shows the TAMM configuration including the WPP replacing generator Gen 03. The small-signal analysis of the configuration in Figure 5.2 was conducted and the results were compared to the case without wind power generation source focusing on the inter-area and local modes. Figure 5.3 shows the system eigenvalue results with the 100 MW WPP integrated which are compared in Figure 5.4 with the base case without the WPP. Figure 5.4 shows that there were some differences between the system eigenvalue characteristics without and with the 100 MW WPP. The eigenvalue results with the 100 MW WPP had additional eigenvalues when compared to the original case without wind power sources shown in Figure 5.1. In addition, there were also slight changes in the original eigenvalue characteristics when the 100 MW WPP source was included. The results showed that the additional eigenvalues were from the WPP torsional mode between WT rotor and WT generator two-mass model (but these modes are not important for synchronous generators). The torsional mode and the control mode eigenvalues were at -0.412 ± j 8.112 and -90.124 ± j 38.17 oscillating at 1.29 Hz and 6.1 Hz respectively as revealed earlier by the small-signal analysis of the WPP model in Chapter 3. The differences between the system eigenvalue results particularly the inter-

area and local oscillation mode results of the base case without wind power against cases with varying wind power generation sources up to 700 MW are presented further in detail in the following sections.

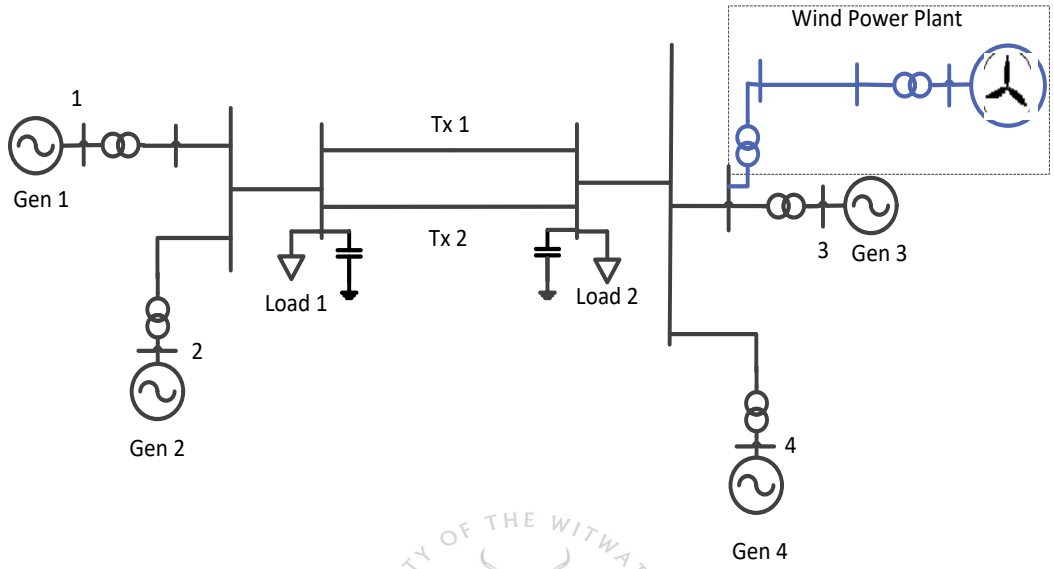

Figure 5.2: Two-Area Multi-Machine (TAMM) system with generator 03 replaced with a Wind Power Plant (WPP)

UNIVERSITY OF THE WITWATERSRAND JOHANNESBURG

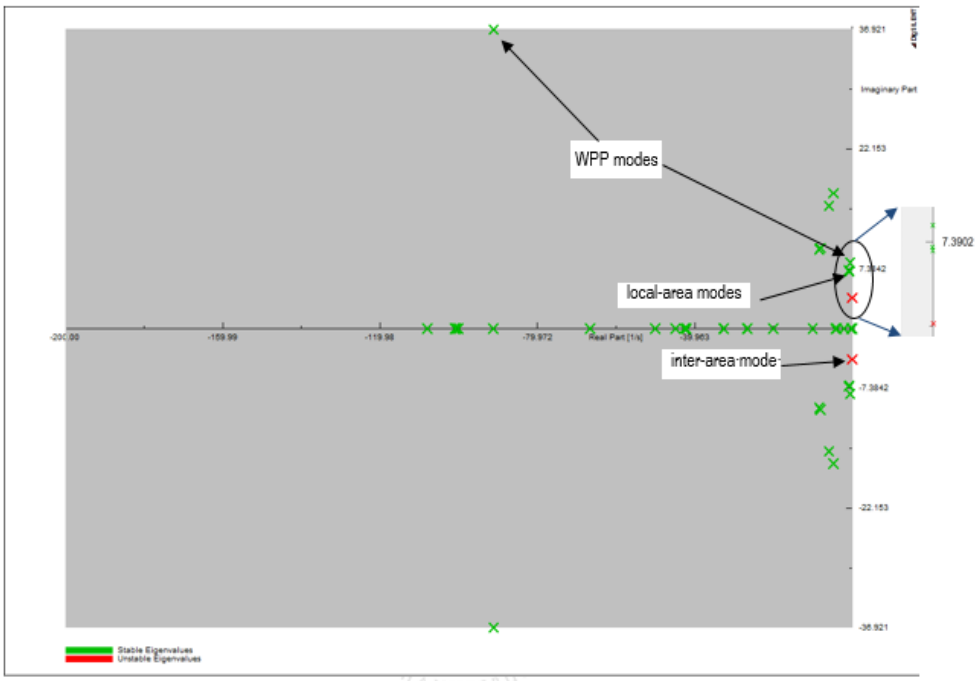

Figure 5.3: Eigenvalue plot of the TAMM system with WPP

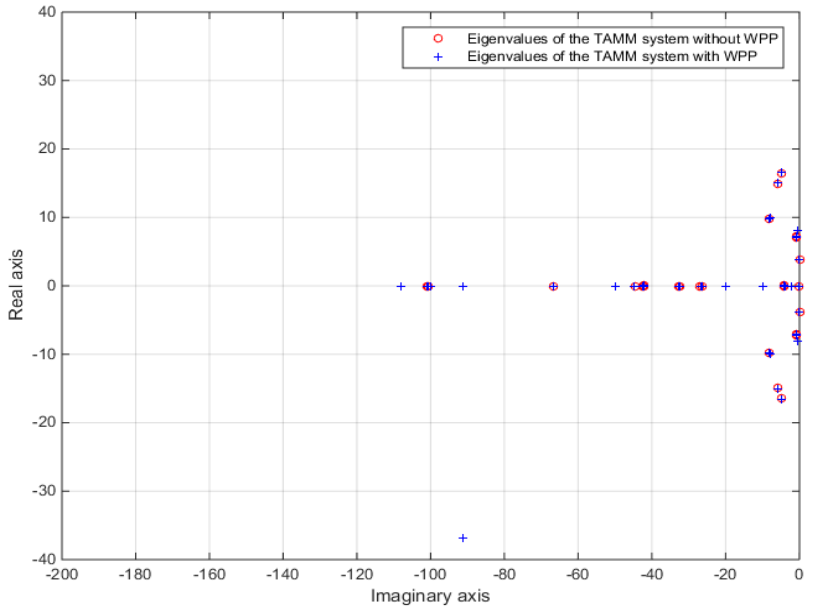

Figure 5.4: Comparison of the eigenvalues of the TAMM system without and with WPP (100 MW)

Inter-area mode behaviour

As the generator, Gen 03 dispatch was varied further from 700 MW to 200 MW in steps of 100 MW while maintaining the generator MVA rating and using wind power to compensate the generator reduced output dispatch the differences between the original eigenvalues without wind power and with increased wind power generation became significant. The inter-area mode eigenvalues and frequency for each scenario considered are provided in Table 5.2. Initially, the inter-area mode eigenvalues (0.05 ± j 3.820) had positive real parts indicating an unstable mode at 0.61 Hz with a damping ratio of -1.22%. When the wind power penetration increased the inter-area mode eigenvalue moved slightly to 0.029 ± j 3.797 with a decrease in frequency of 0.009 Hz to 0.604 Hz and increased damping ratio from -1.22% to -0.77% for 100 MW wind power integration. As the wind power penetration increased to 200 MW to compensate the reduction in the conventional generation dispatch the inter-area oscillation mode eigenvalue moved further left to 0.012 ± j 3.78 which further reduced the frequency from 0.604 Hz to 0.602 Hz with an increased damping ratio of -0.31%. The inter-area mode eigenvalues moved further the left-half of the complex plane and became stable when the wind power penetration was increased to 300 MW (which was 42% of initial conventional generator Gen 03 output dispatch). The inter-area mode eigenvalue moved to -0.005 ± j 3.763 with a reduction in the frequency to 0.599 Hz and an increased damping ratio of 0.14%. Further increase in wind power generation to 400 MW moved the inter-area mode eigenvalue to -0.021 ± j 3.747 consequently resulting in the frequency decreasing further to 0.596 Hz with an increased damping ratio of 0.55%. When the wind power increased to 500 MW the inter-area mode frequency decreased to 0.594 Hz while the damping ratio increased to 0.89%. The decrease in frequency of the inter-area oscillation mode was further observed when 600 MW and 700 MW of wind power generation compensation. For the two cases of 600 MW and 700 MW WPP, the eigenvalues of the inter-area mode were -0.041 ± j 3.726 and -0.042 ± j 3.727 resulting in the mode frequency of 0.593 Hz. The corresponding damping ratios were 1.1% and 1.14% respectively.

Table 5.2: Inter-area oscillation mode with increasing wind power (no PSSs)

Wind power (MW)	Eigenvalue $(\sigma \pm j\omega)$	Frequency (Hz)	Percentage damping ratio $(\zeta \times 100\%)$
0	0.05 ± j 3.820	0.610	-1.22
100	0.029 ± j 3.797	0.604	-0.77
200	0.012 ± j 3.780	0.602	-0.31
300	-0.005 ± j 3.763	0.599	0.14
400	-0.021 ± j 3.747	0.596	0.55
500	-0.033 ± j 3.735	0.594	0.89
600	-0.041 ± j 3.726	0.593	1.10
700	-0.042 ± j 3.726	0.593	1.14

Table 5.3 provides calculated changes in the inter-area mode frequencies and damping ratios with increasing wind power compensating generator Gen 03 output dispatch in area 2. In this dissertation, the change in the frequencies and damping ratios of the inter-area and local oscillation modes with wind power penetration were determined by taking the difference between the case with wind power source and that without wind power. The decrease in frequency with wind power from the original case without the wind power varied from 0.006 Hz to 0.017 Hz for 100 MW to 700 MW of wind power integration. At the same time, the change of the inter-area oscillation mode damping ratios from the original case without wind power were calculated and are provided in Table 5.3. The variation between minimum and maximum increase of the inter-area mode damping ratio was from 0.45% for 100 MW to 2.36% for 700 MW wind power integration.

Table 5.3: Percentage change in inter-area mode frequency with reference to case without wind power

Wind power (MW)	**Frequency (Hz)**	**Percentage damping ratio ($\boldsymbol{\zeta \times 100\%}$)**	**Frequency decrease with reference to case without wind power (Hz)** $(f_n - f_0)$	**Percentage change in damping ratio with reference to case without wind power (%)** $(\zeta_n - \zeta_0)$
0	0.610	-1.22%	-	-
100	0.604	-0.77%	0.006 Hz	0.45%
200	0.602	-0.31%	0.008 Hz	0.91%
300	0.599	0.14%	0.011 Hz	1.36%
400	0.596	0.55%	0.014 Hz	1.77%
500	0.594	0.89%	0.016 Hz	2.11%
600	0.593	1.10%	0.017 Hz	2.32%
700	0.593	1.14%	0.017 Hz	2.36%

where: f_0 = mode frequency without wind power integrated, f_n = mode frequency with *n* MW of wind power integrated
ζ_0 = mode damping ratio without wind power integrated, ζ_n = mode damping ratio with *n* MW of wind power integrated

The inter-area power flows for each integration scenario considered were monitored and compared against the case without wind power integration and are presented in Table 5.4. The resulting power flows from area 1 to area 2 for the scenarios investigated remained fairly constant with increasing wind power compensating the reduced synchronous generation output dispatch. This was because in each of the two interconnected areas the supply and load demand were not altered.

Table 5.4: Different load flows for the integration of WPPs of different capacity for the inter-area mode investigation

Wind power penetration level (in MW)	0	100	200	300	400	500	600	700
Inter-area active power (MW)	404.4	404.4	404.4	404.4	404.3	400.2	400.2	400.2

Local oscillation mode behaviour

Figure 5.5 and Figure 5.6 show the configurations used to investigate the impact of wind generation on the local modes between generators, Gen 01 and Gen 02 of area 1 and generators Gen 03 and Gen 04 of area 2 separately. The generators Gen 02 and Gen 04 with the highest participation factor towards area 1 and area 2 local modes respectively were selected and gradually reduced their dispatch outputs. Wind power was introduced to compensate the reduction in the generator dispatch in a similar approach used when considering generator Gen 03 of area 2 for the inter-area mode study. The eigenvalue analysis of the configurations shown in Figure 5.5 and Figure 5.6 were conducted separately and the results with 100 MW of wind power integrated were similar to those in Figure 5.3 and Figure 5.4.

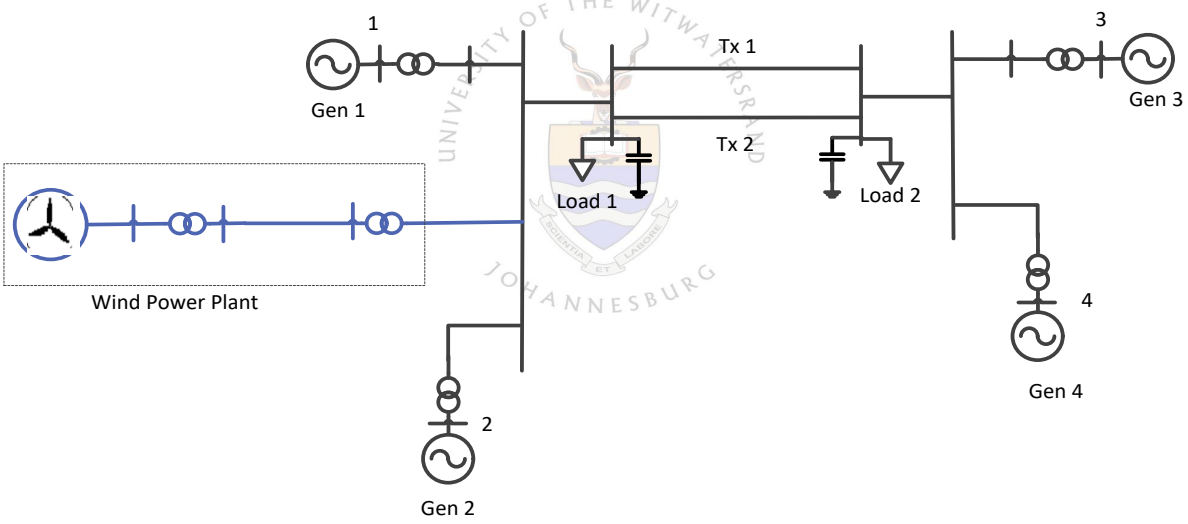

Figure 5.5: Two-Area Multi-Machine (TAMM) system with generator 02 replaced with a Wind Power Plant (WPP) (no PSSs)

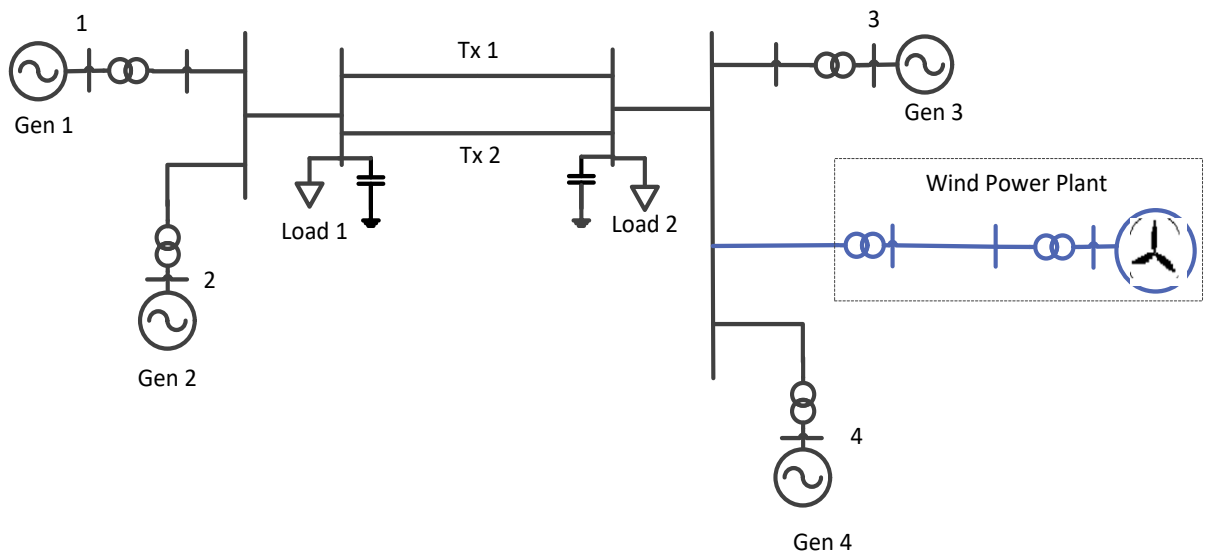

Figure 5.6: Two-Area Multi-Machine (TAMM) system with generator 04 replaced with a Wind Power Plant (WPP) (no PSSs)

Table 5.5 shows area 1 local mode characteristics when generator Gen 02 output dispatch was gradually reduced from 700 MW to zero output in steps of 100 MW while being compensated with wind power using the configuration in Figure 5.5. Table 5.5 also provides the area 2 local mode characteristics between generators Gen 03 and Gen 04 as generator Gen 02 in area 1 reduced dispatch was gradually replaced with wind power. From Table 5.5 the frequency and damping ratio of the area 2 local mode barely changed. This would be expected since generators Gen 03 and Gen 04 of area 2 which participated in the area 2 local mode were not altered. In contrast, there were significant changes in the characteristics of the area 1 local mode. It can thus be inferred that wind power generation in one area exporting power does not affect the local oscillation modes in another area far from the wind farm location.

Table 5.5: Local oscillation mode with increasing wind power (no PSSs) (as generator Gen 02 in area 1 dispatch was gradually replaced with wind power)

Wind power (MW)	Area 1 local mode characteristic			Area 2 local mode characteristic		
	Eigenvalue $(\sigma \pm j\omega)$	Frequency (Hz)	Percentage damping ratio $(\zeta \times 100\%)$	Eigenvalue $(\boldsymbol{\sigma \pm j\omega})$	Frequency (Hz)	Percentage damping ratio $(\zeta \times 100\%)$
100	-0.765 ± j 6.931	1.10	10.97%	-0.623 ± j 7.235	1.151	8.6%
200	-0.878 ± j 6.829	1.09	12.75%	-0.618 ± j 7.235	1.151	8.5%
300	-0.968 ± j 6.719	1.07	14.25%	-0.613 ± j 7.236	1.152	8.4%
400	-1.031 ± j 6.613	1.05	15.40%	-0.608 ± j 7.237	1.152	8.4%
500	-1.068 ± j 6.531	1.04	16.13%	-0.604 ± j 7.238	1.152	8.3%
600	-1.081 ± j 6.487	1.033	16.44%	-0.599 ± j 7.239	1.152	8.2%
700	-1.075 ± j 6.496	1.034	16.33%	-0.594 ± j 7.241	1.152	8.2%

With reference to the area 1 local mode without wind power, generators Gen 01 and Gen 02 were oscillating at 1.12 Hz with a damping ratio of 9.1%. In comparison to the original case without wind power generation, the integration of 100 MW from wind power resulted in the local mode frequency decreasing by 0.02 Hz to 1.10 Hz while the damping ratio increased to 10.97%. Further increase of wind power to 200 MW to compensate generator Gen 02 reduced dispatch resulted in area 1 local mode frequency decreasing further to 1.09 Hz with increased damping ratio of 12.75%. For 300 MW of wind power compensating a reduction in the conventional generation output dispatch the area 1 local mode frequency further decreased by 0.02 Hz to 1.07 Hz while the damping ratio increased by 1.5% to 14.25% in comparison to the case with 200 MW of wind power. The frequency of the local mode decreased progressively by 0.02 Hz to 1.05 Hz while the damping ratio increased to 15.4% for 400 MW of wind power. As wind power penetration increased to 500 MW and 600 MW compensating the conventional generation reduced dispatch output the area 1 local mode frequency further decreased by 0.01 Hz to 1.04 Hz and 1.03 Hz. For these two cases the damping ratio increased to 16.13% and 16.44% respectively. For 700 MW wind power generation integration compensating the full output dispatch of Gen 02 the local mode frequency slightly increased from 1.033 Hz to 1.034 Hz with a decrease in damping to 16.33%.

Table 5.6 provides the power flows between area 1 and area 2 when generator Gen 02 dispatch output was varied and compensated with wind power. In this case, significant changes in the inter-area power flows between area 1 and area 2 were observed and compared to the base case without wind power. The significant differences in the power flows can be explained based on the power flow directions over and above the generation and load requirements in the exporting area and the WPP losses. The losses of the WPP were determined to be

around 3% for 100 MW WPP and the losses also increases with the increasing WPP dispatch output. As the synchronous generator dispatch output reduced the amount of exported power was reduced in order to compensate for the WPP losses to meet the local load requirements.

Table 5.6: Inter-area active power flows for the integration of WPPs of different capacity for the area 1 local mode investigation

Wind power penetration level (in MW)	**0**	**100**	**200**	**300**	**400**	**500**	**600**	**700**
Inter-area active power (MW)	404.4	397.6	394.8	392	389	386.2	383.4	380.6

Table 5.7 shows the area 2 local mode characteristic when generator Gen 04 dispatch output in area 2 was gradually compensated with wind power from 700 MW to zero output in steps of 100 MW using the configuration shown in Figure 5.6. Table 5.7 also provides the area 1 local mode characteristic as generator Gen 04 of area 2 dispatch output was varied and replaced with wind power. Similar to the previous case when area 1 local mode was investigated, the results in Table 5.7 shows that local mode frequency and damping ratio in the area without wind power integration remained unchanged. In this case, area 1 local mode frequency and damping ratio remained unchanged. This was because the dispatch of generators Gen 01 and Gen 02 participating in area 1 local mode were not altered.

Table 5.7: Area 2 local oscillation mode with increasing wind power (no PSSs) (as generator Gen 04 in area 2 dispatch was gradually replaced with wind power)

Wind power (MW)	**Area 2 local mode characteristic**			**Area 1 local mode characteristic**		
	Eigenvalue $(\sigma \pm j\omega)$	**Frequency (Hz)**	**Percentage damping ratio** $(\zeta \times 100(\%))$	**Eigenvalue** $(\sigma \pm j\omega)$	**Frequency (Hz)**	**Percentage damping ratio** $(\zeta \times 100(\%))$
100	-0.763 ± j 7.178	1.142	10.6%	-0.644 ± j 7.016	1.117 Hz	9.1%
200	-0.855 ± j 7.042	1.121	12.1%	-0.640 ± j 7.014	1.116 Hz	9.1%
300	-0.941 ± j 6.931	1.103	13.5%	-0.640 ± j 7.014	1.116 Hz	9.1%
400	-1.005 ± j 6.828	1.087	14.6%	-0.640 ± j 7.014	1.116 Hz	9.1%
500	-1.046 ± j 6.751	1.075	15.3%	-0.639 ± j 7.014	1.116 Hz	9.1%
600	-1.068 ± j 6.719	1.069	15.7%	-0.639 ± j 7.013	1.116 Hz	9.1%
700	-1.071 ± j 6.744	1.073	15.7%	-0.639 ± j 7.012	1.116 Hz	9.1%

With reference to the area 2 local mode without wind power generation, the generators in area 2 i.e. Gen 03 and Gen 04 were oscillating at 1.15 Hz with a damping ratio of 8.6% which changed with the introduction of 100 MW from wind power source to compensate for decrease in synchronous generator dispatch. The resulting area 2 local mode frequency decreased to 1.142 Hz and the damping ratio consequently

increased from 8.6% to 10.6%. Further increase in the wind power to 200 MW to compensate generator Gen 04 reduced dispatch resulted in area 2 local mode frequency decreasing to 1.121 Hz with increased damping ratio of 12.1%. For 300 MW of wind power integrated to compensate a reduction in the conventional generation dispatch, the area 2 local mode frequency decreased by 0.08 Hz to 1.103 Hz while the damping ratio increased to 13.5%. Area 2 local oscillation mode frequency decreased by 0.016 Hz to 1.087 Hz with 400 MW of wind power generation compensating conventional generation and the damping ratio increased to 14.6%. For 500 MW of wind power in area 2 the local oscillation mode frequency further decreased to 1.075 Hz while the damping ratio increased to 15.3%. When 600 MW of wind power compensating the reduction in generator Gen 04 dispatch, the local mode frequency decreased to 1.069 Hz with increased damping ratio of 15.7%. For 700 MW of wind power, the area 2 local mode frequency slightly decreased by 0.004 Hz from 1.069 Hz when 600 MW of wind power was considered to 1.073 Hz while the damping ratio remained constant at 15.7%. Figure 5.7 graphically shows the increase in the local mode damping ratios with increasing wind power compensating a reduction in conventional synchronous generator dispatch. As explained earlier, the local mode frequencies in the two areas decreased with wind power compensating the reduction in the synchronous generator output dispatch.

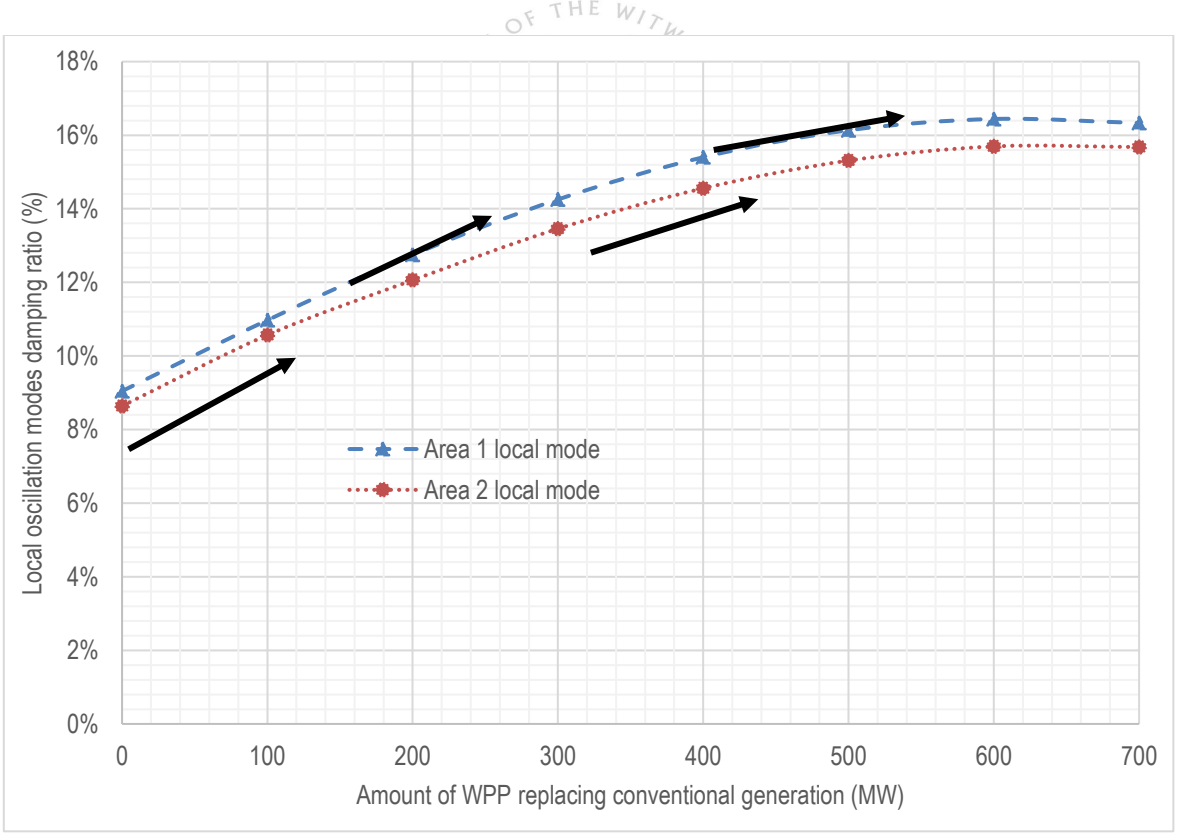

Figure 5.7: Local oscillation modes damping ratios with gradual increase in wind power without PSSs

Table 5.8 provides the percentage change of local oscillation modes frequency and damping ratios with increasing wind power penetration relative to the base case without wind power generation. Area 1 local mode percentage changes in Table 5.8 were calculated by considering f_0 = 1.12 Hz and ζ_0 = 9.1% as local mode frequency and damping ratio respectively without wind power integrated while f_n and ζ_n are the area 1 local mode frequency and damping ratio at different wind power integration levels as provided in Table 5.5. For the area 2 the local mode frequency f_0 and damping ratio ζ_0 with wind power 1.15 Hz and 8.8% respectively while f_n and ζ_n are the local mode frequency and damping ratio respectively with various level of wind power integrated as provided in Table 5.7. The percentage change calculation suggests that when wind power is integrated in the area receiving power the local mode frequency is less sensitive than the frequency of the local mode of the area sending power when the wind power source is integrated within the area. The local mode frequencies decreased by 0.8% to 8.1% and 2% to 9% when the wind power was separately integrated in the receiving area and exporting area respectively for the same amount of wind power capacity. The resulting damping ratios of the local modes were less sensitive when the wind power was integrated in the area receiving power. The damping ratios increase varied from minimum to maximum of 1.87% to 7.34% in the exporting and 1.8% to 6.9% in the area receiving power.

Table 5.8: Local modes characteristic with increasing wind power compensating synchronous generator dispatch variation

Area 1 local mode characteristic			**Area 2 local mode characteristics**	
Wind power (MW)	**Percentage decrease in frequency with reference to case without wind power** $(f_n - f_0) \times 100\%$	**Percentage increase in damping ratio with reference to case without wind power (%)** $(\zeta_n - \zeta_0)$	**Percentage decrease in frequency with reference to case without wind power** $(f_n - f_0) \times 100\%$	**Percentage increase in damping ratio with reference to case without wind power (%)** $(\zeta_n - \zeta_0)$
100	- 2%	1.87%	- 0.8%	1.8%
200	- 3%	3.65%	- 2.9%	3.3%
300	- 5%	5.15%	- 4.7%	4.7%
400	- 7%	6.30%	- 6.3%	5.8%
500	- 8%	7.03%	- 7.5%	6.5%
600	- 9%	7.34%	- 8.1%	6.9%
700	- 9%	7.23%	- 7.7%	6.9%

Table 5.9 shows the power flows from area 1 to area 2 observed when generator Gen 04 in area 2 was gradually replaced with wind power. The results indicate that the export from area 1 to area 2 did not change significantly because the generation and load requirements in area 1 which were not altered.

Table 5.9: Different load flows for the integration of WPPs of different capacity for the area 2 local mode investigation

Wind power penetration level (in MW)	**0**	**100**	**200**	**300**	**400**	**500**	**600**	**700**
Inter-area active power (MW)	404.4	400.4	404.4	404.4	404.4	404.2	404.2	404.2

Based on the results when wind power generators operate in parallel with conventional synchronous generators compensating reduction in the synchronous generator dispatch the frequencies of inter-area and local oscillation modes decrease while damping ratios increased. The base case without wind power had the synchronous generators operating at higher outputs and the transmission system was heavily loaded. Thus, the system was heavily congested under which the damping ratios of the oscillation modes were low and reducing the output of the generator with the highest participation towards the inter-area mode de-loads the synchronous generator which changes its operating point. The change in the operating point together with the observed changes in the power flows result in the overall operating conditions changing and contributes to the change of the mode characteristics. In this case, it can be argued that the damping ratios of the inter-area and local modes increased because the generators, with highest participating towards the modes, output dispatch were reducing, i.e. operating at a lower output hence it was being lightly loaded, with increasing wind power penetration. This can however be associated with a decrease or an increase in the oscillation mode frequencies for which in this case the frequencies decreased. Another observation is that the local modes are more sensitive to the wind power penetration than the inter-area modes if the generators with high participation towards the modes are compensated with wind power.

5.1.2. Wind Power Supplying Increasing System Load

Figure 5.8 and Figure 5.9 show the TAMM configurations used to investigate the impact of wind power on inter-area and local oscillation modes when wind power source is used to supply increasing system load with the synchronous generators operating without the designed PSSs. The load active power in each area was gradually increased in 100 MW steps to 700 MW while the WPP was varied to supply the load. Similar to the previous cases investigated, the WPP output compensating for the load increase was attained by changing the number of parallel generators and pad-mount transformers which were initially set to 50 while the number of parallel lines of the collector cables and the main transformer were set to 1 for a 100 MW WPP.

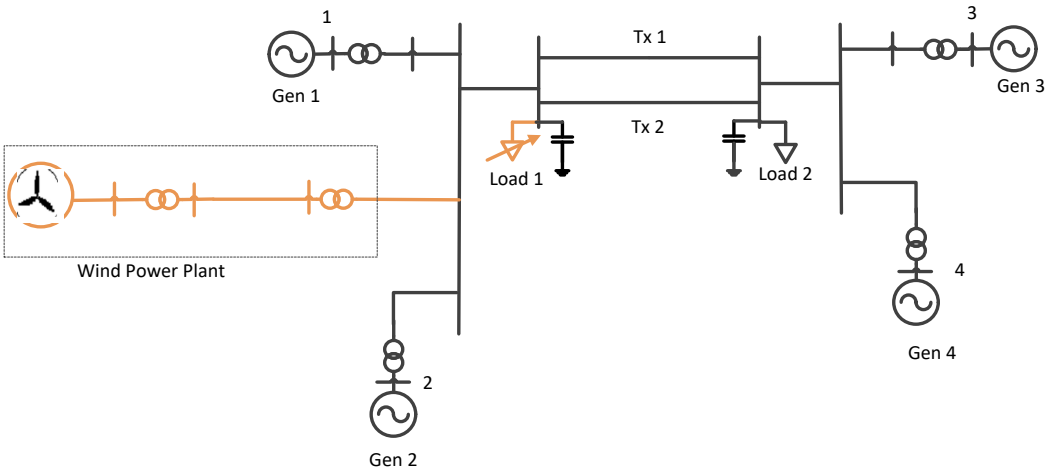

Figure 5.8: Two-Area Multi-Machine (TAMM) system with Wind Power Plant (WPP) in area 1 supplying increasing load (Load 1) (no PSSs)

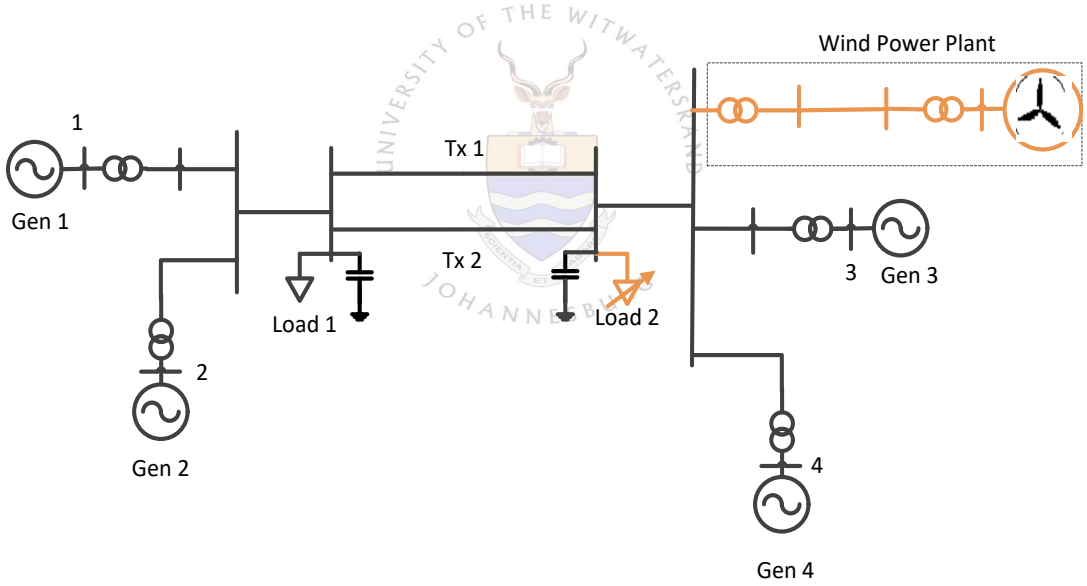

Figure 5.9: Two-Area Multi-Machine (TAMM) system with Wind Power Plant (WPP) in area 2 supplying increasing load in area 2 (no PSSs)

Wind power supplying increasing system load in area 1

Figure 5.10 and Figure 5.11 show the behaviour of the inter-area and local mode frequencies and damping ratios when wind power is used to supply the area 1 load increase respectively. The results indicate that when wind power generation is used to supply increasing load in parallel with the synchronous generators the frequencies and damping ratios of inter-area and local modes decrease.

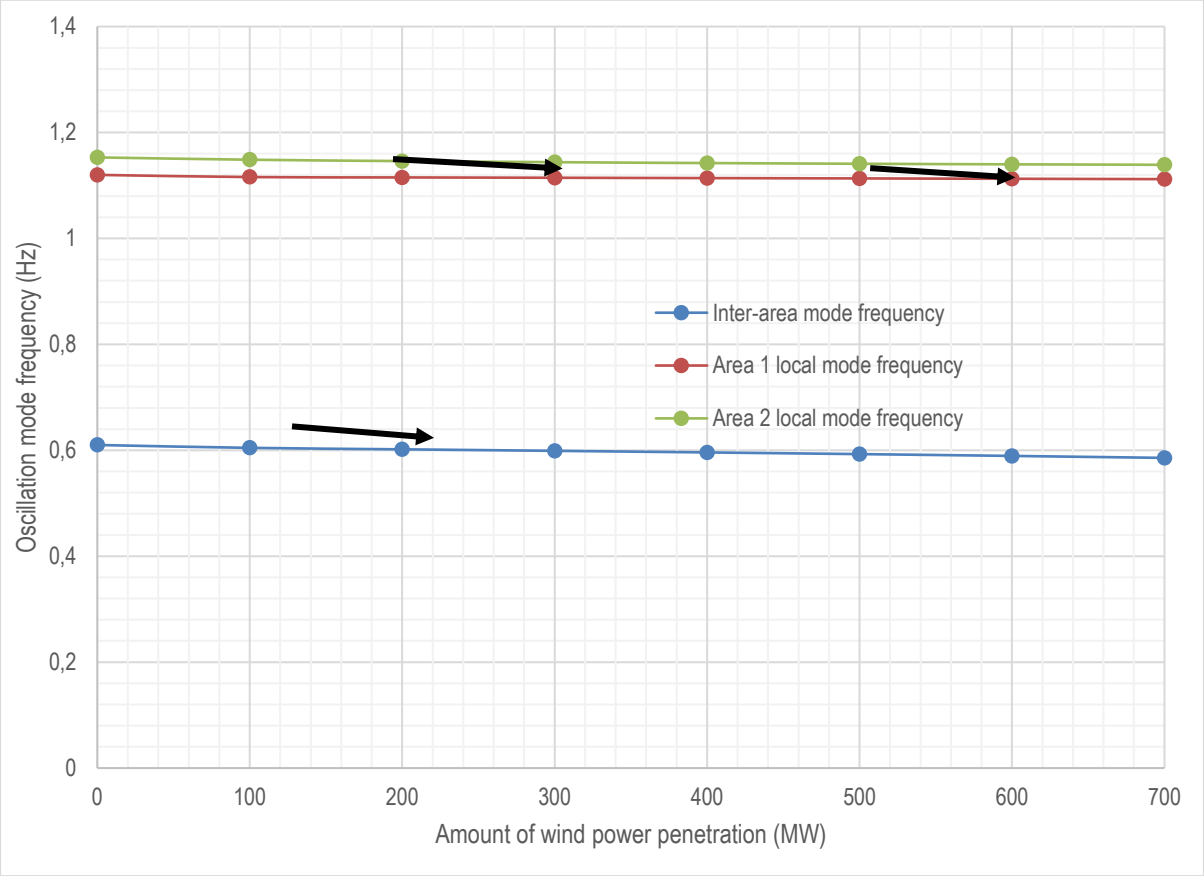

Figure 5.10: Inter-area and local oscillation modes' frequency variation with wind power supplying increasing area 1 load (no PSSs)

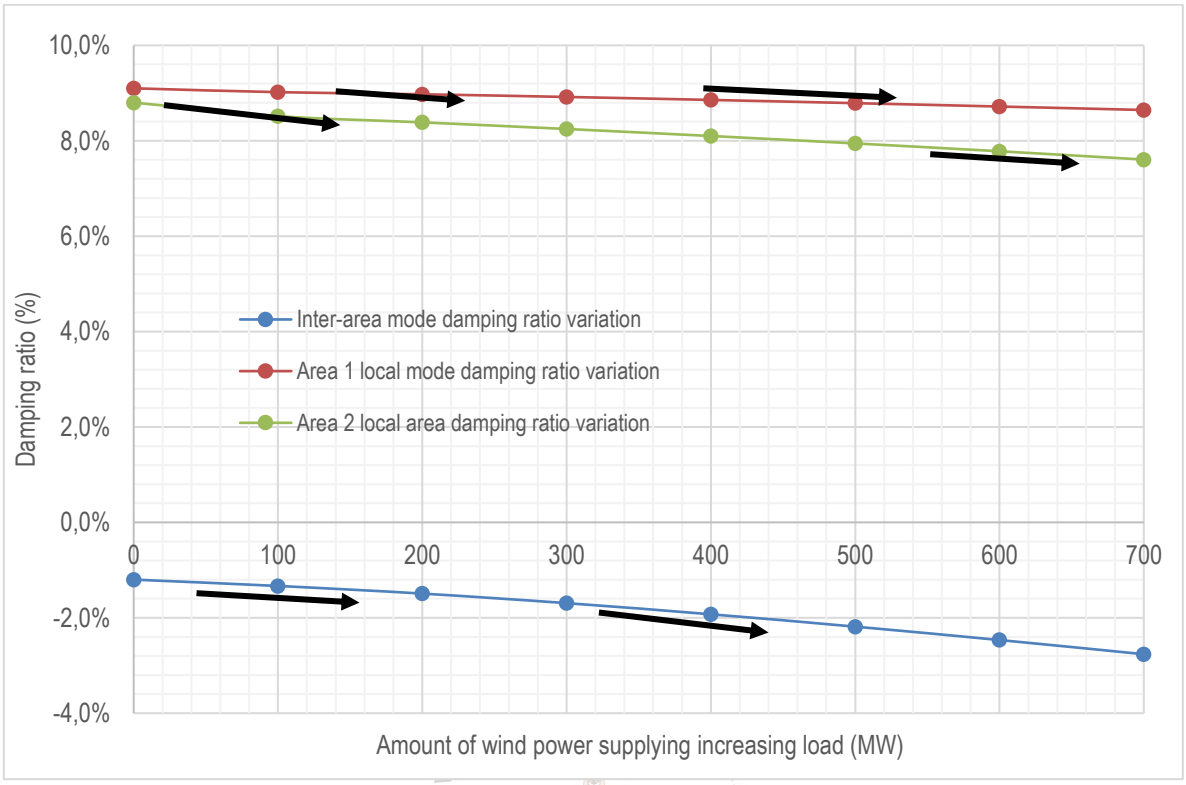

Figure 5.11: Inter-area and local modes damping ratios variation with wind power supplying increasing area 1 load (no PSSs)

Table 5.10 provides the inter-area mode characteristics when wind power was used in parallel with synchronous generators to supply the increasing system load. The results show that when the area 1 load was increased by 100 MW and using wind power to compensate the system load increase, the frequency of the inter-area mode decreased by 0.007 Hz from 0.61 Hz while the damping ratio decreased by 0.13% from -1.20% to -1.33% in comparison to the base case without wind power. When the load was further increased to 200 MW the inter-area mode frequency further decreased by 1.1% which correspond to a decrease of 0.011 Hz from 0.61 Hz while the damping ratio further decreased by 0.29% from the -1.2%. When 300 MW of load was considered and supplied from the WPP, the frequency of the inter-area mode progressively decreased by 0.015 Hz while the damping ratio further decreased by 0.49% from -1.2%. For 400 MW of increased load the frequency of the inter-area mode decreased by 0.018 Hz while the damping ratio decreased by 0.73% from -1.2%. When 500 MW of increased load the frequency and damping ratio of the inter-area mode further decreased by 0.022 Hz and 0.99% respectively. For 600 MW of wind power supplying the same amount of load increase, the inter-area oscillation mode frequency and damping ratio further decreased by 0.026 Hz and 1.27% respectively. The maximum decrease in the inter-area mode frequency and damping ratio of 0.03 Hz and 1.56% respectively were observed when load in area 1 was increased to 700 MW and wind power was introduced to supply the load.

Table 5.10: Inter-area oscillation mode characteristic with wind power supplying increasing area 1 load (no PSSs)

Wind power (MW)	Eigenvalue $(\sigma \pm j\omega)$	Frequency (Hz)	Percentage damping ratio $(\zeta \times 100\%)$	Frequency decrease with reference to case without wind power (%) $(f_n - f_0)$	Percentage change in damping ratio with reference to case without wind power (%) $(\zeta_n - \zeta_0)$
100	0.051 ± j 3.791	0.603	-1.33%	0.007 Hz	- 0.11%
200	0.056 ± j 3.766	0.599	-1.49%	0.011 Hz	- 0.29%
300	0.063 ± j 3.741	0.595	-1.69%	0.015 Hz	- 0.49%
400	0.072 ± j 3.717	0.592	-1.93%	0.018 Hz	- 0.73%
500	0.081 ± j 3.693	0.588	-2.19%	0.022 Hz	- 0.99%
600	0.090 ± j 3.669	0.584	-2.47%	0.026 Hz	- 1.27%
700	0.101 ± j 3.644	0.580	-2.76%	0.030 Hz	- 1.56%

Table 5.11 shows the local modes characteristic when wind power supplied the increasing system load in area 1. The results show that the frequencies and damping ratios of the area 1 local oscillation modes decreased with increasing wind power penetration while Area 2 local mode frequency remained constant with decrease in the damping ratio.

Table 5.11: Local oscillation modes characteristic with wind power supplying increasing area 1 load

Wind power (MW)	Area 1 local mode characteristic			Area 2 local mode characteristic		
	Eigenvalue $(\sigma \pm j\omega)$	Frequency (Hz)	Percentage damping ratio $(\zeta \times 100\%)$	Eigenvalue $(\sigma \pm j\omega)$	Frequency (Hz)	Percentage damping ratio $(\zeta \times 100\%)$
100	-0.633 ± j 6.995	1.113	9.02%	-0.618 ± j 7.236	1.152	8.52%
200	-0.629 ± j 6.978	1.111	8.97%	-0.609 ± j 7.235	1.151	8.39%
300	-0.623 ± j 6.963	1.108	8.92%	-0.599 ± j 7.234	1.151	8.25%
400	-0.618 ± j 6.950	1.106	8.86%	-0.588 ± j 7.234	1.151	8.10%
500	-0.612 ± j 6.938	1.104	8.79%	-0.577 ± j 7.234	1.151	7.94%
600	-0.606 ± j 6.928	1.103	8.72%	-0.565 ± j 7.235	1.151	7.78%
700	-0.600 ± j 6.918	1.101	8.65%	-0.552 ± j 7.235	1.152	7.61%

Table 5.12 provides the calculated percentage change of frequency and damping ratio of area 1 and area 2 local modes with wind power source supplying area 1 load increase. Area 1 local mode frequency decreased by 0.004 Hz from 1.117 Hz corresponding to area 1 local mode frequency without wind power while the damping ratio decreased by 0.08% from 9.1% when the system load was increased by 100 MW. When the area 1 load active power was increased to 200 MW with wind power supplying the increasing load, the frequency of the area 1 local mode decreased by 0.006 Hz and the damping ratio further decreased by 0.13% to 8.97%. Similar trend in the area 1 local mode was seen for 300 MW active load being supplied from wind power, the local mode frequency and damping ratio decreased by 0.009 Hz and 0.18% respectively in comparison to the case without wind power. For 400 MW of wind power supplying load increase the frequency and damping ratio of the area 1 local oscillation mode decreased by 0.011 Hz and 0.24% respectively. When 500 MW of wind power supplied the same amount of the area 1 active load the frequency and damping ratio of the local oscillation mode progressively decreased by 0.013 Hz and 0.31% respectively. Table 5.12 shows that when 600 MW of wind power was considered the area 1 local mode oscillation frequency further decreased by 0.014 Hz and the damping ratio decreased by 0.38%. Further trend in the reduction of the area 1 local mode was observed when 700 MW of wind power was considered. For 700 MW of wind power, the area 1 local mode frequency and damping ratio decreased by 0.016Hz and 0.45% respectively.

UNIVERSITY OF THE WITWATERSRAND

Table 5.12: Local modes change in frequency and damping ratio when wind power supplies increasing load in area 1 (no PSSs)

Wind power (MW)	**Area 1 local mode characteristic**		**Area 2 local mode characteristic**	
	Change in frequency $(f_n - f_0)$	**Change in damping ratio (%)** $(\zeta_n - \zeta_0)$	**Change in frequency** $(f_n - f_0)$	**Change in damping ratio (%)** $(\zeta_n - \zeta_0)$
100	0.004 Hz	- 0.08%	0.002 Hz	- 0.280%
200	0.006 Hz	- 0.13%	0.001 Hz	- 0.410%
300	0.009 Hz	- 0.18%	0.001 Hz	- 0.550%
400	0.011 Hz	- 0.24%	0.001 Hz	- 0.700%
500	0.013 Hz	- 0.31%	0.001 Hz	- 0.860%
600	0.014 Hz	- 0.38%	0.001 Hz	- 1.020%
700	0.016 Hz	- 0.45%	0.002 Hz	- 1.190%

It is important to note that, the area 2 local mode characteristic changed with increasing wind power supplying increasing area 1 active load. This would not be expected since only the area 1 active load was altered and that the effects of such changes would be less anticipated in another area. The area 2 local mode frequency were less sensitive to the area 1 load change as provided in Table 5.12 where the frequency decrease of area 2 local mode was within 0.002 Hz while for area 1 local mode frequency varied from 0.004 Hz to 0.016 Hz. The damping

ratios of the local mode progressively decreased with increasing wind power supplying the increasing area 1 system load with the receiving area damping ratios being more sensitive than the sending area where the wind power source is integrated.

Table 5.13 provides the resulting power flows when wind power was introduced in area 1 to supply the increasing system load in area 1. The power flows decreased with increasing wind power supplying increasing system load in area 1. This would be expected since the area 1 load demands could not be met due to the WPP losses and hence the exported power is reduced. The reduced power flow resulted in the system being slightly loaded which causes a change in the system operating condition and hence the characteristics of the system modes.

Table 5.13: Power flow changes when wind power supplies increasing system load in area 1

Wind power penetration level (MW)	**0**	**100**	**200**	**300**	**400**	**500**	**600**	**700**
Inter-area active power (MW)	404.4	394	387.6	380.6	373.4	365.8	357.6	349.2

Wind power supplying increasing system load in area 2

In a separate case, the area 2 load active power was also gradually increased in steps of 100 MW to 700 MW whilst introducing wind power source to supply the load increase. Figure 5.12 and Figure 5.13 show the frequencies and damping ratios variation of the inter-area and local modes with increasing wind power generation supplying increasing system load in area 2. From Figure 5.12 and Figure 5.13 both the frequencies and damping ratios of the inter-area and local modes decreased with increasing wind power supplying load in area 2. These results are similar to the results observed when the load in area 1 was increased and compensated by wind power source in the same area as presented in the previous section although the power flow changes were different.

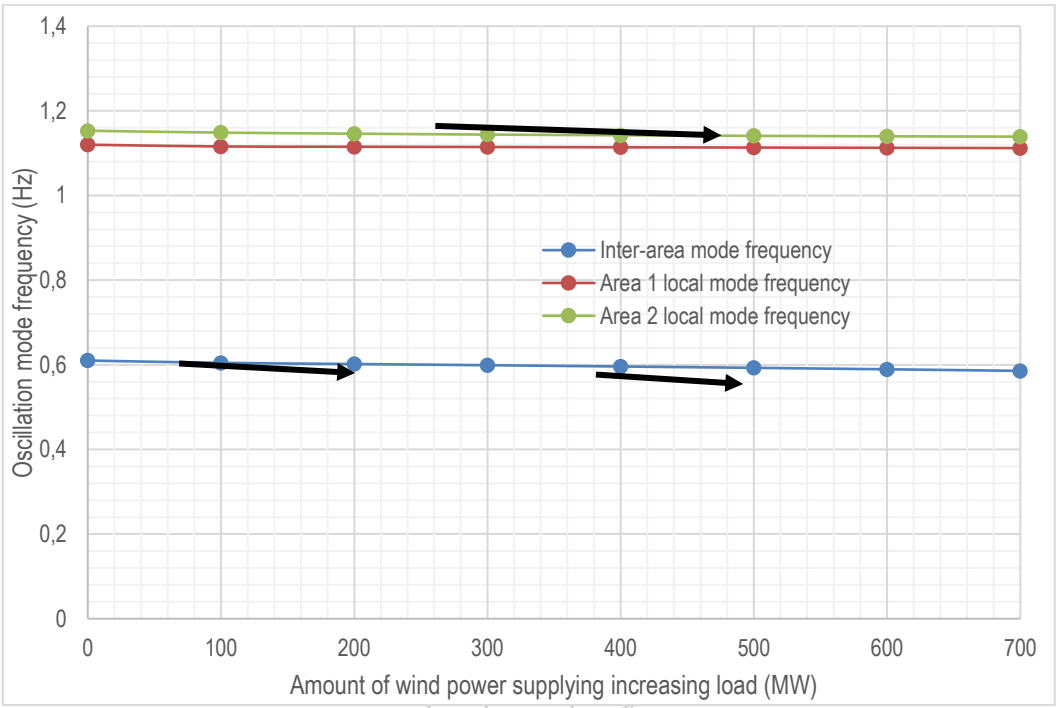

Figure 5.12: Inter-area and local oscillation mode frequency variation with wind power supplying increasing area 2 load (no PSSs)

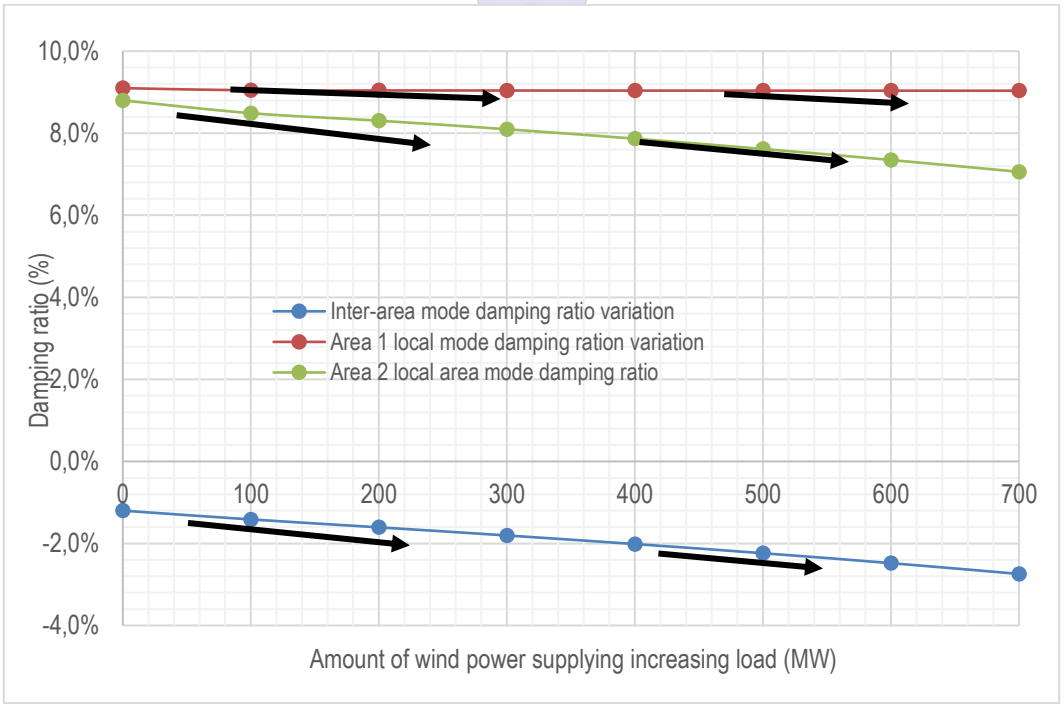

Figure 5.13: Local oscillation mode damping ratio variation with increasing wind power penetration (no PSSs)

Table 5.14 shows the inter-area mode characteristics when wind power was used to supply increasing system load in area 2. The results indicate that when the area 2 load was increased by 100 MW and supplied by wind power the frequency of the inter-area mode decreases from 0.61 Hz to 0.605 Hz with decrease in the damping ratio from -1.22% to -1.41%. When the load in area 2 was increased to 200 MW the inter-area mode frequency further decreased by 0.008 Hz to 0.602 Hz while the damping ratio further decreased to -1.61% when compared to the base case without wind power and increasing load. The inter-area mode frequency and damping ratio progressively decreased by 0.011 Hz and 0.59% respectively when 300 MW of wind power source supplied the increasing load in area 2. This resulted in the frequency and damping ratio of 0.599 Hz and -1.81% respectively. A further increase in area 2 load to 400 MW and wind power supplying the load caused the inter-area mode frequency and damping ratio decreased by 0.014 Hz and 0.82% respectively compared to the base case without wind power source. When 500 MW of wind power supplied the same amount of load increase in area 2 the inter-area oscillation mode frequency and damping ratio decreased by 0.017 Hz and 1.04% respectively. The frequency and damping ratio of the inter-area mode further deceased by 0.021 Hz and 1.26% respectively when 600 MW of wind power was introduced to supply load increase in area 2. The maximum decrease in the inter-area mode frequency and damping ratio were 0.024 Hz and 1.52% respectively relative to the base case without wind power and increased area 2 load for 700 MW load increase being supplied by wind power.

Table 5.14: Inter-area oscillation mode characteristic with wind power supplying increasing area 2 load (no PSSs)

Wind power (MW)	Eigenvalue $(\sigma \pm j\omega)$	Frequency (Hz)	Percentage damping ratio $(\zeta \times 100\%)$	Change in frequency with reference to case without wind power (Hz) $(f_n - f_0)$	Percentage change in damping ratio with reference to case without wind power (%) $(\zeta_n - \zeta_0)$
100	0.054 ± j 3.799	0.605	-1.41%	0.005 Hz	-0.19%
200	0.061 ± j 3.781	0.602	-1.61%	0.008 Hz	-0.39%
300	0.068 ± j 3.763	0.599	-1.81%	0.011 Hz	-0.59%
400	0.075 ± j 3.744	0.596	-2.02%	0.014 Hz	-0.80%
500	0.083 ± j 3.724	0.593	-2.24%	0.017 Hz	-1.02%
600	0.092 ± j 3.703	0.589	-2.48%	0.021 Hz	-1.26%
700	0.101 ± j 3.679	0.586	-2.74%	0.024 Hz	-1.52%

Based on the inter-area results provided here and from the previous section when there was load increase in area 1 supplied by wind power in the same area i.e. the exporting area, the frequency of the inter-area mode is less sensitive when the wind power is integrated in the area receiving power. This observation is based on the change in the inter-area mode frequencies provided in Table 5.10 and Table 5.14. When wind power was integrated in the area exporting power the inter-area mode frequency varied from 0.007 Hz to 0.03 Hz for 100 MW to 700

MW load increase. For the same amount of load increase being supplied by wind power in the receiving area the inter-area mode frequency varied from 0.005 Hz to 0.024 Hz. In both cases wind power integrated in the exporting and receiving areas, the negative damping ratio gets larger (i.e. the inter-area mode gets more negatively damped, less stable) as wind power is added to meet increased load. In the case of both the reduction in mode frequency and the reduction in mode damping the effect is slightly less pronounced when wind power is integrated into the receiving end area of the transmission system. This can be argued to be as a result of the unchanging power flows between the two areas.

Table 5.15 shows the corresponding behaviour of the local modes when area 2 load was gradually increased in steps of 100 MW with wind power supplying the load. It can be observed from Table 5.15 that the area 2 local mode frequency and damping ratio also decreased while area 1 local mode characteristic did not change significantly. The percentage change in the area 2 local mode frequency and damping ratio were calculated and are given in Table 5.16. Area 2 local mode frequency and damping ratio decreased with the introduction of wind power to supply the load increase. The resulting frequency and damping ratio decreased by 0.44% and 0.31% respectively with reference to the original case without wind power and increasing system load in area 2. When 200 MW of load was compensated by wind power source, the area 2 local mode frequency decreased by 0.70% to 1.146 Hz with a 0.49% decrease in damping ratio from 8.49% to 8.31%. For 300 MW wind power supplying increasing load of the same amount the area 2 local mode frequency and damping ratio further decreased from their original case without wind power to 1.144 Hz with a damping ratio of 8.1%. The decrease in the local mode frequency and damping ratio in area 2 were observed when area 2 load was also increased to 400 MW. This resulted in the frequency decreasing to 1.142 Hz with a decreased damping ratio of 7.87%. When the load in area 2 was increased to 500 MW and being compensated by wind power the local mode frequency decreased by 0.009 Hz while the damping ratio also decreased by 0.93% from the original case without wind power and increase in the load. A similar trend was observed for the cases when 600 MW and 700 MW of wind power was supplied to supply the same amounts of increasing loads in area 2. The area 2 local mode frequencies decreased to 1.14 Hz and 1.139 Hz for 600 MW and 700 MW of wind power supplying the equivalent loads in area 2 respectively while their damping ratios decreased to 7.35% and 7.06% respectively.

UNIVERSITY OF THE WITWATERSRAND JOHANNESBURG

Table 5.15: Local oscillation modes characteristic with wind power supplying increasing area 2 load (no PSSs)

Wind power (MW)	Area 1 local mode characteristic			Area 2 local mode characteristic		
	Eigenvalue $(\sigma \pm j\omega)$	Frequency (Hz)	Percentage damping ratio $(\zeta \times 100\%)$	Eigenvalue $(\sigma \pm j\omega)$	Frequency (Hz)	Percentage damping ratio $(\zeta \times 100\%)$
100	-0.637 ± j 7.011	1.116	9.05%	-0.615 ± j 7.217	1.149	8.49%
200	-0.636 ± j 7.007	1.115	9.04%	-0.600 ± j 7.201	1.146	8.31%
300	-0.636 ± j 7.003	1.115	9.04%	-0.584 ± j 7.188	1.144	8.10%
400	-0.635 ± j 6.999	1.114	9.04%	-0.566 ± j 7.177	1.142	7.87%
500	-0.635 ± j 6.995	1.113	9.04%	-0.548 ± j 7.169	1.141	7.62%
600	-0.634 ± j 6.991	1.113	9.04%	-0.528 ± j 7.162	1.140	7.35%
700	-0.634 ± j 6.987	1.112	9.04%	-0.506 ± j 7.157	1.139	7.06%

Table 5.16: Local mode change in frequency and damping ratio when wind power supplies increasing load in area 2 (no PSS)

Wind power (MW)	Area 1 local mode characteristic		Area 2 local mode characteristic	
	Change in frequency $(f_n - f_0) \times 100\%$	Change in damping ratio (%) $(\zeta_n - \zeta_0)$	Change in frequency $(f_n - f_0) \times 100\%$	Change in damping ratio (%) $(\zeta_n - \zeta_0)$
100	-0.41%	-0.05%	-0.44%	-0.31%
200	-0.48%	-0.06%	-0.70%	-0.49%
300	-0.55%	-0.06%	-0.90%	-0.70%
400	-0.61%	-0.06%	-1.07%	-0.93%
500	-0.67%	-0.06%	-1.21%	-1.18%
600	-0.74%	-0.06%	-1.31%	-1.45%
700	-0.81%	-0.06%	-1.39%	-1.74%

The power flow between area 1 and area 2 observed in this case are provided in Table 5.17 which shows that the power flows were constant for the various scenarios considered. The constant power flows are explained by the fact that the exporting area load and generation demand were not altered.

Table 5.17: Power flow changes when wind power supplies increasing system load in area 2

Wind power penetration level (in MW)	**0**	**100**	**200**	**300**	**400**	**500**	**600**	**700**
Inter-area active power flow (MW)	404.4	400.2	400.2	400	400	400	399.6	399.6

The key findings for this case when wind power is introduced to supply increasing loads is that the frequencies and damping ratios of the both inter-area and local modes decrease with increasing wind power. However, the damping ratio of the inter-area and local oscillation modes contrasted to the previous cases investigated shows the opposite behaviour. In this case, the damping ratios of inter-area and local modes decreased while for the previous case the damping ratios increased. The differences between these two cases is that the generators in this case were not de-loaded but remained at high output hence the system remained stressed and that there was a load increase in the system. It was however expected that the damping ratios of the inter-area and local modes would increase particularly when the wind power and load increase were considered in area 1 where the inter-area power flows significantly decreased thus in a way reducing the system strain and hence would improve damping characteristics of the modes, as found earlier. It is therefore argued that the increasing the system load, in general, has an adverse effect on the system damping which consequently reduces the inter-area and local modes damping ratios.

5.2. Impact of Wind Generation on Power System Stabilizers (PSSs) Tuned for Damping Inter-Area and Local Oscillation Modes

This section presents the results of the impact of wind generation on the inter-area and local modes when the synchronous generators were equipped with PSSs. The damping ratios are the key parameters which were used to assess the impact of wind power on the PSSs tuned for the damping of the inter-area and local modes. The approach used considered increasing the system load active power and compensate the load increase with wind power. This was the same approach used in the previous section but with the generators equipped with PSSs. For convenience Table 5.18 provides the TAMM system small-signal stability characteristics when the generators were equipped with PSSs. These modes were tracked and analysed to understand the effects of wind power on the PSS tuned for damping inter-area and local modes.

Table 5.18: TAMM system small-signal characteristic with PSS in service without wind generation

	Inter-area oscillation mode	Area 1 local oscillation mode	Area 2 local oscillation mode
Eigenvalue	-0.612 ± j 3.524	-4.173 ± j 4.961	-4.04 ± j 5.209
Frequency (Hz)	0.56 Hz	0.79 Hz	0.83 Hz
Damping ratio (%)	17.1%	64.4%	61.2%

5.2.1. Wind power supplying increasing load with generators equipped with PSSs

The behaviour of both the inter-area and local modes with tuned PSSs in the presence of a significant amount of wind power was investigated by integrating wind power source in each area separately to compensate for the system load active power increase in steps of 100 MW. The same TAMM system configurations in Figure 5.8 and Figure 5.9 but with the PSSs installed on the synchronous generators were used. Both inter-area and local mode frequencies and damping ratios were expected to decrease as the approach used was similar to the previous case, but the generators did not include PSSs.

UNIVERSITY OF THE WITWATERSRAND JOHANNESBURG

Inter-area mode behaviour with tuned PSSs

Table 5.19 provides the PSS tuned inter-area mode characteristics obtained when wind power supplied increasing load in area 1 and area 2 separately. The results in Table 5.19 indicate that wind power causes the frequency and damping ratio of the inter-area mode to decrease. These observations further confirm the results obtained in the previous cases when the PSSs were not in service. Figure 5.14 and Figure 5.15 show the damping ratio and frequency variation of the inter-area mode with increasing wind power and load. The percentage change of the inter-area mode damping ratio with increasing wind power and increasing load from the base case without wind power were calculated to determine the extent of impact of wind power on the damping of the tuned inter-area oscillation modes.

Table 5.19: Inter-area mode characteristics with increasing wind power supplying increasing system load (with PSSs)

Wind power (MW)	Inter-area mode characteristic when load 1 is increased and compensated with wind power located in area 1			Inter-area mode characteristic when load 2 is increased and compensated with wind power located in area 2		
	Eigenvalue $(\sigma \pm j\omega)$	Frequency (Hz)	Percentage damping ratio $(\zeta \times 100\%)$	Eigenvalue $(\sigma \pm j\omega)$	Frequency (Hz)	Percentage damping ratio $(\zeta \times 100\%)$
100	-0.597 ± j 3.504	0.558	16.8%	-0.594 ± j 3.511	0.559	16.7%
200	-0.583 ± j 3.482	0.554	16.5%	-0.578 ± j 3.496	0.556	16.3%
300	-0.568 ± j 3.460	0.551	16.2%	-0.561 ± j 3.479	0.554	15.9%
400	-0.552 ± j 3.438	0.547	15.9%	-0.543 ± j 3.460	0.551	15.5%
500	-0.537 ± j 3.415	0.543	15.5%	-0.525 ± j 3.440	0.547	15.1%
600	-0.520 ± j 3.392	0.540	15.2%	-0.507 ± j 3.417	0.544	14.7%
700	-0.504 ± j 3.368	0.536	14.8%	-0.486 ± j 3.393	0.540	14.2%

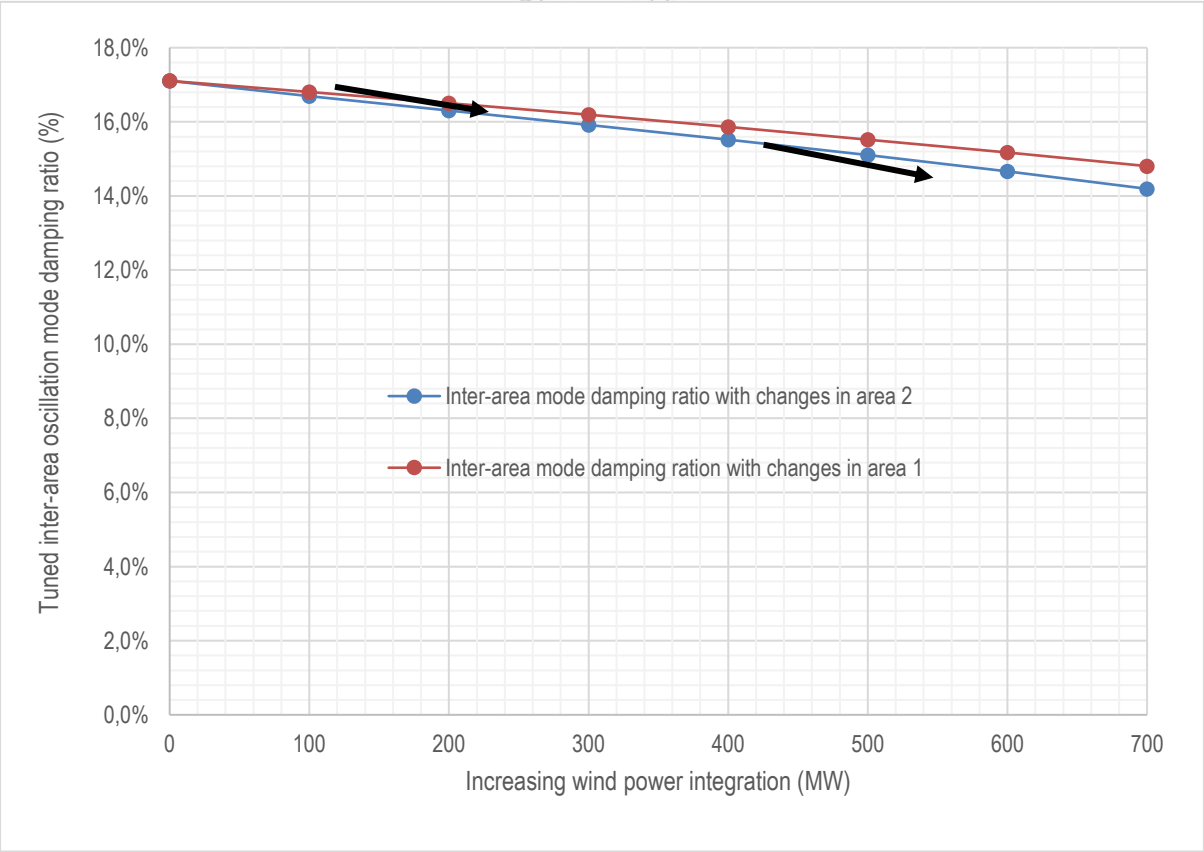

Figure 5.14: Inter-area oscillation mode damping ratio variation with increasing wind power (with PSSs)

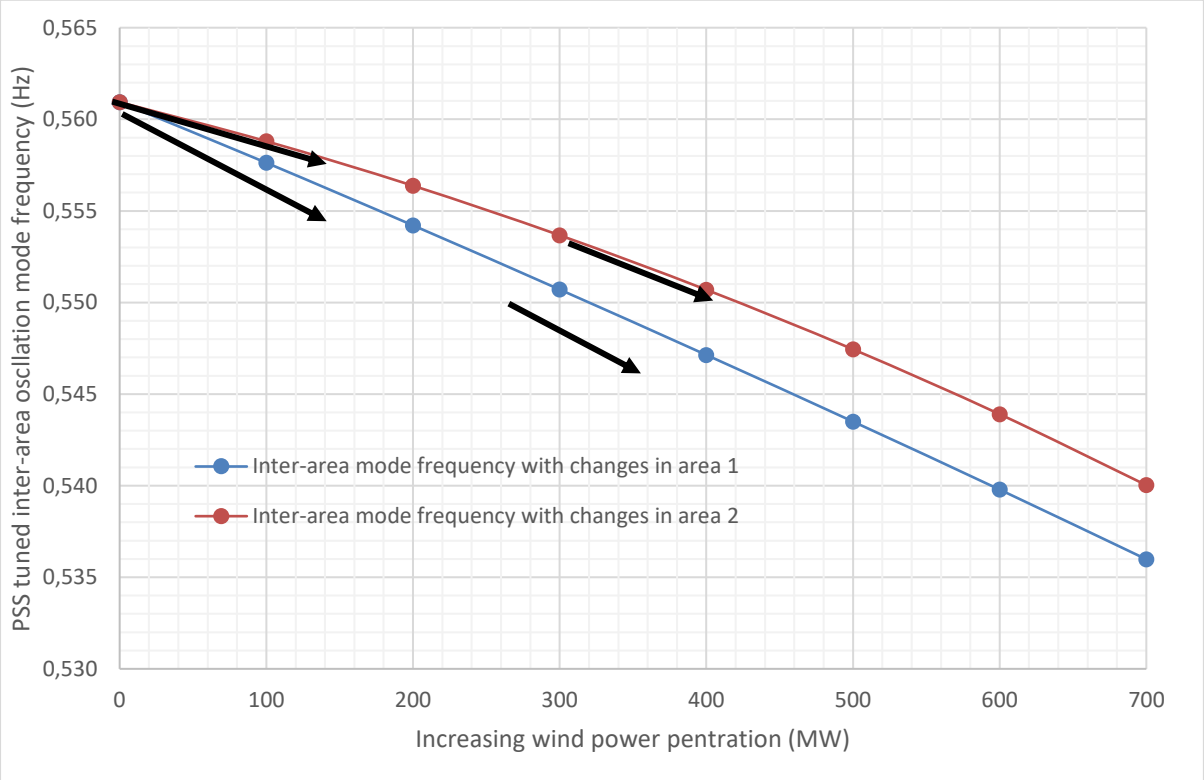

Figure 5.15: Inter-area oscillation mode frequency variation with wind power (with PSSs)

Table 5.20 provides the determined percentage decrease in the inter-area mode damping ratios with increasing wind power against the case without wind power. When 100 MW of wind power was introduced in area 1, i.e. area exporting power, the inter-area mode damping ratio decreased by 0.3% from 17.1% to 16.8% whereas when the same amount of wind power was introduced in area 2 (i.e. the receiving area) the inter-area mode damping ratio was more sensitive since the damping ratio decreased by 0.4% to 16.7%. When 200 MW of wind power was considered in area 1 the inter-area mode damping ratio decreased by 0.601% from the nominal inter-area mode damping ratio of 17.1%. For the same amount, 200 MW wind power connected in area 2 to compensate the load increase the inter-area mode damping ratio decreased by 0.8%. For 300 MW of wind power in area 1 and area 2 the inter-area mode damping ratio decreased by 0.915% and 1.2% respectively from the 17.1% damping ratio. When 400 MW of wind power was connected in area 1 and area 2 the inter-area mode damping ratio further decreased by 1.242% and 1.6% from the nominal damping ratio of 17.1% respectively. For 500 MW of wind power in area 1 and area 2 the inter-area oscillation mode damping ratio further decreased by 1.583% and 2% respectively. The inter-area oscillation mode damping ratio decreased by 1.936% and 2.4% when 600 MW of wind power was integrated in area 1 and area 2 respectively. The maximum decrease in the inter-area oscillation mode damping ratios were observed when 700 MW of wind power was connected in area 1

and area 2. The inter-area oscillation mode damping ratio decreased by 2.3% and 3% from the 17.1% damping provided by PSSs when 700 MW of wind power was integrated in area 1 and area 2 respectively.

Table 5.20: Percentage change in the tuned inter-area mode's damping ratio with increasing wind power (with PSSs)

Wind power (MW)	Inter-area mode characteristic when load 1 is increased and compensated with wind power located in area 1		Inter-area mode characteristic when load 2 is increased and compensated with wind power located in area 2	
	% damping ratio without wind power ($\zeta \times 100$)	% damping ratio decrease with wind power ($\zeta \times 100$)	% damping ratio without wind power ($\zeta \times 100$)	% damping ratio decrease with wind power ($\zeta \times 100$)
100	16.8 %	-0.30%	16.7%	-0.4%
200	16.5 %	-0.601%	16.3%	-0.8%
300	16.2 %	-0.915%	15.9%	-1.2%
400	15.9 %	-1.242%	15.5%	-1.6%
500	15.5 %	-1.583%	15.1%	-2.0%
600	15.2 %	-1.936%	14.7%	-2.4%
700	14.8 %	-2.301%	14.2%	-2.9%

In addition to the trend is that the inter-area oscillation mode frequency and its damping ratio decreases with increasing wind power and increasing load, Figure 5.14 and Figure 5.15 and the analysis above show that inter-area mode frequency and damping ratio are more sensitive to the wind power when the wind power source was considered in the area exporting power in comparison to the case when the wind power source is integrated in the area receiving power, area 2. This result suggests that the power flow directions affect the inter-area modes characteristics. It can further be inferred that when wind power is connected in area opposite to the system power flows the inter-area mode is significantly affected.

To further investigate the behaviour of the PSS tuned inter-area mode the system configuration in Figure 5.16 was used. This configuration considered a WPP connected between the two interconnected areas by looping in and out of one of the interconnection line (Tx 2) to supply an increasing load in area 2. This configuration resulted in the power flow changes provided in Table 5.21.

Table 5.21: Power flows when wind power was integrated between the two interconnected areas

Wind power penetration level (in MW)	**0**	**100**	**200**	**300**	**400**	**500**
Inter-area active power flow (MW)	404.4	404.1	399.1	399.4	398.8	396.4

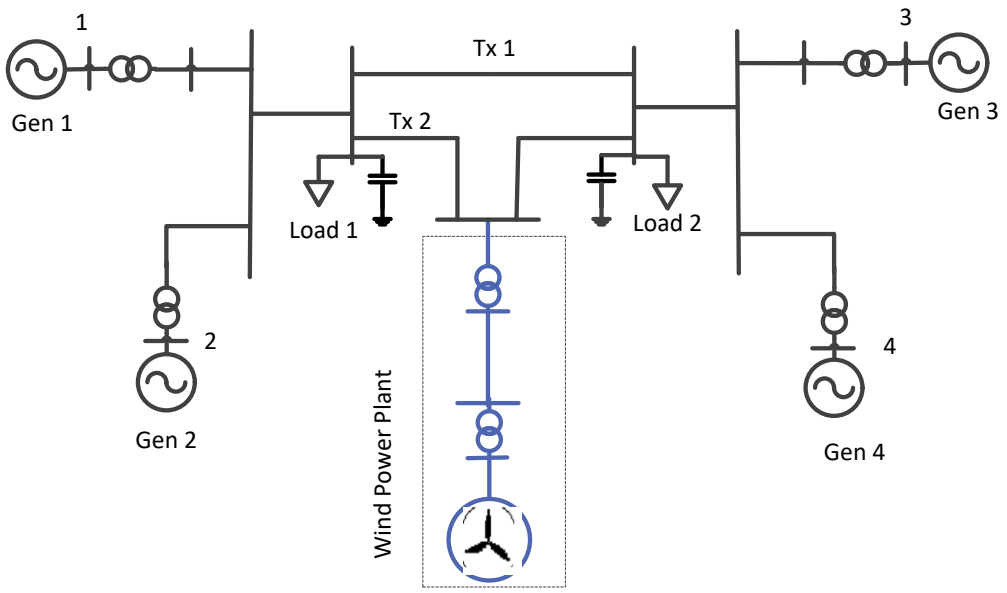

Figure 5.16: Wind power connected between the two interconnected areas

Table 5.22 provides the frequency and damping ratio of the inter-area mode obtained when wind power supplied increasing load in area 2 based on the configuration in Figure 5.16. The frequency of the inter-area mode decreased with increasing wind power penetration while its resulting damping ratio decreased and then increased with increasing wind power. When 100 MW of wind power was connected to supply load increase of 100 MW in area 2 the damping ratio decreased by -0.4% with reference to the nominal damping ratio of 17.1%. When the load was further increased to 200 MW to supply increasing load the inter-area mode damping ratio further decreased by 0.5% from 17.1% inter-area mode damping ratio without wind power. However, additional wind power generation source caused the damping ratio of the inter-area mode increase. For 300 MW the inter-area mode damping ratio decreased by 0.3% from the original case without wind power source which gradually increased by 0.2% when 500 MW of wind power was considered. This behaviour suggests that depending on the location of the wind power generation source, wind power can have negative or positive impacts on power system small-signal stability requirements. In addition, for the case studies examined, this investigation suggests that under heavy loading introduction of the wind power sources without de-loading the heavily loaded synchronous generators participating towards the system modes wind power may adversely affects the system damping requirements. Conversely, the introduction of wind power generation source to de-load the highly stressed synchronous generators participating towards the system modes result in improved system damping requirements.

Table 5.22: Inter-area mode characteristic when load 2 is increased and compensated with wind power located in area 2 (with PSSs)

Wind power (MW)	Eigenvalue $(\sigma \pm j\omega)$	Frequency (Hz)	Percentage damping ratio (%) $(\zeta \times 100)$	Percentage change in damping ratio (%) $(\zeta \times 100)$
100	-0.588 ± j 3.473	0.553	16.7%	-0.4%
200	-0.578 ± j 3.431	0.546	16.6%	-0.5%
300	-0.573 ± j 3.365	0.535	16.8%	-0.3%
400	-0.562 ± j 3.260	0.519	17.0%	-0.1%
500	-0.532 ± j 3.038	0.483	17.3%	0.2%

Local modes behaviour with tuned PSSs

Table 5.23 provides the local mode characteristics when wind power was integrated to supply increased load using configurations shown in Figure 5.8 and Figure 5.9. The results provided in Table 5.23 shows that the PSS tuned local mode frequencies increased with wind power penetration while their resulting damping ratio decreased. Figure 5.17 shows the increasing local mode frequencies with increasing wind power penetration. The frequency increase in the local modes were not expected since the previous case without the PSSs instead showed a decrease in both the inter-area and local modes with increasing wind power. It can be argued that this increase in frequency of the local modes in the presence of the wind power with increasing system loads suggest that the change in operating conditions are causing PSSs to introduce more synchronizing torque than the damping torque at local mode frequencies. However, this could be challenged when PSSs are properly tuned to provide optimum damping without introducing more synchronising torque as revealed by the PSSs effect on the local mode frequency in the previous chapter.

Table 5.23: Local mode characteristics with increasing wind power with PSSs (with PSSs)

Wind power (MW)	PSS tuned local oscillation mode in area 1 for the configuration shown in Figure 5.8	PSS tuned local oscillation mode in area 2 for the configuration in Figure 5.9
100	-3.972 ± j 5.293 0.842 Hz, ζ = 60.0%	-4.123 ± j 5.033 0.801 Hz, ζ = 63.4%
200	-3.913 ± j 5.371 0.855 Hz, ζ = 58.9%	-4.079 ± j 5.101 0.812 Hz, ζ = 62.4%
300	-3.860 ± j 5.433 0.866 Hz, ζ = 57.8%	-4.038 ± j 5.167 0.822 Hz, ζ = 61.6%
400	-3.809 ± j 5.512 0.877 Hz, ζ = 56.9%	-3.982 ± j 5.228 0.832 Hz, ζ = 60.6%
500	-3.761 ± j 5.578 0.888 Hz, ζ = 55.9%	-3.946 ± j 5.260 0.837 Hz, ζ = 60%
600	-3.715 ± j 5.643 0.898 Hz, ζ = 55%	-3.923 ± j 5.299 0.843 Hz, ζ = 59.5%
700	-3.669 ± j 5.706 0.908 Hz, ζ = 54.1%	-3.902 ± j 5.345 0.851 Hz, ζ = 59%

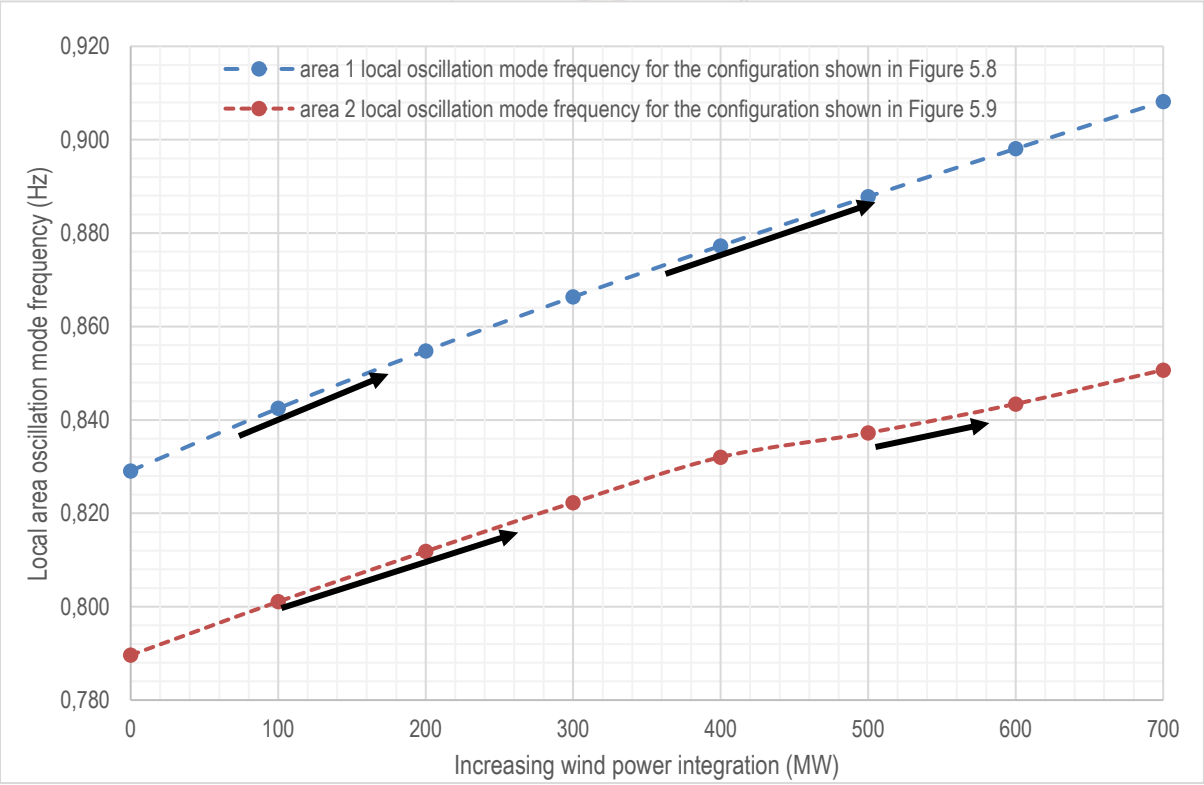

Figure 5.17: Local oscillation mode frequency change with increasing wind power (with PSSs)

Figure 5.18 shows the PSS tuned local modes damping ratio variation with increasing wind power. The figure shows that the damping ratio of the local modes decreased with increasing wind power. The percentage decrease in the damping ratio of the PSSs tuned local mode are provided in Table 5.24. In area 1 the percentage decrease of the local oscillation mode damping ratio varied from a minimum of -1.2% to a maximum of -7.2% from the local mode damping ratio of 61.2% for the original case without wind power but with the designed PSSs. Similarly, in area 2 the calculated percentage decrease in the damping ratios of the local mode varied from -1% to -5.4% from the 64.4% area 2 local mode damping ratio with designed PSSs. The results presented here when wind power was used to supply increasing system load suggest that significant amount of wind power penetration has a negative impact of the damping requirements of both the inter-area and local modes of power systems. However, the local modes damping ratios are more sensitive to wind power as revealed by the results above in Table 5.20, Table 5.22 and Table 5.24.

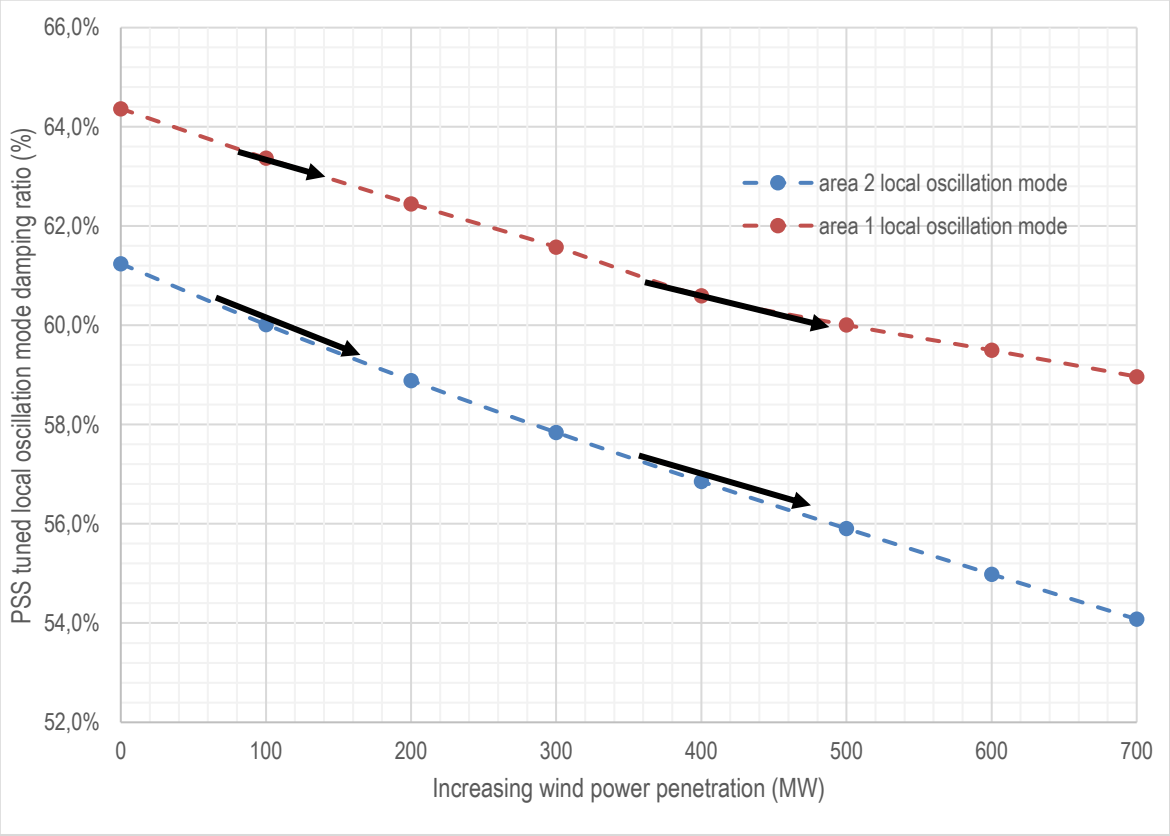

Figure 5.18: Local oscillation mode damping ratio with increasing wind power (with PSSs)

Table 5.24: Local modes damping ratio changes with increasing wind power (with PSSs)

Wind power (MW)	Area 1 local mode characteristic when load 1 is increased and compensated with wind power located in area 1		Area 2 local mode characteristic when load 2 is increased and compensated with wind power located in area 2	
	% damping ratio without wind power ($\zeta \times 100$)	% damping ratio decrease with wind power ($\zeta \times 100$)	% damping ratio without wind power ($\zeta \times 100$)	% damping ratio decrease with wind power ($\zeta \times 100$)
100	60.0%	-1.2%	63.4%	-1.0%
200	58.9%	-2.4%	62.4%	-1.9%
300	57.8%	-3.4%	61.6%	-2.8%
400	56.9%	-4.4%	60.6%	-3.8%
500	55.9%	-5.3%	60.0%	-4.4%
600	55.0%	-6.3%	59.5%	-4.9%
700	54.1%	-7.2%	59.0%	-5.4%

The corresponding generator behaviour in the presence of wind power was compared to the case without wind power and is presented next to further confirm the modal analysis results presented in previous sections in this chapter. Since the PSSs performance is also evaluated using the non-linear time domain simulations, the generator rotor behaviour was investigated in the presence of the wind power sources. A transient disturbance was applied to the test system and assessing the generator rotors for each integration step (every 100 MW of wind power for the cases) investigated in the previous sections. The disturbance was a 3-phase fault on transmission line (Tx 1) applied at 1.5 seconds and cleared by disconnecting the transmission line after 500 milliseconds. Figure 5.19 and Figure 5.20 show generator Gen 01 rotor angle response with increasing wind power while Figure 5.21 and Figure 5.22 the same variables but for Gen 02. The figures illustrate that the generators rotor angle settles in 10 seconds for all the cases with increasing wind power integration which indicate that although the PSSs damping capabilities will be adversely affected as revealed by the modal analysis the PSSs can still provide adequate damping in the presence of wind power. However, the initial and peak values of the generator rotor angle positions in the presence of the wind power changes with increasing wind power penetration as shown in the Figure 5.19 to Figure 5.22. The changes in generator rotor angle positions are due to changes in the system operating conditions with wind power which have been exhibited throughout the cases investigated in this dissertation.

5.3. Summary

This chapter has presented the impact of wind power on the inter-area and local oscillation modes of the power system using an aggregated WPP model. The first part focused on the impact of wind power generation on the inter-area and local oscillation modes when the generators

were operating in automatic excitation control without PSSs and then with PSSs. The results indicated that the introduction of wind power causes the power flows to change and hence the operating conditions. The change in the operating conditions alter the inter-area and local modes characteristic. In this investigation it was found that the inter-area and local oscillation mode frequencies decrease with increasing wind power penetration. Further to that it was found that inter-area and local oscillation mode damping ratios may decrease and increase in some cases with the wind power. However, the damping ratio changes were insignificant which suggests that already installed PSSs need not be re-tuned to accommodate the introduction of the wind power.

UNIVERSITY OF THE WITWATERSRAND
JOHANNESBURG

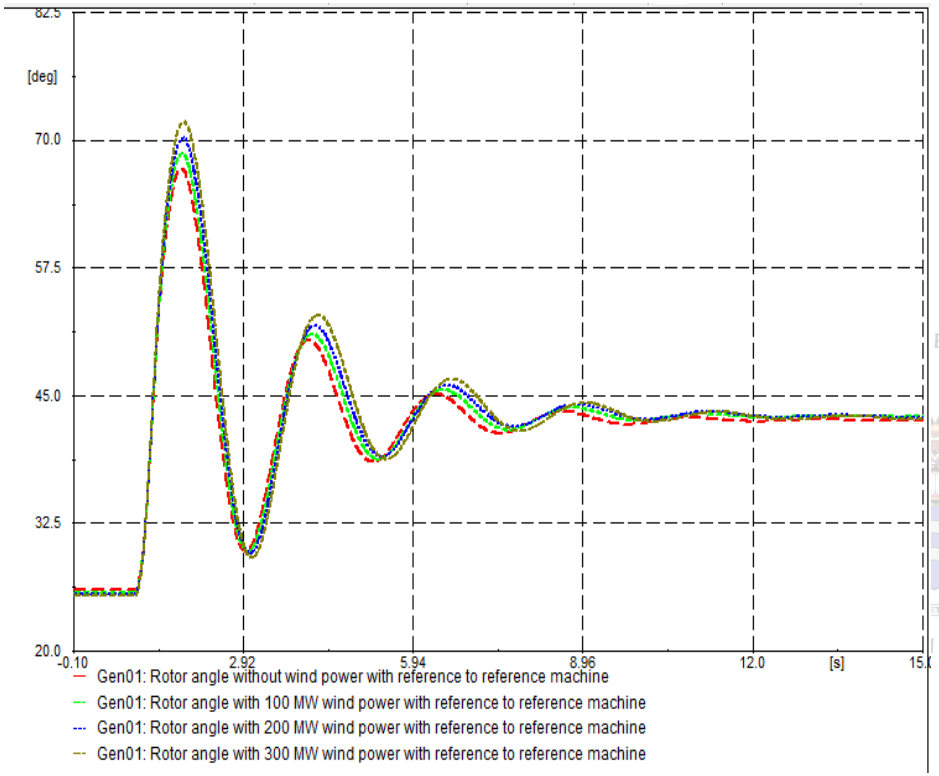

Figure 5.19: Generator 01 rotor angle response with 100 – 300 MW wind power with reference to the reference machine response with increasing wind power with PSSs

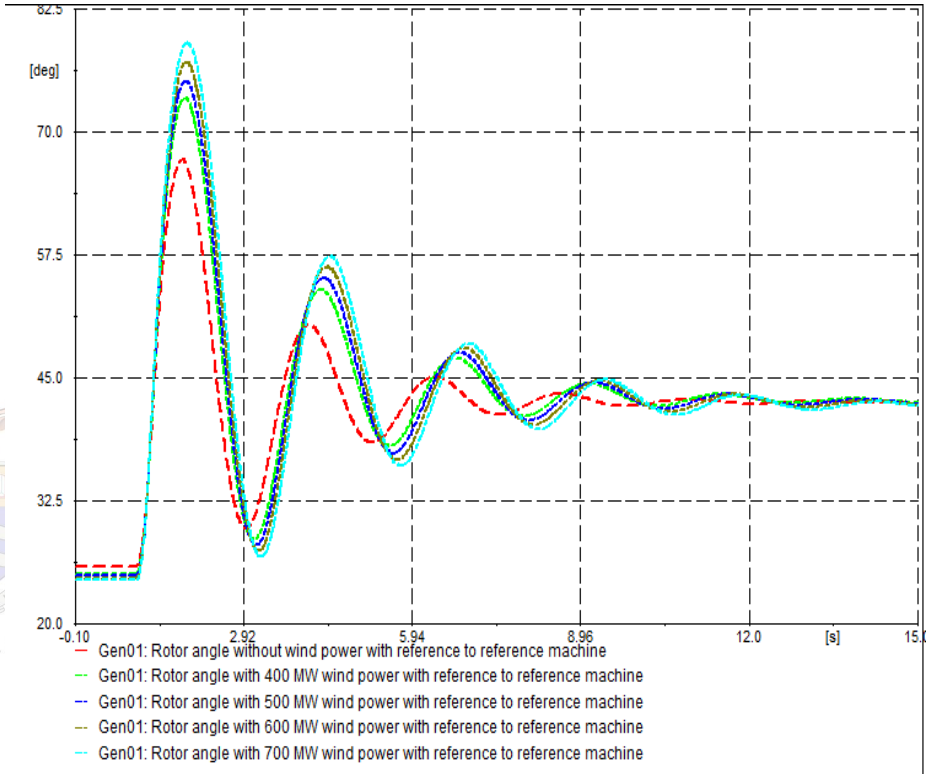

Figure 5.20: Generator 01 rotor angle response with 400 – 700 MW wind power with reference to the reference machine response with increasing wind power with PSSs

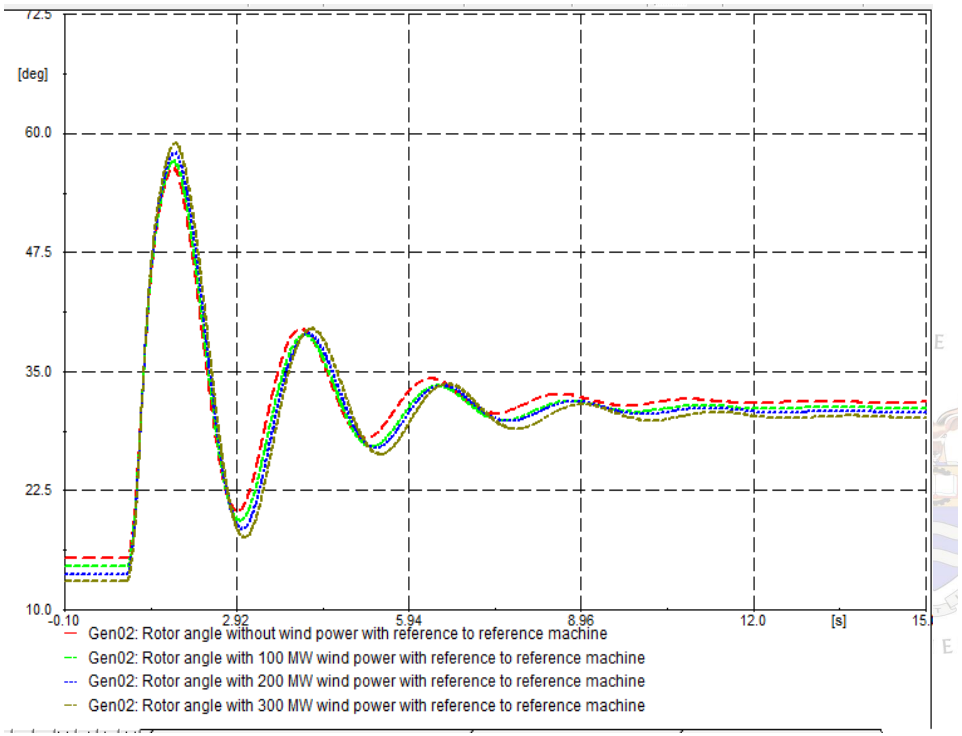

Figure 5.21: Generator 02 rotor angle response with 100 – 300 MW wind power with reference to the reference machine response with increasing wind power with PSSs

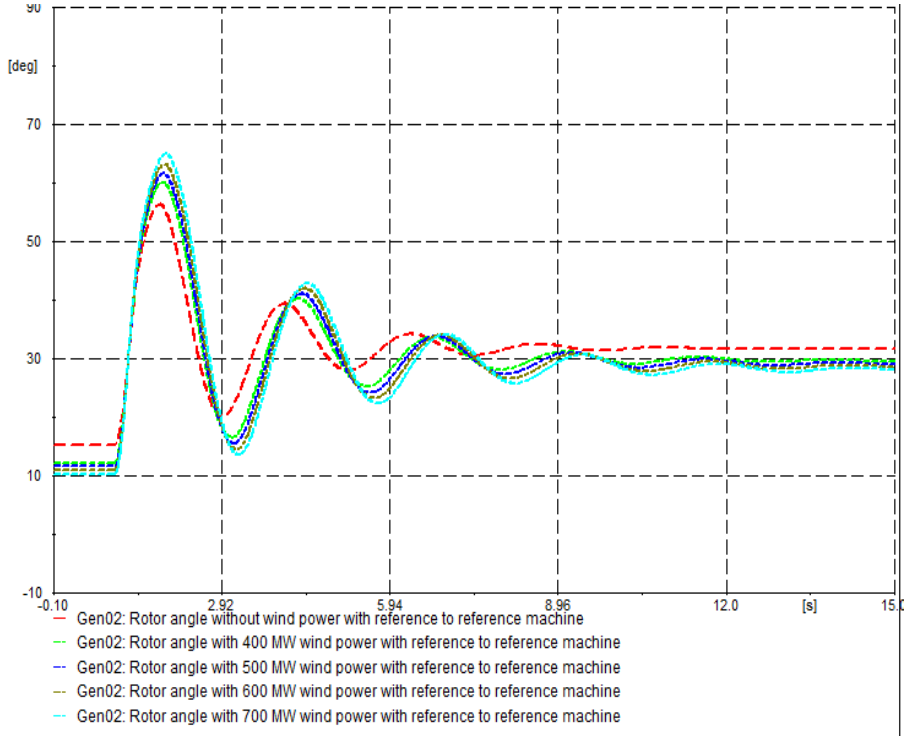

Figure 5.22: Generator 02 rotor angle response with 400 – 700 MW wind power with reference to the reference machine response with increasing wind power with PSS

CHAPTER 6 : CONCLUSION AND RECOMMENDATION

This research work has investigated the impact of wind power on the inter-area and local oscillation modes of power systems through a wide range of simulations. The work has been performed using IEC 61400-27-1 (2015) Type 4 WTG WPP of varying capacities integrated into a small-scale multi-machine test system environment with inherent inter-area and local modes. This research work also considered the impact of wind power on the inter-area and local oscillation modes with PSSs present.

The objective of this work was to investigate the impact of wind power generation on the power system small-signal stability. This study was guided by two sub-questions, the first one aimed to investigate the ability of PSSs to provide damping to both local and inter-area modes. In this dissertation PSSs were designed using classical control design methods namely the phase-lead and root locus. The design approach targeted the local modes and optimizing the PSS gains to improve the inter-area oscillation mode damping. The extent of the damping was achieved by optimizing the PSS gains. The PSSs were tested under various operating conditions and they were found to adequately provide additional damping to both local and inter-area oscillation modes.

The second sub-question examined the impact of the Type 4 WTG WPPs on the inter-area and local oscillation modes when the generators have PSSs. The impact of wind power generation on the inter-area and local oscillation modes of power systems were investigated through careful observation of the movement of the oscillation mode eigenvalues for different wind power generation levels. It was found that Type 4 WTs WPPs do not introduce new electromechanical low frequency oscillation modes. The eigenvalue results of the test system with all the synchronous generators without and with PSSs with varying wind power penetration into the test system found that the oscillation modes frequencies decrease. Based on this work it can be argued that the location and purpose of the wind power generation source can positive or negatively impact on power system's small-signal stability. This is especially when wind power sources are operated in parallel with the conventional synchronous generators, whereby this investigation has shown that the damping ratio increases when WPP compensate the decreasing conventional synchronous generators' dispatch. On the other hand, when wind power supplies an increasing system load the damping ratio of the oscillation modes decrease with increasing wind power penetration. As a result, there is no general statement on the impact of wind power on the power system small signal stability. However, it can be argued that impact of wind power on the power system small signal stability is dependent on the power system characteristics including generator operating conditions, power flows and the location of the wind power generation source. It is recommended based on this investigation that wind power integration into electric power system grids consider the assessment of the system small-signal stability as this is a unique characteristic of the network and that future grid codes and standard planning practices consider the system small-signal stability requirements when integrating wind generation.

REFERENCES

[1] ExxonMobil, The Outlook for Energy: A view to 2040, 2016, Available on: http://cdn.exxonmobil.com

[2] J. G. Wright, P. M. Tuson and J. M. Van Coller, "Studies for wind energy facility grid code compliance in South Africa," *IEEE Power and Energy Society Conference and Exposition in Africa: Intelligent Grid Integration of Renewable Energy Resources (PowerAfrica)*, Johannesburg, pp. 1 - 7, 2012.

[3] P. Kundur, *Power system stability and Control*, New York: McGraw-Hill, Inc, 1994.

[4] J. G Slootweg, "Wind Power Modelling and Impact on Power System Dynamics," PhD Thesis Delft University of Technology, 2003.

[5] Nersa, "Grid Connection Code for Renewable Power plants connected to the electricity Transmission system or the distribution system in South Africa, Version 2.8," July 2014.

[6] P. Kundur, J. Paserba, V. Ajjarapu, G. Andersson, A. Bose, C. Canizares, N. Hatziargyion, D. Hill, A. Stankovic, C. Talyor, T. Van Custem and V. Vittal, "Definition and classification of power system stability IEEE/CIGRE joint task force on stability terms and definitions," in *IEEE Transactions on Power Systems*, Vol. 19, No. 3, pp. 1387 – 1401, Aug 2004.

[7] G. Rogers, *Power System Oscillations*, Boston, Kluwer, 1999.

[8] M. J. Gibbard, P. Pourbeik and D. J. Vowles, *Small-Signal Stability, Control and Dynamic Performance of Power Systems*, University of Adelaide Press, Adelaide, 2015.

[9] IEEE Recommended Practice for Excitation System Models for Power System Stability Studies, in *IEEE Std. 412.5 - 2005 (Revision of IEEE Std 421.5-1992)* pp. 1 – 93, April 2006

[10] D. J. Vowles, C. Samarasinghe, M. J. Gibbard and G. Ancell, "Effect of wind generation on small-signal stability — A New Zealand Example," *2008 IEEE Power and Energy Society General Meeting - Conversion and Delivery of Electrical Energy in the 21st Century*, Pittsburgh, PA, pp. 1-8, 2008.

[11] S. S. Mvuyana, "Small Signal Stability Assessment of the Eskom Network Based on Measurements," MSc Thesis, University of the Witwatersrand, 2014.

[12] A. Ellis and E. Muljadi, "Wind power plant representation in large-scale power flow simulations in WECC," *2008 IEEE Power and Energy Society General Meeting - Conversion and Delivery of Electrical Energy in the 21st Century*, Pittsburgh, PA, pp. 1-6, 2008.

[13] DigSilent GmbH, "DigSilent Power Factor 15 User Manual," 2015

[14] A. Golieva, “Low Short Circuit Ratio Connection of Wind Power Plants, MSc Thesis,” TU Delft, 2014.

[15] A. Ghosh, G. Ledwich, O. P. Malik, G. S. Hope, “Power System Stabilizer Based on Adaptive Control Techniques,” in *IEEE Transaction on Power Apparatus and Systems*, Vol. PAS – 103, No. 8, pp. 1983 – 1989, 1984.

[16] S. Chen and O. P. Malik, “H- infinity optimization-based power system stabilizer,” in *IEE Proc, Gener,Transm, Distrib*, Vol. 142, No. 2, pp. 179 – 184, 1995.

[17] S. S. Lee, Y. N. Yoon, J. K. Park and S. Y. Li, “Non-Linear Adaptive Decentralised Stabilization Control for Multi-Machine Power Systems,” *International Journal of Control, Automation and Systems*, Vol. 7, No. 3, pp. 389 – 397, 2009.

[18] F.de Mello and C. Concordia, “Concepts of Synchronous Machine Stability as Affected by Excitation Control,” in *IEEE Transactions in Power Apparatus and Systems,* Vols. vol.PAS-88, pp. 316-329, April 1969.

[19] A. Murdoch and G. Boukarim, “Performance criteria and tuning techniques,” *IEEE Tutorial Course-Power System Stabilization via excitation control,* pp. 26 - 43, June 2007.

[20] R. Burebe and L. Hajagos, “Integral of accelerating power type stabilizers,” *IEEE Tutorial Course-Power System Stabilization via Excitation Control ,* pp. 35-43, 2007.

[21] E. V. Larsen and D. A. Swann, "Applying Power System Stabilizers Parts I, II & III" in *IEEE Transactions on Power Apparatus and Systems*, Vol. PAS-100, No. 6, pp. 3017-3024, June 1981.

[22] D. C. Lee, R. E. Beaulieu and J. R. R. Service, “A power system stabilizer using speed and electrical power inputs-Design and Field experience” *IEEE Transaction on Power Apparatus and Systems,* Vol. PAS-100, pp. pp 4151-4157, 1981.

[23] P. Kundur, G. R. Berube, L. M. Hajagos and R. Beaulieu, "Practical utility experience with and effective use of power system stabilizers," *2003 IEEE Power Engineering Society General Meeting (IEEE Cat. No.03CH37491*), pp. 1777-1785 Vol. 3, 2003.

[24] P. Kundur, M. Klein, G. J. Rogers and M. S. Zywno, "Application of power system stabilizers for enhancement of overall system stability," *in IEEE Transactions on Power Systems*, Vol. 4, No. 2, pp. 614-626, May 1989.

[25] K. Katsuhiko, *Modern Control Engineering*, 3rd Edition, University of Minnesota, 1997.

[26] B. Pai and B. Chaudhuri, *Robust Control in Power Systems*, Springer Science & Business Media, 2005L

[27] K. K. Kaberere, K. A. Folly and A. I. Petroianu, "Assessment of commercially available software tools for transient stability: experience gained in an academic environment," *2004 IEEE Africon. 7th Africon Conference in Africa (IEEE Cat. No.04CH37590)*, Vol.2, pp. 711 – 716, 2004

[28] IEEE Task Force on Load Representation for Dynamic Performance, “Load Representation for Dynamic Performance Analysis,” *IEEE Transactions on Power Systems,* Vol. 8, No. 2, pp. 472-482, 2 May 1993.

[29] D. GmbH, “DigSilent PowerFactory Technical Reference Documentation: Two-winding Transformer (3-phase),” 2014.

[30] J. D. Glover, M. S. Sarma and T. J. Overbye, *Power system analysis and design*, 5th Ed, Global Engineering, 2012.

[31] J. Turu and S. Muratel, “Novel On-site LVRT Testing Method for Full Converter Wind Turbines”, Bachelors Thesis, Tongji University, 2014.

[32] P. Jain, *Wind Energy Engineering*, New York : McGraw Hill, 2011.

[33] H. Zhao, “Coordinated control of wind power and energy storage, PhD Thesis,” Technical University of Denmark (DTU), 2014.

[34] L. Meegahapola and D. Flynn, "Impact on transient and frequency stability for a power system at very high wind penetration," *IEEE PES General Meeting*, Minneapolis, MN, pp. 1-8, 2010.

[35] J. Fortmann, S. Engelhardt, J. Kretschmann, C. Feltes and I. Erlich, "New Generic Model of DFG-Based Wind Turbines for RMS-Type Simulation," in *IEEE Transactions on Energy Conversion*, Vol. 29, No. 1, pp. 110-118, March 2014

[36] IEC 61400-27 Working Group, “IEC 61400-27 Working Group, Wind Turbines- Part 27-1: Electrical simulation models for wind power generation-Wind Turbines” Final Draft International Standard (FDIS),” 2015.

[37] N. W. Miller, J. J. Sanchez-Gasca, W. W. Price and R. W. Delmerico, "Dynamic modeling of GE 1.5 and 3.6 MW wind turbine-generators for stability simulations," 2003 IEEE Power Engineering Society General Meeting (IEEE Cat. No.03CH37491), 2003, pp. 1977-1983 Vol. 3

[38] J. G. Slootweg, S. W. H. de Haan, H. Polinder and W. L. Kling, "Modeling wind turbines in power system dynamics simulations," *2001 Power Engineering Society Summer Meeting. Conference Proceedings (Cat. No.01CH37262)*, Vancouver, BC, Canada, Vol.1, pp. 22 – 26, 2001.

[39] D. GmbH, “DigSilent PowerFactory Technical Reference Documentation: Static Generator,” 2014.

[40] G. Tsourakis, B. Nomikos and C. Vournas, “Effect of wind parks with doubly fed asynchronous generators on small-signal stability,” in *Electric Power Systems Research*, Vol. 79, No. 1, pp. 190 – 200, 2009.

[41] E. Muljadi, C. P. Butterfield, A. Ellis, J. Mechenbier, J. Hochheimer, R. Young, N. Miller, R. Delmerico, R. Zavadil and J. C. Smith, "Equivalencing the collector system of a large wind power plant," *2006 IEEE Power Engineering Society General Meeting*, Montreal, Que., pp. 1 – 9, 2006.

[42] N. Kshatriya, “Power System Controller Design by Optimal Eigenvalue Assignment, PhD Thesis, University of Manitoba, 2010”.

[43] I. Kamwa, R. Grondin and G. Trudel, "IEEE PSS2B versus PSS4B: the limits of performance of modern power system stabilizers," in IEEE Transactions on Power Systems, Vol. 20, No. 2, pp. 903 - 915, May 2005.

[44] P. Kundur, M Klein, G. Rogers, M. Zywno, “Application of power system stabilizers for enhancement of overall system stability,” IEEE Transactions of Power System, Vol. 4, pp. 614–626, May 1989.

[45] P. Kundur, G. R. Berube, L. M. Hajagos and R. Beaulieu, "Practical utility experience with and effective use of power system stabilizers," *2003 IEEE Power Engineering Society General Meeting (IEEE Cat. No.03CH37491)*, Vol. 3., pp. 1777-1785, 2003.

[46] M. Klein, G. J. Rogers and P. Kundur, "A fundamental study of inter-area oscillations in power systems," in *IEEE Transactions on Power Systems*, vol. 6, no. 3, pp. 914-921, Aug 1991.

APPENDIX A

Generator 01 – 04 Governor parameters

The IEEEG1 governor parameters used in this dissertation are provided in Table A.1.

Table A.1: IEEE governor parameters

Description	Name	Value	Unit
Controller Gain	K	25	[p.u.]
Governor Time Constant	T1	0.001	[s]
Governor Derivative Time Constant	T2	0.001	[s]
Servo Time Constant	T3	1	[s]
High Pressure Turbine Factor	K1	0.3	[p.u.]
High Pressure Turbine Factor	K2	0	[p.u.]
Intermediate Pressure Turbine Time Constant	T5	9	[s]
Intermediate Pressure Turbine Factor	K3	0.4	[p.u.]
Intermediate Pressure Turbine Factor	K4	0	[p.u.]
Medium Pressure Turbine Time Constant	T6	0.5	[s]
Medium Pressure Turbine Factor	K5	0.3	[p.u.]
Medium Pressure Turbine Factor	K6	0	[p.u.]
High Pressure Turbine Time Constant	T4	0.4	[s]
Low Pressure Turbine Time Constant	T7	0	[s]
Low Pressure Turbine Factor	K7	0	[p.u.]
Low Pressure Turbine Factor	K8	0	[p.u.]
HP Turbine Rated Power(=0->PNhp=PgnnHp)	PNhp	0	[MW]
LP Turbine Rated Power(=0->PNlp=Pgnnlp)	PNlp	0	[MW]
Valve Closing Time	Uc	-0.1	[p.u./s]
Minimum Gate Limit	Pmin	0	[p.u.]
Valve Opening Time	Uo	0.1	[p.u./s]
Maximum Gate Limit	Pmax	0.95	[p.u.]